TASK 3.1.5
PHYSICS-BASED MODELING TOOLS FOR HIGH TEMPERATURE SUPERCONDUCTING MVDC CABLES
Year One – Deliverable(s)

Submitted to:
The Office of Naval Research

Contract: N00014-14-1-0198

Submitted by:
FSU – S. Pamidi(Lead), L. Graber, C.H. Kim, J.G. Kim, V. Pothavajhala

01/14/2015

1 TASK DESCRIPTION

This effort in this Task synergistically interacts with 5.2.4 and 5.2.5. by using the results of the tasks to refine the models and feed the model optimizations to improve the designs of hardware components developed in 5.2.5.

As the HTS technology components are still under development, prototype testing to validate the designs and capture their attributes to aid in model development and refinement is essential. The task will take advantage of the infrastructure at FSU-CAPS to facilitate the proposed component technology development and prototype testing and validation with the systems view in focus. In particular, this task will focus on generating scalable electrical and thermal models for HTS cables that can be used in systems analysis to quantify the benefits, risks, and identifying potential challenges that needs to be tackled for successful implementation of HTS cables on AES. This task will also involve collecting and maintaining the relevant data on HTS cables that would be necessary to update the electrical models developed as the technology matures and new design features are added. There are many efforts underway throughout the world on developing HTS cables for terrestrial utility applications and some of the development can directly be implemented for HTS cables for Navy MVDC system applications. This task will review the ongoing development to assess the relevance to the Navy of various design features of the superconducting components and cryogenic system components and collecting and maintaining the data necessary to create electrical models.

2 YEAR ONE DELIVERABLES

- Domain-specific high-level electrical and thermal models of HTS cables.

3 APPENDIX OF REPORTS SUBMITTED

A. Summary of Year 1 efforts
B. Paper - Experimental and model based studies on current distribution in superconducting DC cables
C. Book Chapter - Gaseous Helium Cooled Superconducting Power cables
D. Presentation - Effects of Longitudinal Variations in Critical Current and n-Value of Individual Tapes on the Performance of Superconducting Cables
E. Presentation - Study of Gaseous Helium Cooled HTS Cable System Components Using Thermal Network Models
F. Presentation - Cryogenic Thermal Modeling of Helium Gas-Cooled Superconducting Cable System Components
G. Paper - Effects of Longitudinal Variations in Critical Current and n-Value of Individual Tapes on the Performance of Superconducting Cables
H. Paper - Thermal Modeling of Gaseous Helium as a Cryogen for High Temperature Superconducting Cable Components

APPENDIX A

SUMMARY OF YEAR 1 EFFORTS

The ESRDC Task 3.1.5 focuses on quantifying the benefits and assessing the risks involved in using high temperature superconducting (HTS) MVDC power cables for shipboard applications. These goals are accomplished by generating both the electrical and thermal models of HTS cables, validating the models with existing experimental data, and extracting pertinent cable parameters for comparison with the conventional copper cables with similar power ratings. The electrical and thermal models will also be used to conduct other ship systems studies to understand the impact of HTS power cables on the rest of the ship system that arise from the special electrical and thermal characteristics of HTS cables.

The effort of 2014 was a continuation of the modeling work started in 2013 on analysis of risk in HTS cables attributed to the way they are manufactured [3_1_5 reference 1]. The focus was on short cables (30-50 m long) used onboard Navy ships that encounter large variations in load currents including situations where the load currents could reach the design limits of the cables. HTS power cables are fabricated using a large number of superconducting tapes, usually in multiple layers that form parallel networks for current transmission. Uniform distribution of current among the tapes of the cable is essential to ensure reliable operation of the cables. Non-uniform current distribution causes reduction in the rated capacity of the cable and leads to higher losses and cable failure.

Different parameters of superconducting cables such as differences in the resistance of soldered contacts of the tapes to the terminations of the cable, critical current variations among individual tapes and along the length of each tape, index (n) value of superconducting tapes, radial and longitudinal temperature gradients are identified as the primary reasons for non-uniform current distribution. Most of the listed parameters have natural statistical variations of characteristics resulting from the complex structure of second generation high temperature superconducting (2GHTS) coated conductors that are manufactured in batch process involving multiple steps. The dominant reason for non-uniform current distribution in short cables (< 50 m) is the difference in contact resistances at the ends. All the variations in tape characteristics, the contact resistances, and the variation of contacts with aging have statistical fluctuations. The models developed aimed at understanding the role of the variations in each of the individual parameters listed above and more importantly their combined effects on the risks encountered in using a manufactured HTS cable and devising operating protocols that would minimize and mitigate the risks. Monte Carlo methods combined with mathematical models were used to analyze the combined effect of the cable and superconducting tape characteristics on the risks that result from a non-uniform current distribution among the tapes in a cable.

Cryogenic thermal modeling effort adopted the thermal network approach based on the similarity between electrical and thermal fields. Heat transfer was modelled using thermal resistances (resistors), heat capacities (capacitors), temperature differences (voltage sources), and heat fluxes (current sources). Tools for electrical circuit analysis based on Kirchhoff's Laws and the superposition principle were used to analyze thermal networks. Lower computational effort compared to finite element models that facilitates quick parametric and time dependent studies is the motivation for developing the thermal network approach.

The effort on assessing the benifits of HTS cables compared a bipolar HTS cable (based on the technology of the gas-cooled cable developed at CAPS). The studies showed that an HTS cable weighs approximately 7 kg/m including a flexible cryostat while an equivalent copper cable would weigh either 61 kg/m or 122 kg/m, depending on the designed current rating of 3 kA or 6 kA, respectively. Modelling of the electrical characteristics showed that the capacitance per unit length of the HTS cable is comparable to the XLPE cable, the inductance and the resistance are substantially lower. The cable parameters extracted are being used to understand the voltage transients caused by a single rail to ground fault in an ungrounded system such as a shipboard system.

The results of the efforts on the electrical and thermal models were presented at international conferences and published in IEEE Transactions on Applied Superconductivity. Two additional paper(s) are under preparation. The investigators of ESRDC HTS Cable efforts have been invited to write a book chapter on the technology and applications of helium gas cooled HTS cables [reference 2_a book chapter].

Reference 1:

Venkata Pothavajhala, Chul H. Kim, Lukas Graber, and Sastry V. Pamidi, "Experimental and model based studies on current distribution in superconducting DC cables," IEEE Transaction on Applied Superconductivity Vol. 24, 2014, 4800505

Reference 2:

Sastry Pamidi, Chul Han Kim, and Lukas Graber, "Gaseous Helium Cooled Superconducting Power cables," A chapter in Superconductors in the Power Grid, Editor: Christopher Rey, Woodhead Publishing (in print).

4 INTERNATIONAL CONFERENCE PRESENTATIONS IN 2014

1. Venkata Pothavajhala, Chul H. Kim, Lukas Graber, and Sastry V. Pamidi, "Effects of Longitudinal Variations in Critical Current and n-Value of Individual Tapes on the Performance of Superconducting Cables," Presented at Applied Superconductivity Conference 2014, Charlotte, NC, Dates: August 10 through 15, 2014
2. Darshit R. Shah, Chul H. Kim, Lukas Graber, Sastry V. Pamidi, Juan C. Ordonez, "Study of Gaseous Helium Cooled HTS Cable System Components Using Thermal Network Models," Presented at Applied Superconductivity Conference 2014, Charlotte, NC, Dates: August 10 through 15, 2014
3. Nick Suttell, Chul H. Kim, Lukas Graber, Darshit R. Shah, Juan C. Ordonez, Sastry V. Pamidi, "Cryogenic Thermal Modeling of Helium Gas-Cooled Superconducting Cable System Components," Presented at Applied Superconductivity Conference 2014, Charlotte, NC, Dates: August 10 through 15, 2014

5 PUBLISHED WORK IN 2014

1. Venkata Pothavajhala, Chul H. Kim, Lukas Graber, and Sastry V. Pamidi, "Effects of Longitudinal Variations in Critical Current and n-Value of Individual Tapes on the Performance of Superconducting Cables," IEEE Transaction on Applied Superconductivity (in press)
2. Nick Suttell, Chul H. Kim, Lukas Graber, Darshit R. Shah, Juan C. Ordonez, Sastry V. Pamidi, "Thermal Modeling of Gaseous Helium as a Cryogen for High Temperature Superconducting Cable Components," IEEE Transaction on Applied Superconductivity (in press)

APPENDIX B

Experimental and Model Based Studies on Current Distribution in Superconducting DC Cables

Venkata Pothavajhala, *Student Member, IEEE*, Lukas Graber, *Senior Member, IEEE*, Chul Han Kim, *Member, IEEE*, and Sastry Pamidi, *Senior Member, IEEE*

***Abstract*—Current distribution among tapes in superconducting cables has been studied as a function of variations in contact resistance, individual tape critical current, and index (n)-value of individual tapes. It has been shown that besides contact resistances, variations in other superconducting parameters affect current distribution. Variations in critical current and n-value become important at low contact resistances. The effects of collective variations in contact resistances, individual tape critical current, and n-value were studied using Monte Carlo simulations method. Using a validated mathematical model, 1000 cables were simulated with normally distributed random values of contact resistances, individual tape critical current, and n-value. Current distribution in the 1000 simulated cables demonstrated the need for selecting tapes with a narrow distribution in the superconducting parameters to minimize the risk of catastrophic damage to superconducting cables during their operation. It has been demonstrated that there is a potential danger of pushing some tapes closer to their critical current before the current in the cable reaches its design critical current.**

***Index Terms*—Current distribution, direct current, mathematical model, Monte Carlo method, superconducting DC cable.**

I. Introduction

HIGH TEMPERATURE superconducting DC cables have the advantages of high current density and low losses compared to non-superconducting cables [1]. Studies also show that superconducting DC distribution systems are feasible and offer a reduction in cost [2]. The attractiveness and feasibility of DC superconducting transmission was studied and published recently by the Electric Power Research Institute [3]. Other potential applications include DC superconducting submarine power cables [4], and DC electric railway lines to increase the transportation capacity [5]–[7].

Superconducting power cables are fabricated using a large number of superconducting tapes, usually in multiple layers that form parallel networks for current transmission. Uniform distribution of current among the tapes of the cable is one of the important issues to ensure reliable operation of the cables and to devise risk mitigation techniques [8]. Non-uniform current distribution causes reduction in the rated capacity of the cable and also leads to higher losses [9]. Current sharing is also an important issue in resistive superconducting fault current limiters [10], [11].

Efforts are underway to understand the reasons for non-uniform current distribution by mapping the circumferential magnetic field using hall sensors [12]. Different parameters of superconducting cables such as differences in the resistance of soldered contacts of the tapes to the terminations of the cable, critical current variations among individual tapes and along the length of each tape, index (n) value of superconducting tapes, radial and longitudinal temperature gradients, are to be considered in understanding non-uniform current distribution. Most of the listed parameters have natural statistical variations of characteristics resulting from the complex structure of second generation high temperature superconducting (2GHTS) coated conductors that are manufactured in batch process of multiple steps. The dominant reason for non-uniform current distribution in short cables (< 30 m) is the differences in contact resistances at the ends. All the variations in tape characteristics, the contact resistances, and the variation of contacts with aging have statistical fluctuations. It is necessary to understand the role of the variations in each of the individual parameters listed above and more importantly their combined effect on the current distribution in a manufactured cable. This will help in assessing the risk in operating high power density superconducting DC power cables and to devise methods to mitigate the risk. Superconducting AC power cables will be affected by similar issues, but the focus of this paper is superconducting DC cables fabricated from 2G HTS tapes. The role of these variations is magnified in cables cooled with gaseous helium because the lower heat capacity of helium gas and the much higher power densities supported by the cables operated in 50–60 K temperature range [13]. The goal of the effort described in the paper is to assess the role of the combined statistical variations in cable characteristics in non-uniform current distribution manifested by pushing some individual tapes closer to their respective critical current before the current in the cable reached its design critical current. Monte Carlo methods combined with a mathematical model are used to analyze the combined effect of some cable and tape characteristics on current distribution among the tapes in a cable.

Experimental results on a simple network of parallel superconducting tapes were used to validate the developed mathematical model that was used to simulate and analyze current distribution in a set of 1000 tapes with statistical variations in some critical parameters.

Manuscript received July 16, 2013; accepted September 10, 2013. Date of publication September 18, 2013; date of current version September 30, 2013. This work is supported by the Electric Ship Research and Development Consortium (ESRDC) established by the Office of Naval Research (ONR).

The authors are with Center for Advanced Power Systems, Florida State University, Tallahassee, FL 32310 USA (e-mail: pothavajhala@mail.caps.fsu.edu; pamidi@caps.fsu.edu; grabber@caps.fsu.edu; ckim@caps.fsu.edu).

Color versions of one or more of the figures in this paper are available online at http://ieeexplore.ieee.org.

Digital Object Identifier 10.1109/TASC.2013.2282568

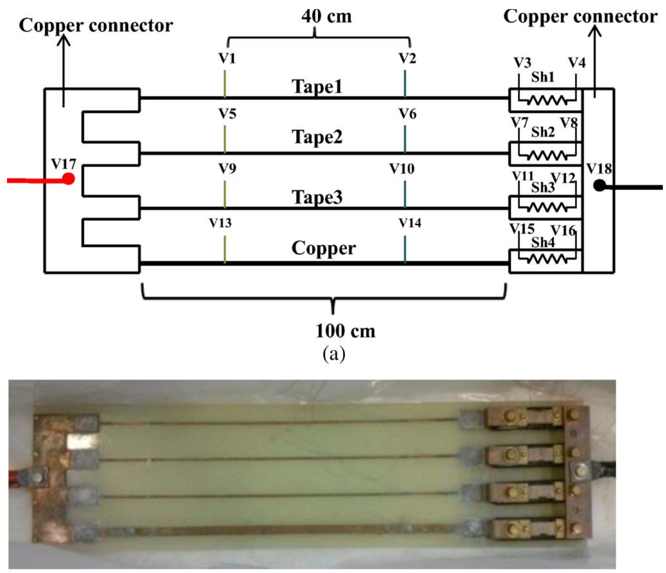

(b)

Fig. 1. (a). Equivalent circuit of the experimental setup. Tape1, 2, and 3 are 2 GHTS tapes and a copper tape arec in a parallel network. Sh1, Sh2, Sh3, Sh4 are calibrated shunts (b). The experimental setup used.

II. Experiments on Distribution of Current in 2G HTS Cables

The experimental setup consisted of three 2GHTS tapes produced by SuperPower Inc. and one copper tape in a parallel network [Fig. 1(b)]. The copper tape was used to replicate the copper conductor used in HTS cables to serve as stabilizer providing an alternative path for the current during a quench.

Each superconducting tape is 100 cm long, 4.2 mm wide and 0.1 mm thick with non-ferromagnetic hastalloy substrate and copper stabilizer. The copper tape has the dimensions of 12 mm × 0.2 mm. A standard caliberated shunt was attached at one end of each tape to measure current through individual tapes [$R_{Sh1} - R_{Sh4}$ in Fig. 1(a)]. Voltage taps were also attached on each HTS tape with a separation of 40 cm to measure the voltage drop across each of the tapes. The electric field criterion of 1 μV/cm was used to to record the invidual critical current, I_c of the tapes. Additional voltage taps were attached to enable measurement of the contact resistances and the resistance of the copper plate connecting the tapes.

A. Measurement of Critical Current

The critical current I_c of each tape was measured using the I-V plots and the using the 1 μV/cm electric field criterion.

B. Measurement of Index (n) Value

The n-values were determined from the experimental slopes of the respective $\log(V) - \log(I)$-graph by approximating the equation $V \propto I^n$.

C. Measurement of Contact Resistances

The contact resistances of the solder joints in a cable are usually not equal for all of the tapes because of differences in solder joint quality and aging [14]. After measuring the critical currents and the index value of each tape, all the tapes were

TABLE I
Characteristics of Tapes Used in Experiment

Tape	Critical current	Index (n) value [±5%]	Contact resistance
1	98 A	37	60 μΩ
2	110 A	35	80 μΩ
3	107 A	39	90 μΩ
4 (Copper)	-	-	140 μΩ

connected in a parallel network as shown in Fig. 1(b), and current was ramped up to 600 A. The contact resistances of three 2G HTS tapes and the copper tape were calculated using the voltage drop across the contacts and the current obtained using the respective shunt resistance.

D. Measurement of Current Through Individual Tapes

The resistances of the shunts used were measured in an open bath of liquid nitrogen (LN_2) to get accurate values of the currents through tapes. It was observed that there was about 7% decrease of resistance of the standard shunts from room temperature to LN_2 temperature. The newly obtained values of shunt resistances were used to calculate the current across each tape in the network.

III. Mathematical Model of the Cable

A mathematical model was developed to calculate the current through individual tapes in a parallel network given the total current, individual tape I_cs, n-values, and contact resistances. For the model, the number of superconducting tapes was limited to due to the limitations of the number of non-linear equations that can be solved simultaneously. The validity of the model was verified using the experimental results.

The values of contact resistances, critical currents and the index numbers were taken from the experimental data and then the mathematical model was used to solve for currents in individual branches. The voltage across each HTS tape was modeled using the electric field criterion and the critical current as:

$$V = E_c l \left(\frac{I}{I_c}\right)^n$$

where E_c is the electric field criterion, l is the length of cable, I is the current through the tape, I_c is the critical current, and n is index value. The following equations were solved simultaneously with the help of the scientific computing software package Maple 16 for obtaining the individual branch currents in Fig. 2, using the function 'fsolve'

$$\begin{aligned}
I_0 &= I_1 + I_2 + I_3 + I_4\\
V_0 &= I_1(50\ \mu\Omega + 10\ \mu\Omega + 233\ \mu\Omega + 2.1\ \mathrm{m}\Omega) + E_c l \left(\frac{I_1}{I_{c1}}\right)^{n1}\\
V_0 &= I_2(50\ \mu\Omega + 30\ \mu\Omega + 232\ \mu\Omega + 1.7\ \mathrm{m}\Omega) + E_c l \left(\frac{I_2}{I_{c2}}\right)^{n2}\\
V_0 &= I_3(80\ \mu\Omega + 10\ \mu\Omega + 239\ \mu\Omega + 3.1\ \mathrm{m}\Omega) + E_c l \left(\frac{I_3}{I_{c3}}\right)^{n3}\\
V_0 &= I_4(90\ \mu\Omega + 0.2\ \mathrm{m}\Omega + 50\ \mu\Omega + 234\ \mu\Omega + 2.2\ \mathrm{m}\Omega).
\end{aligned}$$

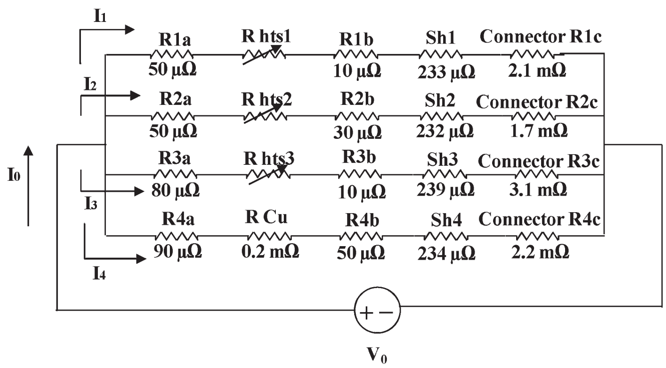

Fig. 2. Mathematical equivalent model of the setup in Fig. 1, with the values of the parameters obtained from the experiment.

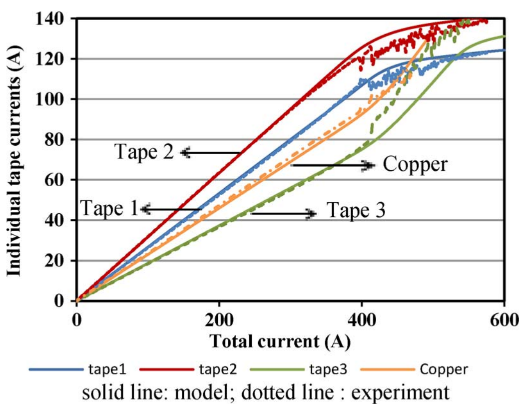

Fig. 3. Comparison of the total current vs. individual tape currents obtained through the experiments and the mathematical model.

The currents through individual tapes as obtained from the measurements and from the mathematical model against the total current through the network shown in Fig. 2 are plotted in Fig. 3.

As can be seen from Fig. 3, the calculated and experimental current values agree validating the cable model. The plots show differences in the extent of current sharing among the tapes of the network that represents a simple cable. It can be observed that the current through the copper tape is higher than the Tape 3. This is because the overall resistance of the branch 3 (3.429 mΩ) is more than branch 4 (2.774 mΩ) as shown in Fig. 2, highlighting the importance of contact resistances. Current sharing was determined by differences of I_c, n-value, and resistance along the electrical path. Resistances originate from the contacts and usually the resistance of copper lead is arbitrary for cable. This paper assesses the influences of contact resistance.

IV. SIMULATIONS

The mathematical model developed was used to study the effect of each of these parameters individually and collectively on the distribution of current among the tapes in superconducting cables. When studying one individual parameter, all other parameters were kept constant at the predetermined values. The model cable contains eight tapes with a design current of 800 A based on a critical current of 100 A per tape; slight reduction of cable critical current due to self-field effects is neglected for the study.

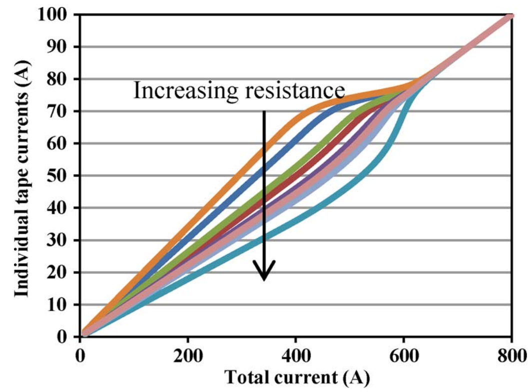

Fig. 4. Individual tape currents for different values of contact resistances: 33.2 nΩ, 37.0 nΩ, 42.9 nΩ, 45.3 nΩ, 49.1 nΩ, 50.8 nΩ, 53.3 nΩ, and 62.8 nΩ; $I_c = 100$ A for all tapes; n = 30 for all tapes.

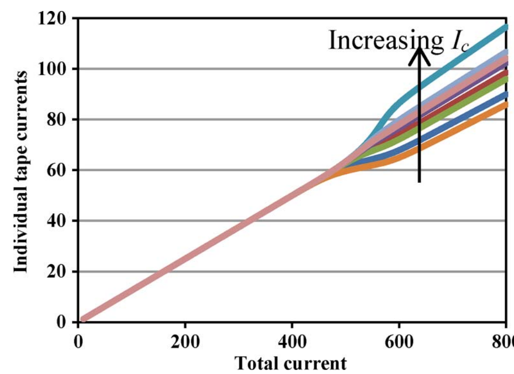

Fig. 5. Individual tape currents for different I_c: 83.16 A, 87.03 A, 92.87 A, 95.29 A, 99.12 A, 100.81 A, 103.26 A, 112.82 A; $n = 30$ for all tapes; all tapes have equal contact resistance of 50 $n\Omega$.

A. Effects of Variation of Contact Resistance

The current distribution in different tapes of a 8-tape cable with normally distributed random values for the contact resistances with average of 50 nΩ and standard deviation of 20 nΩ was plotted in Fig. 4. The contact resistances represent the sum of joint resistances at both ends of the tape connections and the resistance due to a connector (as used in the experiment) was not included because such a connector does not exist in an actual cable.

To analyze the effects of higher contact resistances, the current distribution for higher magnitudes of contact resistances were calculated with tape I_c equal to 100 A and n values equal to 30 for all tapes in all the cases.

As expected, at higher values of contact resistances the unevenness in the current distribution was significant at higher currents but for lower contact resistances the current distribution was mostly equal at higher currents.

B. Effects of Variation of Critical Current

The mathematical model was solved for different normally distributed random values for I_c with a mean of 100 A and a standard deviation of 10 A. The results of the model are plotted in Fig. 5.

Though the tapes have different I_cs, when the contact resistances of them are equal, all of them carry same current until

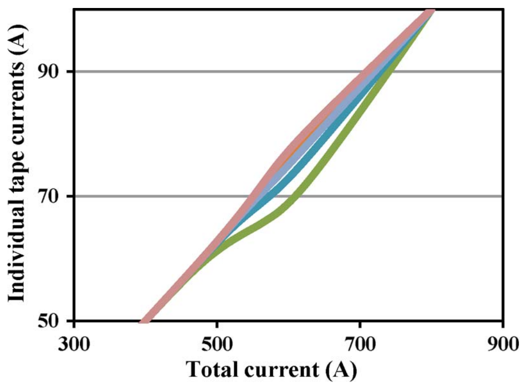

Fig. 6. Current distribution for different n values of tapes: 33.8, 31.4, 22.1, 32.5, 26.7, 32.1, 29.9, and 33.9. The contact resistance of each tape was equal to 50 nΩ and the $I_c s$ were equal to 100.

the total current approaches 8 (number of tapes) times the least I_c of tapes. The unequal current distribution starts earlier if the contact resistances are of the order of nΩ. The effect of I_c variations on current distribution were also investigated for varying levels of contact resistances. The current distributions were calculated for different I_c values (as in description of Fig. 5) and fixed contact resistances of the tapes for 5 cases: at 5 nΩ, 50 nΩ, 500 nΩ, 5 $\mu\Omega$, 50 $\mu\Omega$. The n value was kept at 30 for all tapes in all the cases. It was observed that as the contact resistances increase the current distribution was less sensitive to the difference in the critical currents of the tapes. The deviation of the tape current from the mean was more prominent for lower values of contact resistances than for higher.

C. *Effects of Variation of Index Value*

The current distribution was obtained for different normally distributed random n values with an average of 30 and standard deviation of 3.

As seen in Fig. 6, the effect of change in n value (within the values chosen) on the current distribution is much less when compared to the effect of variation of contact resistance and I_c.

V. Analysis Using Monte Carlo Method

When cables are not manufactured using tapes of similar properties, the current sharing among the tapes would not be equal. To analyze the extent of unevenness in the current distribution, 1000 cables were simulated using Monte Carlo method. Randomly generated values were for the contact resistance, I_c and n value which were used to solve the equations of the circuit. These values were chosen such that they are close to their average values with which the cables are actually designed. The contact resistances were generated with an average value of 50 nΩ and standard deviation (σ) of 20 nΩ. I_cs of the tapes have average of 100 A and σ of 10 A, n-values have average of 30 and σ of 3.

Maple 16 was used to generate the random values for the tape parameters and to solve the system of non-linear equations to get the current distribution in individual tapes. Individual tape currents were calculated at cable current of 680 A and 720 A which are 85% and 90% of design I_c of the cable. At

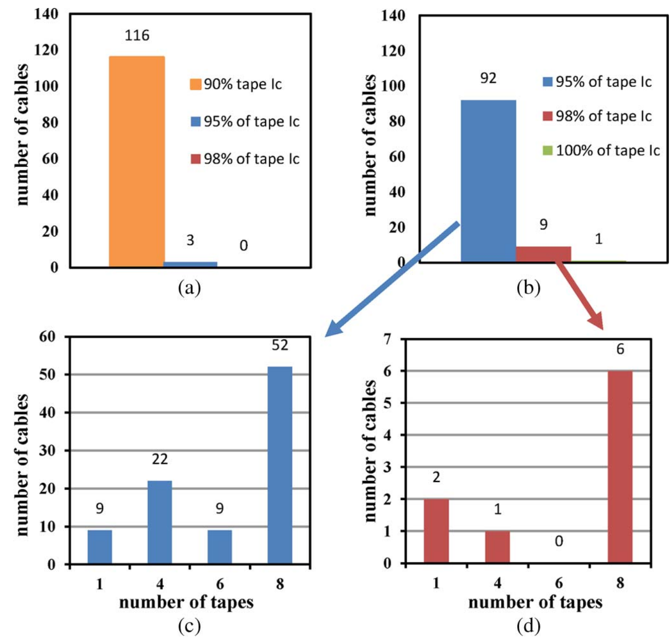

Fig. 7. Number of cables with at least one of their tapes exceeding their given fractional I_c at (a) 85% (b) at 90% design I_c of the cable, number of tapes which exceeded (c) 95% and (d) 98% of their I_c at 90% cable design I_c.

85% of the design cable critical current, out of the 1000 cables simulated, two cables have all their 8 tapes and 1 cable with one exceeding 95% of their I_c. At 90% design cable I_c, six cables have all eight tapes, two cables have one tape each, and one cable has two tapes exceeding 98% of their I_c values. These details are shown in Fig. 7(d). Such situations could lead to damage of the tapes that are closer to their I_c for longer time. When the extent of variations in the tape parameters increases, these tendencies of multiple tapes close to their critical current also tend to increase. Fig. 7(a), (b) show the number of cables and their corresponding range of tapes that exceed (c) 95% and (d) 98% of their I_c at 90% cable design I_c.

Based on the results of the Monte Carlo analysis it can be seen that out of the 1000 cables simulated, approximately 10% of the cables fall in the risky zone that some of their tapes carry high currents because of the combined effect of differences in contact resistances, I_c and n which may lead to their damage.

VI. Conclusion

The experimental and model based studies on the current distribution in superconducting DC cable show that it is important to select tapes with a narrow distribution of properties while manufacturing superconducting cables. Critical current is the second major issue to be considered after the contact resistance of the tapes. When the contact resistances are low (in the order of nΩ), even small variations in the critical current and the n-value of individual tapes can lead to significant variation in the distribution of current at higher fractions of cable design critical current. Significant spread in individual tape parameters can lead to situations in which some tapes carry a current close to their critical current well before the cable as a whole reaches its design critical current. Such an uneven current sharing can lead to catastrophic damage to the cables.

REFERENCES

[1] J. X. Jin, J. L. Zhang, Y. G. Guo, and Y. D. Zhan, "Next generation of DC power transmission technology using High Tc superconducting cables," in *Proc. AUPEC*, Dec. 2007, pp. 1–6.

[2] M. Furuse, S. Fuchino, N. Higuchi, and I. Ishii, "Feasibility study of low-voltage DC superconducting distribution system," *IEEE Trans. Appl. Supercond.*, vol. 15, no. 2, pp. 1759–1762, Jun. 2005.

[3] S. Eckroad, "Program on Technology Innovation: Superconducting DC Cable," Electric Power Research Institute (EPRI) , Palo Alto, CA, USA, Final Rep., 2009.

[4] T. Ishigohka, "Possibility of DC underwater superconducting power cable cooled by long length heat pipe," in *Proc. IEEE PES Transmiss. Distrib. Conf. Exhib.: Asia Pacific IEEE/PES*, Oct. 2002, pp. 1294–1297.

[5] H. Ohsaki, Z. Lv, N. Matsushita, M. Sekino, T. Koseki, and M. Tomita, "Superconducting power cable application in DC electric railway systems," *IEEE Trans. Appl. Supercond.*, vol. 23, no. 3, p. 3600705, Jun. 2013.

[6] M. J. Gouge, J. A. Demko, P. W. Fisher, C. A. Foster, J. W. Lue, J. P. Stovall, U. Sinha, J. Armstrong, R. L. Hughey, D. Lindsay, and J. Tolbert, "Development and testing of HTS cables and terminations at ORNL," *IEEE Trans. Appl. Supercond.*, vol. 11, no. 1, pp. 2351–2354, Mar. 2001.

[7] J. F. Maguire, F. Schmidt, S. Bratt, T. E. Welsh, and J. Yuan, "Installation and testing results of long island transmission level HTS cable," *IEEE Trans. Appl. Supercond.*, vol. 19, no. 3, pp. 1692–1697, Jun. 2009.

[8] J.-H. Kim, C. H. Kim, V. Pothavajhala, and S. V. Pamidi, "Current sharing and redistribution in superconducting DC cable," *IEEE Trans. Appl. Supercond.*, vol. 23, no. 3, p. 4801304, Jun. 2013.

[9] S. Choi, S.-J. Suh, W. Nah, Y. H. Ma, K.-W. Ryu, J. H. Kim, J. Joo, M.-H. Sohn, and Y.-K. Kwon, "Influence of non-uniform current distribution on AC transport current loss in Bi-2223/Ag tapes," *IEEE Trans. Appl. Supercond.*, vol. 16, no. 2, pp. 154–157, Jun. 2006.

[10] T. Nitta, T. Matsumura, J. Baba, M. D. Ainslie, S. Torii, H. Kado, T. Kumagai, and M. Shibuya, "Tests for conceptual design of 6.6 kV class superconducting fault current limiter with YBCO thin film elements," *IEEE Trans. Appl. Supercond.*, vol. 19, no. 3, pp. 1954–1967, Jun. 2009.

[11] M. D. Ainslie, J. Baba, V. Salvucci, T. Nitta, T. Fukunaga, M. Shibuya, S. Torii, T. Matsumura, and T. Kumagai, "Superconducting fault current limiter design using parallel-connected YBCO thin films," *IEEE Trans. Appl. Supercond.*, vol. 19, no. 3, pp. 1918–1921, Jun. 2009.

[12] K. Sim, S. Kim, S. Lee, J. Cho, and T. K. Ko, "The estimation of current distribution on the HTS cable by measuring the circumferential magnetic field," *IEEE Trans. Appl. Supercond.*, vol. 20, no. 3, pp. 1981–1984, Jun. 2010.

[13] P. J. Ferrara, M. A. Uva, and J. Nowlin, "Naval ship-to-shore high temperature superconducting power transmission cable feasibility," *IEEE Trans. Appl. Supercond.*, vol. 21, no. 3, pp. 984–987, Jun. 2011.

[14] M. Takayasu, L. Chiesa, L. Bromberg, and J. V. Minervini, "Cabling method for high current conductors made of HTS tapes," *IEEE Trans. Appl. Supercond.*, vol. 21, pp. 2340–2344, Jun. 2011.

APPENDIX C

A Chapter in Superconductors in the Power Grid
(Editor: Dr. Christopher Rey)

Gaseous Helium Cooled Superconducting Power Cables

Authors: ***Sastry Pamidi, Chul Han Kim, and Lukas Graber***

Center for Advanced Power Systems, The Florida State University, Tallahassee, FL 32310, USA

Gaseous Helium Cooled Superconducting Power Cables

Abstract

The chapter starts with a brief history of superconducting cable development to relate the technical challenges faced by the contemporary developers with those encountered by the early developments in 1960s and 70s. The chapter reviews various cryogenic media used and proposed for cooling superconducting cables. The main focus of the chapter is to describe the benefits and the associated technical challenges of using closed loop cryogenic helium gas circulation for cooling high temperature superconducting cable systems. Many potential applications of gaseous helium cooled high temperature superconducting cables are discussed. Major technical challenges specific to the development of gaseous helium cooled superconducting power cables are described. The need for the development of new cryogenic dielectric material systems for realizing medium voltage power cables is emphasized. Available technology for producing and circulating cryogenic helium gas at sufficiently large mass flow rates needed for power cables is discussed. The chapter concludes with a brief description of ongoing research and development efforts on helium gas cooled high temperature superconducting cables.

Key Terms: Power cables; high temperature superconductors; high power density; power rating tunability; novel cryogenic cooling methods; cryogenic helium circulation; cryogenic dielectrics; high voltage insulation; cable termination; high pressure gas circulation

Gaseous Helium Cooled Superconducting Power Cables

1. History of Superconducting Cables

The desire for taking advantage of application of superconductors in power transmission and distribution cables has existed since the 1960s when commercial low temperature superconducting wires (LTS) started becoming widely available [1-13]. Superconducting power cables have been believed to facilitate meeting increasing demand for electrical power in urban areas while reducing environmental consequences, dealing with right of way challenges, maintaining urban esthetics, and addressing society's unease about perceived electromagnetic interferences [7, 12]. The daunting necessity of cooling LTS cables to < 10 K with helium did not deter the superconducting cable development programs in the 1960s. A variety of competing designs were explored for both AC and DC superconducting cables [7-9]. Studies were conducted to analyze and quantify technical and economic benefits of deploying long superconducting cables in electric power grids [12]. Prototype cables made from LTS were developed and demonstrated in the 1970s and early 1980s in the US, Europe, and Russia [10-13]. Interestingly, the design approaches utilized and the technical challenges faced in the early superconducting cable developments are almost identical to the challenges faced today by the developers of high temperature superconducting (HTS) cables [1-13]. The cost, complexity, and inefficiencies of cryogenic equipment and the lack of suitable high voltage dielectric materials for cryogenic applications are a few of the common obstacles faced in the 1970s by LTS cable developers and contemporary HTS cable developers. Notwithstanding the high costs involved and technical challenges faced, several prototype LTS cables in the late last century, and HTS cables during the past 15 years were successfully demonstrated. The investments responsible for rapid development of superconducting cable technology were a result of broad public support and governments' interest in the development of clean, reliable, and efficient electrical power infrastructure. The projected transition of electricity production to include distributed solar and wind energy sources typically located in remote locations will necessitate moving large quantities of power from the sources to the consumers in urban areas. HTS cables will be suitable to tackle the challenge with low losses.

The majority of recent HTS cable demonstrations have been in urban areas with limited space for expansion of power cables and have been three phase AC cables with varying voltage ratings [14-20]. The lengths of the HTS cable segments demonstrated to date are at or below 1 km. A detailed design of a long distance DC HTS transmission cable has been undertaken by the Electric Power Research Institute (EPRI) to assess the commercial and technological viability of such a cable [21-22]. Several HTS cable demonstration projects are underway to install and test in the near future. HTS cables, both AC and DC type, that have been demonstrated during the past 15 years were cooled with pressured and subcooled liquid nitrogen in the temperature range of 65-77 K. Gaseous helium, gaseous hydrogen, and liquid air have been investigated as alternatives to liquid nitrogen in the DC cable design study by the EPRI [23]. Liquid hydrogen is another potential option for cooling superconducting cables if the safety concerns associated with it can effectively be addressed. A superconducting cable project utilizing MgB_2 superconductor and liquid hydrogen as the coolant has been successfully demonstrated recently in Russia [24]. There have been a few developments in using gaseous helium for cooling HTS cables [25-28]. Grand visions of creating energy flow systems have been proposed that combine both the delivery of liquid fuels such as liquid hydrogen and liquefied natural gas that provide cryogenic environment with transmission of electricity through superconducting cables [29-32]. The idea has been further explored recently by EPRI in the light of high temperature superconducting cable developments [33].

Discovery of many HTS materials in late 1980's and early 1990s has spurred renewed interest in superconducting power applications including power cables mainly because of the higher Tcs (up to 135 K) that allow the use of inexpensive and widely available liquid nitrogen as the coolant for maintaining the required operating temperatures [14-20]. The lengths as well as the power ratings of the demonstrated cables have gone up since the early 2000s. The longest superconducting power cable to date is the 1 km long HTS cable integrated into the power grid in the German city of Essen on May 12, 2014 [20] (see also Chapters 5 and 6 in this book).

The various HTS cable demonstration projects, funded by the federal agencies of respective countries in partnership with the participating utilities, have proved the technical feasibility of HTS power cables. There are, however, a few challenges associated with costs of HTS conductor and cryogenic equipment as well as the lack long-term reliability data that are hindering the realization of widespread commercial applications of HTS cables. The demonstrations are usually terminated after a few years due to the costs involved in continuing their operation [31]. Future successful implementation of HTS cables in electrical power utility infrastructure depends on technical advancements in developing simpler and more efficient cryogenic systems and low cost superconductor manufacturing processes. Development of new cryogenic dielectric materials that will allow reliable factory testing of the cables at room temperature before their installation is also necessary [21]. These developments will facilitate broad acceptance of HTS cable technologies by local utilities and electrical grid operators by reducing the capital investments, operational expenditures, and enhancing the reliability.

2. Introduction to gaseous helium cooled superconducting cables

The interest in developing gaseous helium (GHe) cooled superconducting power cables exists because of their potential in achieving significantly higher power densities compared to their liquid nitrogen (LN2) cooled counterparts. Besides the enhanced power densities, GHe cooled HTS cables provide several other benefits. The advantages of GHe cables relative the LN2 cooled cables are discussed below.

a. Enhanced power density

The lowest operating temperature for a LN2 cooled cable is 63 K, the freezing temperature of N_2. Hence the operating temperature window for LN2 cooled devices is 63 K to 77 K. The operating temperature of gaseous helium cooled power cables can be as low as 4 K, but large cable systems will have to limit the operating temperature to 20 K due to low efficiencies of cryogenic systems below 20 K. Critical current density of HTS materials and cables depends on the operating temperature, improving significantly at lower temperatures (see for example Chapter 2). For example, a typical commercial second generation (2G) HTS conductor operating at 20 K can carry 6-8 times the current it can carry at 77 K in self-field [34]. Thus, in principle, a GHe cooled HTS cable operating at 20 K and 50 K can support 8 times and 3 times the power densities respectively, compared to a similar HTS cable operating at 77 K. The higher power density feature of GHe cooled HTS cables is particularly beneficial for severely congested areas and maritime and aviation applications where space and weight reductions translate into substantial savings in fuel consumption. The US Navy has been exploring GHe cooled HTS power cables for future all-electric ship to take advantage of the substantially higher power densities in GHe HTS cables [35]. Exploratory studies conducted on the technical feasibility and benefits of GHe cooled HTS cables for commercial ship applications concluded that they are more efficient than the copper counterparts for high capacity and long cable applications [36].

b. Power rating tunability

As discussed above, the power rating of an HTS cable depends on its operating temperature. Hence, if the cryogenic system is designed appropriately, a GHe cooled HTS cable power capacity rating can be modified by operating it at a higher or lower temperature depending on the demand. When the power transmission demand is low, the operating temperature can be increased while still serving the loads at significantly lower operating expenses on cryogenic systems. Similarly, the power capacity rating of an HTS cable can be increased by operating it at a lower temperature to meet higher demands for transmission loads, albeit at higher operating expenses on cryogenic systems. The power rating tunability feature is beneficial for HTS cables connected in power transmission networks incorporating intermittent and seasonal power sources such as solar and wind energy and/or serving loads that change with the time of the day.

c. Ease of power system design optimization

The wider operating temperature window of GHe cables enables greater flexibility for a power system designer in optimizing the entire system based on a given constraint than their LN2 cooled counterparts. If the design constraint is limited available space or minimization of superconductor material cost, a lower operating temperature could be utilized to obtain a higher power density. If the constraint is to minimize the number of cryogenic systems in a substation that houses an HTS transformer or HTS fault current limiter besides an HTS cable, a single serial cryogenic fluid loop can be utilized by tolerating larger temperature gradient between the inlet and outlet gas streams of the loop. Helium gas allows a large temperature gradient without a phase change.

d. Cables that tolerate large elevation changes

Long HTS cables require large mass flow rates of the cryogenic fluid at high pressures to limit the temperature rise along the cable to a desired value. If the terrain is not flat with large elevation changes, the pressure variations and associated temperature variations in a LN2 cooled cable could be large requiring complex cryogenic and mechanical designs. Moreover, LN2 could go into a two-phase flow thus negatively affecting thermal and dielectric performance of the cable. Pressure and temperature variations in GHe cooled cables due to elevation changes would be significantly lower. Hence GHe cooling is more suitable for HTS cables going through a terrain with significant elevation changes. The EPRI study on long distance superconducting DC cables discussed in detail the effect of terrain changes on the cryogenic systems [23].

e. Safer operation in closed spaces

In closed or confined spaces such as buildings, tunnels and ships, LN2 cooled cables pose a safety hazard when there is a system breach due to loss of vacuum or rupture of cryogenic vessels. Rapid evaporation of LN2 leads to depletion of oxygen from the environment causing asphyxiation hazard. The much lower inventory of helium in a GHe cooled HTS cable and its lower density than that of air, significantly lower the risk of asphyxiation hazard. The potential asphyxiation hazard is one of the primary reasons for US Navy opting to focus on GHe cooled HTS cables and other devices instead of their LN2 cooled counterparts [37-38]. Similar hazards exist if an HTS cable run through long tunnel ruptures and release large amount of nitrogen gas that will stay stagnant in the tunnel. High fraction of nitrogen in the air prevents access for quick repairs needed for restoring the operation of the cable system.

3. Potential Applications of GHe cables

GHe cooled HTS cables can be used everywhere LN2 cooled cables are used. The potential of allowing operating at temperatures lower than achievable with LN2 cooled cables, GHe HTS cables will have additional superconducting material choices that need to be operated in 20-30 K range. Potential HTS materials for cables, and their pros and cons will be discussed in a later section. Considering the benefits discussed in the previous section, there are several specialized applications where GHe cooled HTS cables have significant advantages over their LN2 cooled counterparts. A few of the potential applications are discussed below. The applications discussed below utilize low voltages of < 2 kV. To apply GHe cooling for higher voltage cables, further research on new dielectric materials and improved dielectric design is required. The limitations of GHe cooled cables in terms of dielectrics will be discussed in detail in later sections.

a. Naval and aviation applications

Higher power densities achievable with GHe cooled HTS cables are particularly advantageous for ship board and aviation applications because of the limited available space and associated fuel costs being a major operating expense. Additionally, confined spaces on board ships or aircraft will not cause safety concerns when GHe is used as the coolant. The US Navy has been exploring GHe HTS power cables for future all-electric ships [25-26, 39]. The interest of the US Navy has been strong since the successful sea trials of GHe cooled HTS degaussing system [38]. Design studies have shown that high amperage (> 5 kA) GHe cooled HTS cables will be more efficient than the copper counterparts on board commercial ships [36]. NASA and the US Air Force have conducted detailed design studies of all-electric aircraft that has HTS cables connecting an HTS motor to the on-board generator [40-41]. GHe HTS cables would be suitable and advantageous for such applications.

b. DC cables for railway feeder applications

Some of the high traffic railway lines use DC feeding systems. The DC feeding systems using copper cables suffer from low efficiency due to the low voltages used typically < 2 kV. The large voltage drops also require a large number of substations along the line. Studies have shown that HTS DC cables bring several benefits including high efficiency, reduction in the number of substations, and handle much higher traffic on the same lines [42-44]. The voltages used for the copper cables are usually low at < 1500 V. GHe cooled HTS cables would increase efficiency and lower the infrastructure costs by eliminating the need for many substations in densely populated regions such as the urban areas of Japan and other countries that have heavy railway traffic.

c. DC Cables for data centers

A typical data center consumes up to 50 times as much electricity as standard office spaces of similar size [45-46]. The number of data centers and the size of a typical data center have been increasing rapidly throughout the developed world. For data security and reliability reasons, redundant electrical distribution networks are used. Enhancing the energy efficiency of data centers has been an ongoing effort. Improving the traditional technologies will bring marginal gains in efficiencies. Introducing HTS DC cables for the powering the data centers will bring significant energy savings. GHe cooled HTS cables are suitable for the application because they are DC cables and the cable runs tend to be indoors. Safety concerns preclude using LN2 cooled cables inside buildings. American Superconductor Corporation has been promoting HTS cables for data center applications [47].

d. Cables that operate in significant elevations

LN2 cooling is not suitable for HTS cables serving loads with significant changes in elevations that cause excessive changes in pressure and associated temperature variations along the length of the cable. The corresponding pressure and temperature variations in GHe cooled cables would be significantly lower [23]. Thus power cables that connect large loads on mountain resorts and other such facilities would be see significant energy savings when replaced with GHe cooled HTS cables. A recent EPRI report discussed the 12 kA power cables at the Raccoon Pumped Hydro Facility as a potential example for cryogenic gas cooled HTS cables [23].

e. Cables for feeder system to connect superconducting magnets at LHC

The Large Hadron Collider (LHC) facility at CERN in Geneva, Switzerland plans to use power cables that supply up to about 150 kA of quasi-DC current from the power converters to the large magnet systems [28-29]. Currently, a combination of copper bus bars and super critical liquid helium (LHe) cooled LTS cables are being used for some such loads. GHe cooled HTS cables are being studied for the application to take advantage of the higher operating temperatures over their LTS counter-parts. GHe cooled HTS cables provide substantial energy savings compared to LHe cooled LTS cables. The availability of 5-20 K helium gas from LHe cooled magnet systems at the facility is an added advantage of GHe cooled HTS cables for the application.

4. Technical issues pertinent to GHe cooled HTS cables

a. HTS Materials

Since the discovery of superconductivity at 36 K in La-Ba-Cu-O system [48], many new superconducting materials commonly known as HTS (or cuprates) were discovered with T_c up to 135 K. Many reviews are available on various aspects of HTS materials [48-53]. Only four of the materials could be developed for commercial production of long length conductors (see also Chapters 5 and 6). To date, all HTS electric power applications have been based on these few materials. Table 1 shows a list of the materials, their critical temperatures (T_c), and references as sources of additional information. Salient features of these practical HTS materials are discussed below as they apply to HTS cable applications. Note, as discussed previously in chapter 2, MgB_2, although technically an LTS material based upon an electron-phonon pairing mechanism is often included in the HTS family because of its unusually high T_c.

Table 1 List of practical HTS materials, their chemical composition, Tc values, and references for additional information.

Material	Common name	T_c (K)	References for additional information
MgB_2	MgB2	39	76-79
$Bi_2Sr_2Ca_1Cu_2O_8$	BSCCO; BSCC0-2223; Bi-2223	85	55-57
$REBa_2Cu_3O_7$	REBCO123; YBCO123; Y-123; 2G HTS	92	66-75
$Bi_2Sr_2Ca_2Cu_3O_{10}$	BSCCO2223; 1G HTS	110	58-65

i. BSCCO2212 conductor

BSCCO2212 with approximate chemical composition of Bi2Sr2Ca1Cu2O8 has T_c of 85-92 K and is made both silver alloy sheathed tape and round wire forms (see also Chapter 3). It is also available in bulk form as rods and tubes mainly for current lead applications [54-57]. Processing of BSCCO2212 involves partial melt processing and hence the fully reacted wire does not tolerate handling due to its brittle nature. Moreover, the material exhibits useful critical current density only at temperatures below 30 K, with excellent critical current density at 4.2 K even in large background magnetic fields. Hence the BSCCO2212 material is primarily being developed for high field magnet applications operating at low temperatures < 30 K, where the coils wound from green wire can be reacted (i.e. wind then react) eliminating the need for handling the wire after partial melt process reaction [56]. Figure 1 shows the typical cross section of round BSCCO wire being developed for high field magnet applications. BSCCO2212 is not suitable for long length power cables because of the difficulty in heat treating long lengths and its inability to tolerate any mechanical handling after the reaction. Besides high critical current density in large background magnetic fields, the round wire form allows ease of winding large magnets without having to worry about anisotropy of superconducting properties that is a problem in other HTS materials [56].

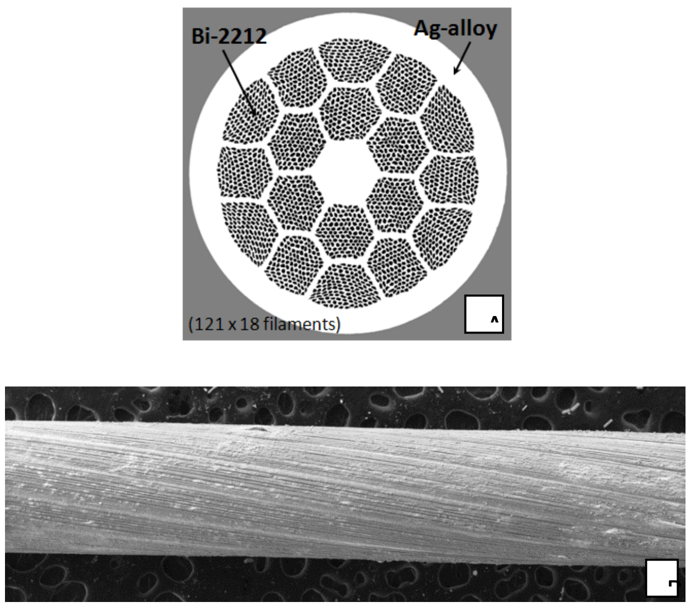

Figure 1 Transverse cross section of a round BSCCO 2212 wire (A) and longitudinal cross section of a twisted BSCCO 2212 wire after etching away the silver (B) (with permission from the Applied Superconductivity Center, National High Magnetic Field Laboratory).

ii. BSCCO2223 conductor (1G HTS)

BSCCO2223, also known as 1G HTS conductor with approximate chemical composition of Bi2Sr2Ca2Cu3O10 with T_c of about 110 K is made as silver alloy sheathed tape. 1G HTS is the first HTS material successfully commercialized in a long length practical conductor. All the early

(1990's and early 2000) HTS power cables and other devices were made from this conductor. As the 1G conductor is available in fully reacted form and comes with several varieties of metal laminated stabilizer options, many large cable demonstration projects were initiated throughout the world [58-61] (see also Chapters 5 and 6). Steady progress has been made in enhancing the performance and reliability of the conductor [62-65]. 1G BSCCO2223 conductor is available in one of several variants depending on the requirements of the application. Of particular importance for HTS cables is the variant that has twisted multifilamentary structure with reduced ac losses to enable AC power cables and other applications [65]. Sumitomo Electric Industries is currently the largest supplier of the 1G conductor with the trade name DI_BSCCO. Figure 2 shows the cross section of BSCCO2223 (1G) tape conductor produced by Sumitomo Electric Industries. Typical commercial conductor is available as nominal 4 mm wide and 0.2 mm thick tape and self-field critical current of 170-200 A at 77 K. Recently, there has been a significant progress in achieving high critical current densities in 1G conductor by using overpressure processing method [62-64].

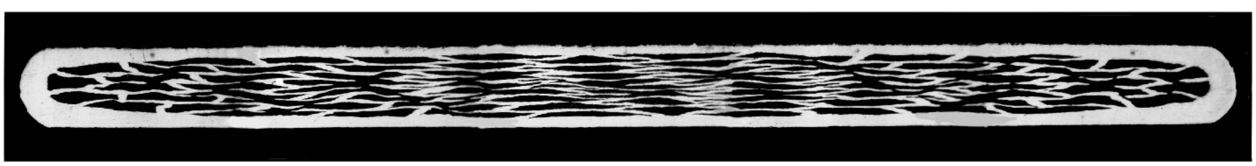

Figure 2 BSCCO 2223 wire cross section reproduced with permission from website of Sumitomo Electric Industries, Ltd.

iii. YBCO1223 conductor (2GHTS)

REBCO1223, also known as second generation (2G) HTS conductor, has a chemical composition of RE1Ba2Cu3O7 with T_c of about 90 K (RE can be one of several rare earth elements). Many manufacturers produce long lengths (~ 100-300 m) of the 2G conductor as coated conductor with a thin layer (1-2 μm) of superconductor on a metal substrate with complex multilayer ceramic buffer layers [66-67] (see also Chapter 4). Multiple intermediate buffer layers are required to achieve the required biaxial texture of the superconducting layer. The terms tape, coated conductor, and wire are used interchangeably throughout this chapter to all refer to the same multilayer REBCO1223 architecture. Figure 3 shows the architecture of the multilayer REBCO1223 2G tape conductor produced by SuperPower Inc. using the Ion Beam Assisted Deposition (IBAD) process. The 2G multilayer REBCO1223 conductor has by far the highest critical current density at 77 K and has the potential to be an inexpensive conductor if the manufacturing challenges are tackled to enhance the yield, performance and uniformity. Many recent long length HTS cable projects have used or being designed for future installations with the 2G conductor [68-71]. The 2G conductor from several manufacturers is amenable to producing specialized HTS cables with small diameters and as multifilamentary and transposed cables [72-75].

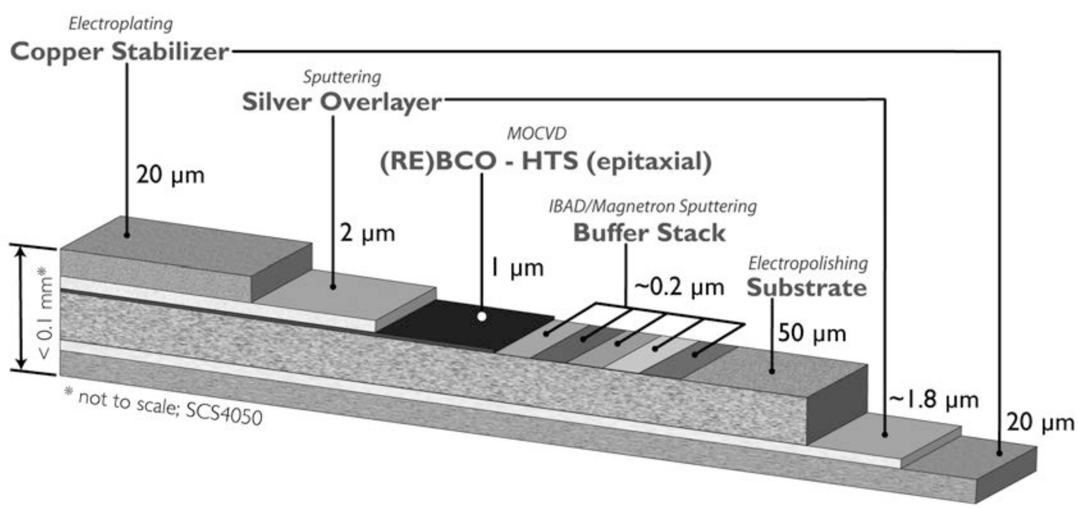

Figure 3 Multilayer architecture of IBAD REBCO1223 tape conductor manufactured by SuperPower Inc. (Image courtesy of SuperPower Inc., a Furukawa Co.)

iv. MgB2 conductor

Magnesium di-boride (MgB_2) is the most recently discovered practical superconducting wires available in long lengths from several manufacturers [76-79]. Although technically an LTS material, because of its unusually high T_c, it is also being considered for superconducting cable applications. Its simple powder-in-tube (PIT) fabrication process (see also Chapter 2), makes MgB_2 the least expensive of the LTS wires being considered for superconducting cable applications, but has the disadvantage of having the lowest T_c of 39 K. It is suitable for applications at operating temperatures of 25 K and lower. It is available as round wire and multifilament architecture from Hyper Tech Research Inc. and Columbus Superconductors. Figure 4 shows the different cross sections of multifilament MgB_2 conductor produced at Hyper Tech Research. Hyper Tech Research currently supplies conductor with self field engineering current density of 2 kA/mm^2 at 20 K, the expected operating temperature of MgB_2 cables and expects to improve the conductor to 5 kA/mm^2 at 20 K in 3 years. High current cables have been demonstrated from MgB2 wires operating at around 20 K using liquid hydrogen as the cryogenic coolant [28-29. 80-81].

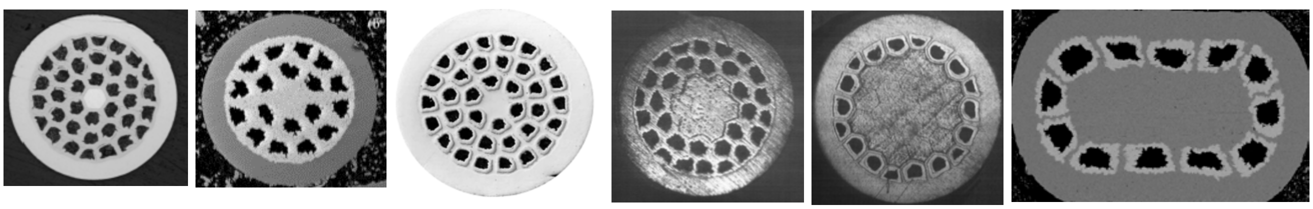

Figure 4 Several cross sections of MgB2 wire available from Hyper tech Research.

5. Dielectric Design Aspects of Helium Gas Cooled HTS Cables

a. Dielectric Properties of Helium Gas

As described in the sections above, there are many benefits for using GHe as the coolant for HTS power cables compared to its LN2 cooled counter-part. However, the dielectric characteristics of GHe are substantially more challenging for the design of an HTS power cable compared to LN2. This is one of the primary reasons why the HTS power cables currently installed in the distribution grid and operating at voltages greater than 10 kV use LN2 as the coolant.

For most HTS cables – more specifically for HTS cables that are of the cold dielectric type, which will be explained in the next section – the cryogenic coolant is part of the dielectric system since it penetrates butt gaps between the layers of the lapped dielectric tape used to insulate the cable. The dielectric breakdown strength of LN2 has been reported to be 19.6 kV/mm [82] in uniform electric fields, independent of pressure and temperature of the liquid, as long as there are no nitrogen gas bubbles present. The formation of nitrogen gas bubbles is usually minimized by subcooling and pressurizing the liquid nitrogen. However, in HTS cable applications the formation of gas bubbles in liquid nitrogen cannot be totally prevented. A decrease of the breakdown strength by approximately a factor two when nitrogen gas bubbles are present has been measured experimentally [83]. Besides the high voltage breakdown strength, LN2 also has a relative permittivity of approximately 1.4 and therefore is not too dissimilar to that of lapped dielectric insulating tape materials such as polytetrafluoroethylene (2.1) or polypropylene (2.2−2.3). When the dielectric materials insulating the HTS cable are reasonably well matched in relative permittivity, there is an advantage for the capacitive electric field in AC applications and during fast voltage transients, leading to an only moderate field enhancement in LN2.

GHe on the other hand has different and more challenging dielectric characteristics than its more robust LN2 counter-part. Gases in low electric fields are generally very good electrical insulators with low dielectric losses, low electrical conductivity, and a relative permittivity very close to unity, leading to HTS cable designs of low losses and low capacitance per unit length. However, the breakdown strength of helium gas is considerably lower than that of liquid nitrogen or even nitrogen gas at equivalent temperature and pressure.

Breakdown strength of a particular gaseous dielectric is a function of its pressure and temperature conditions. The Paschen's Law describes the breakdown voltage between two electrodes as a function of the product of pressure and electrode distance. The function has a minimum breakdown voltage at a certain pressure-distance product, called the Paschen minimum. Starting from the Paschen minimum, the breakdown voltage increases rapidly towards lower pressure-distance products. This zone is important for vacuum dielectrics. The breakdown voltage also increases towards higher pressure-distance products but only gradually. This is the zone of interest for gaseous dielectrics such as GHe cooled HTS devices.

The dielectric strength of a gas is also a function of temperature. The dependency on temperature is not considered in most diagrams of Paschen's Law. Decreasing the temperature has a similar effect as increasing the pressure since both of them increase the density of the gas. Figure 5 shows the Paschen curve of GHe at room temperature along with breakdown voltages of GHe at 77 K and LN2 in the same diagram. Operation at cryogenic temperature around or below 77 K and pressure levels of 1 MPa and higher allow the use of gases with low dielectric strength such as the noble gases helium and neon as an insulation media of HTS devices. The dielectric breakdown strength of GHe at 77 K and 1.0 MPa has been reported to be 4 kV/mm (RMS, 60 Hz) in uniform field (Rodrigo et al., 2014). While this value is good enough to allow designing HTS cables for low to medium voltage applications, it is still approximately five times lower than that of LN2.

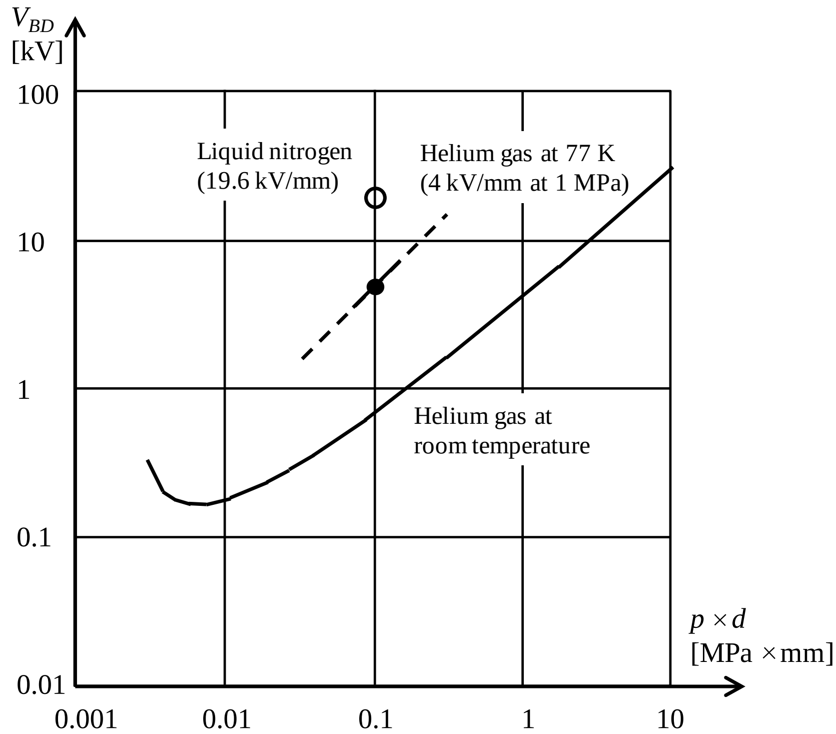

Figure 5 Paschen's Law for helium gas at room temperature [84], breakdown voltage for helium gas at 77 K and 1 MPa [85], as well as breakdown voltage for liquid nitrogen [82].

Solely relying on the Paschen's Law is not sufficient for a complete assessment of dielectric properties. Corona discharges on electrode surfaces appear at voltage levels much lower than breakdown voltage. Since helium gas is located in butt gaps of lapped tape insulation around HTS cables, these corona discharges manifest themselves in high frequency pulses not dissimilar to partial discharge (PD) pulses in solid dielectrics. And like PD pulses in solid dielectrics, these corona discharges can deteriorate the insulation if they occur over an extended period of time. Therefore, the maximum voltage in normal operation should never exceed the PD inception voltage. Figure 6 shows PD inception voltage as a function of gas pressure at a temperature of approximately 50 K

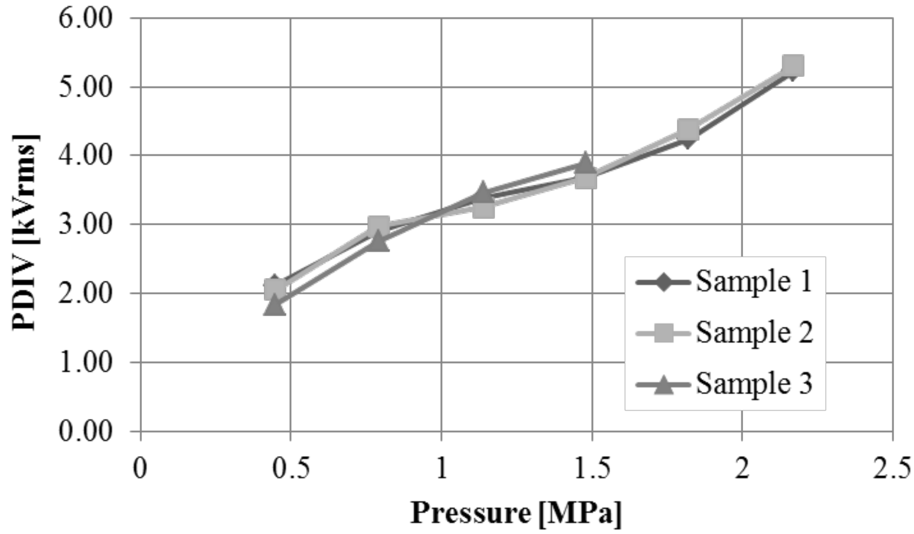

Figure 6 Partial discharge inception voltage as a function of helium gas pressure for three samples of a 1-m HTS model cable [86].

In addition to the low corona onset voltage, GHe has a relative permittivity close to unity, which leads to considerable AC field enhancement in butt gaps. This is especially true in combination with lapped tape made of materials with high relative permittivity such as polyimide (3.4). But also DC fields are expected to be enhanced in butt gaps since GHe has a very low electrical conductivity.

Another breakdown mechanism is surface flashover on the interface of a solid insulator to helium gas. It has been reported that the temperature of the surface has a substantial impact to the voltage limit at which surface flashover occurs. This is especially important at cable terminations where the insulator body of the high voltage bushing may have a temperature much higher than the helium cooling gas itself [87].

b. Two Different Design Philosophies: Cold Dielectrics and Warm Dielectrics

There are two different types of design of HTS power cables, categorized by the type of electrical insulation: a) warm dielectric and b) cold dielectric. In an HTS cable using a "warm dielectric", the electrical insulation is outside the HTS cable cryostat and therefore essentially at room temperature. Warm dielectric materials typically are fabricated with a synthetic rubber insulation such as ethylene propylene rubber (EPR) layer extruded onto the outer wall of the cryostat containing the [88]. An outer armor and screen is added like in conventional non-superconducting power cables. The HTS cable is located inside the flexible cryostat. The HTS cable and the cryostat are on the same voltage potential thus no electrical insulation is required on the HTS cable. It must be noted that using the warm dielectric design, the two poles of a DC cable or the three phases of an AC cable always require separate individual cryostats. The additional volume occupied by the additional cryostat(s) reduces the effective power density compared to HTS cables of using "cold dielectrics," where both poles or all three phases can be contained within a single cryostat.

For an HTS cable using a cold dielectric, the high voltage HTS cable is located inside a cryostat that is at ground potential. Therefore, the HTS cable itself must be electrically isolated from the cryostat. The cryostat might feature a protective plastic layer to simplify handling and help protect against environmental damage to the HTS cable during insertion. However, this protective layer does not need to withstand any electrical field. The HTS cable on the inside of the cryostat typically has a lapped dielectric tape insulation and a conductive return or shield layer. The return or shield layer is at ground potential and can be either made of normal metal tape such as copper or aluminum or made of HTS tape, depending upon the anticipated magnitude of the shielding currents. There is an additional protective layer wrapped around the shield layer to reduce friction when pulling the cable into the cryostat and reduce the risk to damage the shield layer or the inside of the cryostat. Figure 7 depicts the two basic designs [88].

Warm dielectric and cold dielectric HTS cables both have their advantages and disadvantages. Depending on the application, one type can be more advantageous than the other. It has been reported that for retrofitting existing duct or pipe systems, the warm dielectric design is more suitable [89]. Even though the power density of an HTS cable of type warm dielectric is lower than that of its cold dielectric counter-part, it still leads to an increase in power density by a factor of two to three compared to conventional copper or aluminum cables. However, for new systems the cold dielectric design seems to be more favorable since it allows power densities exceeding five times that of conventional power cables [89]. Besides the improved power density of HTS cables of cold dielectrics, they have advantages in reduced AC losses for cables carrying AC current since the HTS shield reduces the radial magnetic field of adjacent conductors. The HTS shield also prevents inductive coupling with nearby metallic materials such as the cryostat [89]. One of the major disadvantages is the tradeoffs required for the cryogenic electrical insulation, especially if GHe cooling is used. The electrical insulation needs to accommodate multiple thermal cycles without either the insulation getting damaged by cracking or the conductors getting damaged by applying excessive strain to the HTS tapes due to mismatching coefficients of thermal expansion. The thermal conductivity of the dielectric is also an essential feature since it allows heat conduction from the HTS conductor to the cryogenic coolant. While a large number of layers of lapped insulating tapes is beneficial to lower the dielectric stress, it is also counterproductive for the thermal management.

The lower complexity of warm dielectric HTS cable is simpler to manufacture and less costly overall [90]

Table 2 summarizes the comparison between warm dielectrics and cold dielectrics.

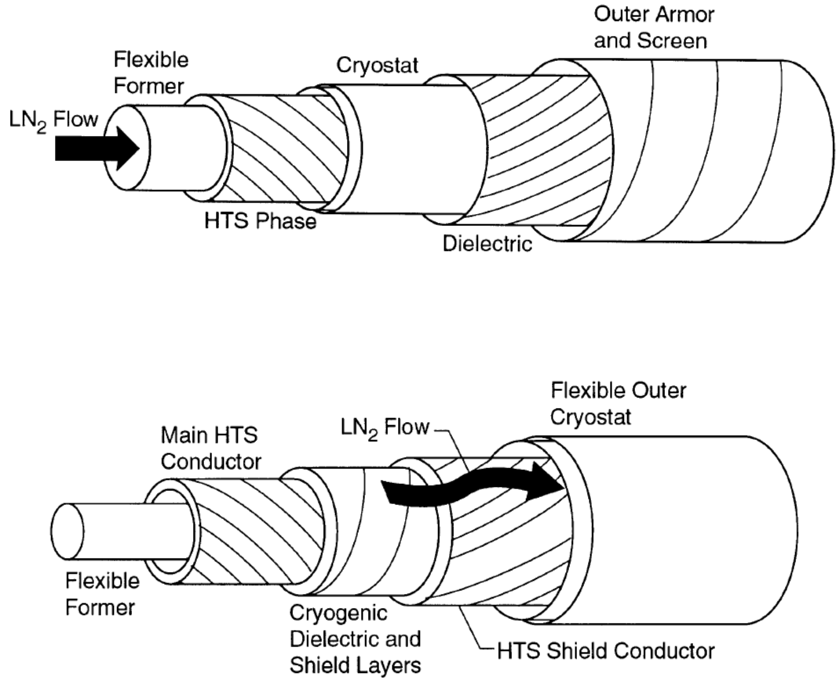

Figure 7 Cable layout considerations: Warm dielectrics (above) versus cold dielectric (below) [88].

Table 2. Comparison of two basic designs of HTS cables.

	Warm Dielectric	Cold Dielectric
Number of cryostats	Each pole/phase in a separate cryostat	Poles/phases can be in the same or in separate cryostats
Type of shield layer	Metal at room temperature (additional losses)	HTS or metal
Magnetic field	Present	Canceled
AC losses	Higher	Lower
Dielectric losses	No heat load to coolant	Heat load to coolant

Power density	2-3x regular power cable	5x regular power cable
Complexity of insulation	Low	High
Complexity of termination	High	Low
Complexity of factory testing	Low (at room temperature)	Generally not possible

c. Lapped Tape Insulation

Most conventional power cables use extruded insulation around the metallic conductor. More precisely, there is a thin inner layer of semi-conductive material extruded onto the conductor, followed by the actual insulating dielectric, finished by another semi-conductive layer. The extruded insulator material is typically either ethylene-propylene rubber (EPR) or cross-linked polyethylene (XLPE). The extrusion process is very carefully controlled to avoid any impurities and voids that could lead to partial discharge under high dielectric stress.

There is no evidence in the technical literature that extruding insulation on HTS conductors has been tried successfully except for very thin layers directly extruded onto HTS tapes. The mismatch in coefficient of thermal expansion between most dielectrics and HTS tapes that may lead to significant strain and potential delamination of the extruded insulation for the HTS tape or delamination of the HTS layer from the underlying metallic substrate [91]. Therefore, for HTS power cables with cold dielectric, the insulation of choice has been wrapping with lapped insulating tape. Insulation materials show substantial shrinkage in cryogenic environments of around 5% or more [89], however, the lack of bonding directly to the surface of the HTS tape, which has a thermal shrinkage closer to 0.3 %, provided by the wrapping insulation technique does not lead to damage of the HTS tapes.

To give an example, the coefficient of linear expansion of PTFE is approximately $140 \cdot 10^{-6}$ K^{-1}, which is considerably higher than that of stainless steel ($17 \cdot 10^{-6}$ K^{-1}) or copper ($16 \cdot 10^{-6}$ K^{-1}) [92]. The mismatch in thermal expansion could lead to high levels of mechanical stress in the HTS cable, potentially damaging the superconducting material if the cable design would not take it into account. A typical solution to avoid problems associated with the mismatch in thermal expansion is to use a dielectric in tape form. The tape is helically wound around the cable along its length, allowing the insulation material to contract without causing stress on the HTS tapes. The material and thickness of the tape are chosen to allow mechanical flexibility at cryogenic temperatures. The materials proposed for lapped tape insulation of HTS cables include polyethylene (PE), polypropylene (PP), polycarbonate, polyethyleneterephtalate (PET), polyamide (Nomex, Nylon), polyimide (Kapton), cellulose (Kraft paper), and polypropylene laminated paper (PPLP) [93].

Electric field grading is an important aspect for any power cable to reduce the electric stress in the dielectric. For this purpose, a semi-conductive layer (often referred to as “semi-con”) is added on the interface between conductor layers and insulation layers to reduce electric field enhancements around edges and protrusions. The semi-conductive layer must be very smooth. For HTS power cables, it is most suitable to use a lapped tape [94]. Typical examples are tapes made of fibrous graphite paper, graphite impregnated polytetrafluoroethylene (PTFE, Teflon), and semi-conducting ethylene propylene rubber (EPR). Their resistivity of semi-con tape can be varied over a wide range and is also a function of frequency, temperature, pressure. For AC power cables, the semi-conductive layer has a substantial impact to the total dielectric losses of the cable. The number of layers of semi-conductive tape is a tradeoff between reducing electric stress and increasing dielectric losses. The number of semi-conductive layers should be kept to the necessary minimum. Ratios of semi-conductor-to-insulation layers of between 1:40 and 1:80 have been suggested [94]. However, this depends on factors such as the content of high frequency components such as power electronic switching harmonics, which can lead to increased interfacial polarization and ultimately lead to cable failure due to shield malfunction [94].

The HTS cable is terminated in metallic termination blocks in order to allow a low electrical resistance interface from the bushing to the HTS cable. The electrical insulation is stripped back for easy access of the terminal blocks. Without additional HTS cable design effort, the electric field would be enhanced around the HTS cable section where the insulation is stripped back to make the low electrical resistance. This high stress region can be avoided by designing the appropriate stress cones. The stress cones are typically made of the same dielectric tape to avoid any mismatch in relative permittivity and electrical conductivity. A gradual increase in the number of insulating layers or an additional triangular sheet of the same material wound around the cable end result in the required conical shape of the stress cone.

d. Differences between AC Cables and DC Cables

There are both obvious and non-obvious differences between DC power cables and AC power cables. The most obvious difference is that a DC cable has two poles. A bipolar cable has a positive pole and a negative pole while a monopole cable has one of them grounded. The two poles can be separate HTS cables each contained in its own cryostat, they can be in the same cryostat, or they can be designed as a coaxial cable.

An AC cable has three phases and a ground pole, which is sometime referred to as the “shield” or “return” phase. In rare cases it can also have a neutral phase, which is typically on ground potential but designed to allow substantial continuous current flow. Similar as for DC cable, the three phases can be in separate cryostats, they can be in the same cryostat, or they can be of tri-axial configuration in a single cryostat (see also Chapter 5).

The AC field distribution in an HTS cable is dominated by the permittivity of the dielectrics. This is called the capacitive field [95]. The capacitive field can be simulated by finite element analysis. It is important to estimate the maximum electric field in butt gaps and insulator surfaces. Even though such analyses do not calculate the breakdown voltage, it helps to determine the weakest location, which could become a source of partial discharge (PD) [95].

If the AC electric fields are too high, it can damage the insulation by constant PD activity. This is a process that can take days to months before the material breaks down. The insulator gets damaged locally at the source of PD, driving an electric tree of degraded material forward in field direction. The local electric field at the branch ends of the tree is enhanced since the tree has a higher conductivity than the surrounding undamaged insulation material thus acts as a perturbance in the otherwise homogeneous electric field. The ultimate breakdown occurs from one of the branches, bridging the remaining distance in the pristine dielectric to the conductor.

Dielectrics under AC fields show dielectric losses. The dielectric losses typically consist of two components: a) polarization losses and b) conductive losses. Under ideal conditions, the AC current flowing in a dielectric material leads the voltage by an angle of 90°. The dielectric losses reduce this angle by a few degrees. These losses are expressed as the “loss tangent,”or is sometimes referred to as the “dissipation factor.” It is defined as the ratio of the active power P_δ divided by reactive power Q_C, where $\tan\delta = \frac{P_\delta}{Q_C}$. The dielectric losses for a certain material can also be expressed by a complex permittivity consisting of both a real part and an imaginary part. Küchler (2005) reports that typical values for dielectric losses at room temperature range from 0.1% (PTFE, PE, quartz) to 10% (filled epoxy resins, polyamide). PPLP insulated HTS cables in LN2 have dielectric losses between 0.2% and 1.1% depending on the applied electric stress [96].

Power systems aspects such as the maximum capacitive load need to be considered when designing AC systems. The capacitive load added by power HTS cables can be considerable. There are indications that HTS power cables could have a higher capacitive load than regular XLPE or EPR power cables [87]. This would limit the maximum length of such cables to avoid problems with grid stability. Details to cable capacitance and grid stability can be found in the power systems literature (see also Chapter 5).

Dielectrics in DC cables are different than their AC counter-parts. The dielectric withstand capabilities of an insulator is typically substantially higher for DC electric fields than AC electric field – values of up to three times higher withstand voltage have been reported for regular high voltage power cables [97]. That being said, the electric field distribution is much more complex than for AC fields and is a function of time. Shown in Figure 8 are the time dependent voltage $v(t)$ and current $i(t)$ versus time commonly observed when charging an insulator with a time varying voltage $\mathrm{d}v/\mathrm{d}t$. The time dependent behavior can be characterized by four distinct regions or phases. In a first phase (Phase I in Fig. 8) during which the voltage is ramped up, the field distribution is of capacitive type, that is dominated by the relative permittivities of the materials. The charging current is mainly a capacitive current $i_C(t) = C \cdot \mathrm{d}v(t)/\mathrm{d}t$ with the total effective capacitance C. In Phase II of Figure 8, the voltage $v(t)$ is constant and the current is dominated by a polarization current $i_P(t)$. The polarization current is responsible for the accumulation of space charges on the interfaces of the insulating tapes as well as within the material of the insulating tapes. In Phase III of Figure 8, a purely resistive field is established that depends on the specific resistivities of the insulating materials. The residual current that remains after the transients decay is a constant resistive leakage current. After switching off the voltage in Phase IV of Figure 8, the local surface charges and space charges remain for a certain moment of time. This can be a slow process with a time constant similar to the polarization time constant in Phase II [95].

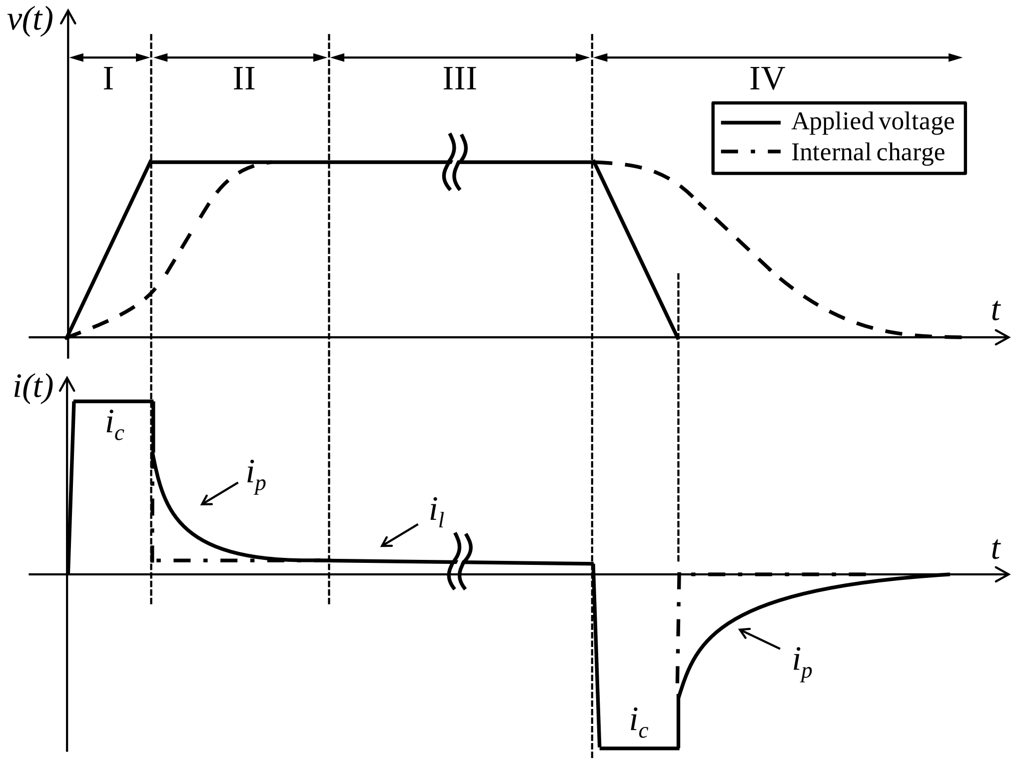

Figure 8 The four phases of dielectric currents in DC fields [95].

Under ideal conditions, DC cables have considerably lower dielectric losses than AC cables. However, this assumes that the supply voltage is pure DC. In most practical applications, there are power electronic rectifiers generating the DC current. This leads to a certain level of voltage ripple in case of a line commutated diode or thyristor rectifiers. In case of a switched-mode IGBT rectifier, high frequency harmonics of the switching frequency should be expected to be present, leading to parasitic dielectric losses. The amplitude and frequency of the voltage ripple and switching harmonics need to be carefully considered for the dielectric design. Hence dielectric losses can still occur under these circumstances.

6. Design Aspects for GHe Cooled HTS Cable Terminations

The terminations of an HTS power cable have the primary function of interfacing the room temperature power source hardware with the superconducting cable operating at cryogenic temperature. Besides the current leads, the terminations must also include helium gas inlet and outlet ports as well as instrumentation to monitor the HTS cable system [25]. The large temperature gradient, along with Joule heating in non-superconducting feed-throughs, result in a substantial heat load to the cryogenic cooling system. For short power cables, the heat load from the terminations can exceed all other heat loads to the cryogenic system. [98] reported a total heat load from ambient of 25 W for each termination for a 3000 A rated HTS cable. The heat load from the flexible cable cryostat is approximately 1-2 W/m depending upon the size (i.e. diameter) of the cryostat. The lower heat capacity of GHe compared to LN2 makes the thermal design of the terminations particularly challenging. An optimization of the conductor cross section in the current leads is most important and usually done by using “McFee Optimization” [99].

The dielectric design of terminations for GHe cooled cables is also demanding. Electric fields are problematic in helium gas at elevated temperature and electric fields in proximity to warm insulator surfaces because of lower density of helium at such spots. Such a situation can be prevented by maintaining low temperature at the insulator bodies of the feed-throughs. The requirement for cold insulator surfaces in helium gas led to the development of hybrid HTS cable terminations (Figure 9) [87, 100-101]. Hybrid terminations include a volume of LN2 to keep the feed through into the GHe section at temperatures close to 77 K and thus increase the density and withstand voltage of helium gas in proximity to the feed through. This design also reduces the heat load to the GHe system. A disadvantage of a hybrid termination is the requirement of a second feed through from ambient into the LN2 chamber.

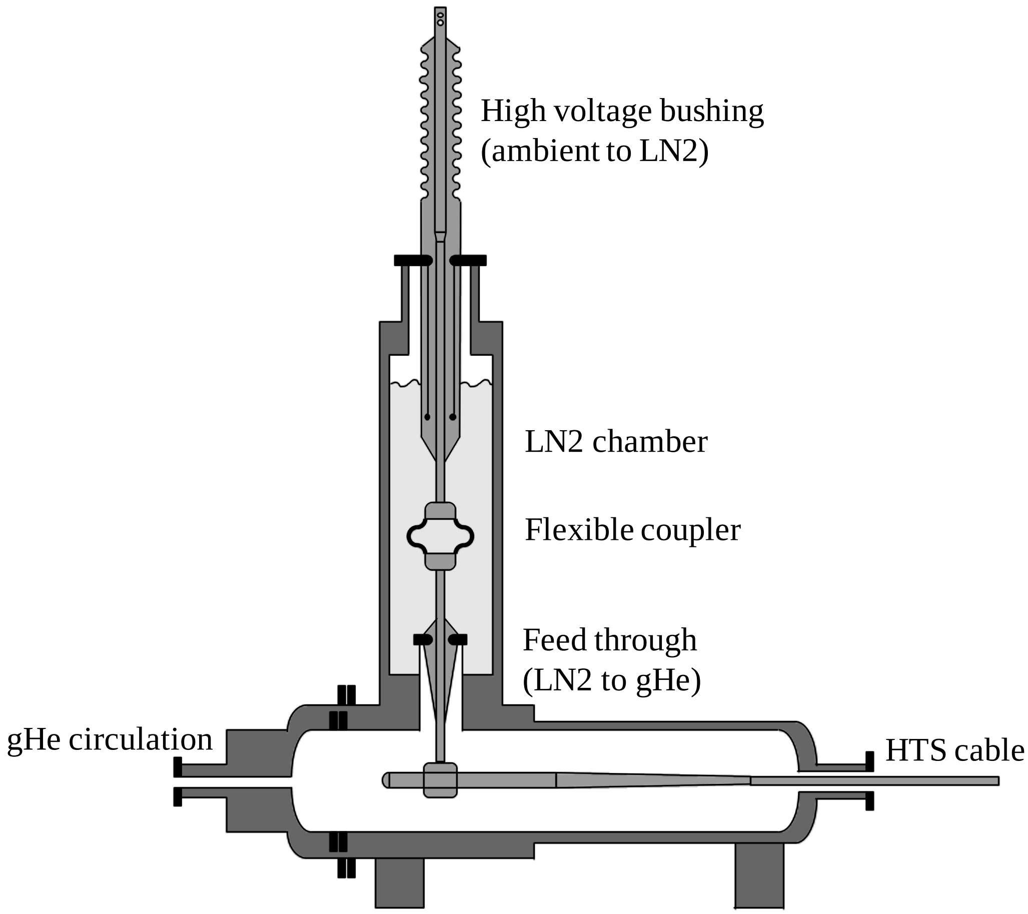

Figure 9 Hybrid HTS cable termination combining LN2 cooling of the power leads with GHe cooling of the HTS cable [100].

7. Cryogenic Helium Circulation Systems

Cryogenic refrigerator is a critical and integral part of any superconducting cable system. Generally, a maintenance free and high efficiency cryogenic refrigerator is the hallmark of a successful and practical superconducting cable system. For liquid nitrogen cooled HTS cables, two general design options exist for providing the required cryogenic environment. The first option is an open loop system where liquid nitrogen is supplied to the cable from a large reservoir tank and evaporated liquid nitrogen is periodically replenished. The supply from the tank is pumped on, pressurized, and circulated through the cable system. Some HTS cable demonstration systems preferred open loop systems because of its simplicity, low maintenance, and to take advantage of higher efficiency of large-scale centralized refrigerators [102-103]. The second option is to use a closed loop system in which a cryo-refrigerator removes the heat from the cryogen between the outlet and inlet to maintain the operating temperature. Some HTS cables preferred closed loop cryogenic systems to avoid the need for trucking liquid nitrogen to the site and the associated uncertainty of supply interruptions [104-106].

For gaseous helium cooled HTS cables, the only viable cooling option is a closed loop circulation of cryogenic helium gas. There are a few methods available to produce cryogenic helium gas. Depending on the operating temperature, a single stage or two stage cryogenic refrigerators can be used [107-108]. Standard liquid helium refrigerators can also be modified to obtain cold helium gas [109-110]. Circulation of helium gas through the cable can be accomplished using cryogenic circulator fans or by using a compressor, either the same compressor of the working gas of the cryocooler or a separate compressor unit [25, 27, 111-112]. The cryogenic helium gas loop could be either the primary loop of the working gas of the cryogenic refrigerator or a secondary loop which is a separate fluid loop, but thermally connected to the primary loop through a heat exchanger that transfers heat from the secondary loop to the primary working gas loop. Some of the options available to produce cryogenic helium gas and to circulate it through a HTS cable system are described below.

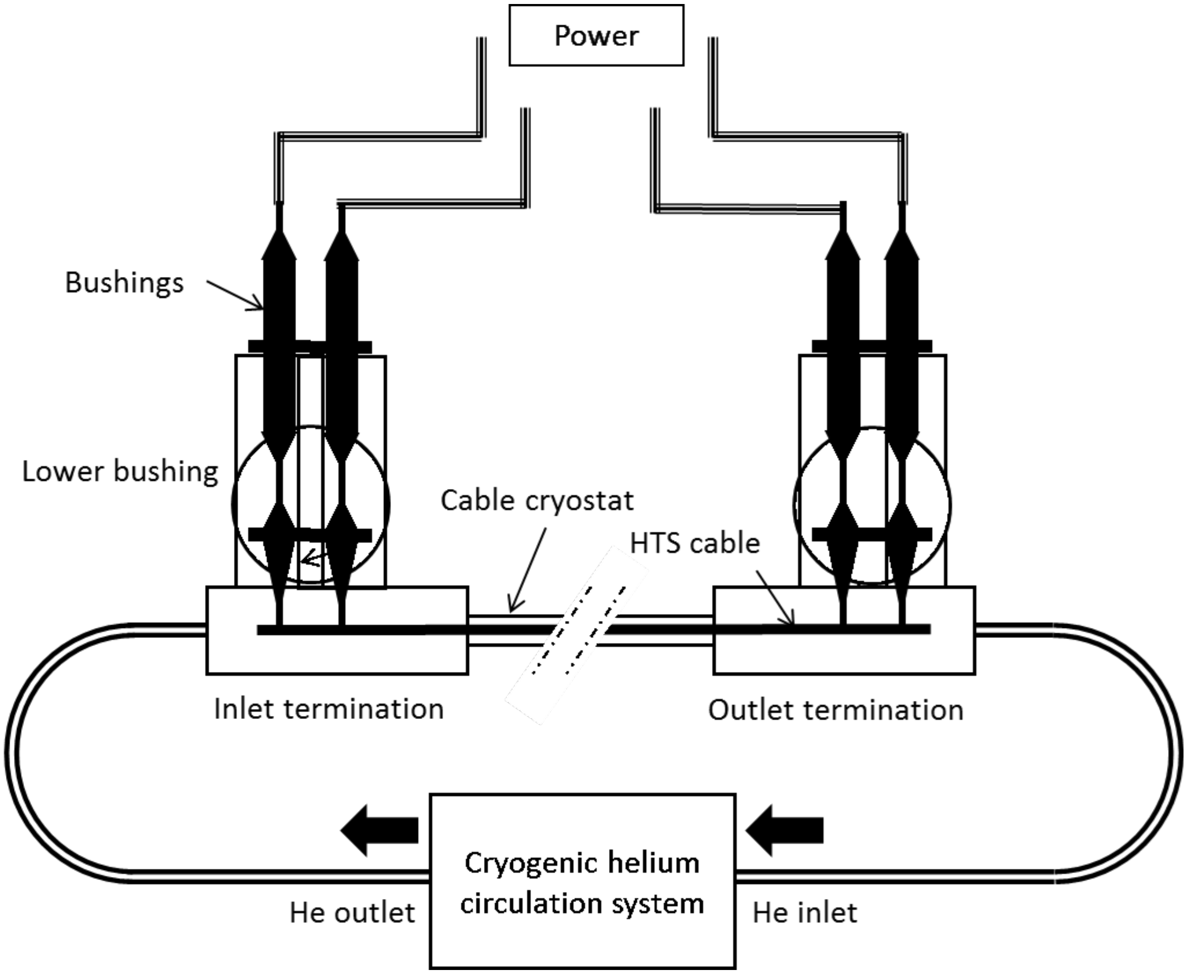

Figure 10 A schematic of a GHe cooled HTS DC cable system with the cryogenic gas circulation system, terminations, cable cryostat and the HTS cable.

Figure 10 shows a schematic of a HTS cable system cooled by gaseous helium circulation. The main components of a helium circulation system are identified in the figure 10. Shown in Figure 10, a cryocooler cold head is represented as the source of cryogenic cooling power, but many kinds of cryocoolers or helium refrigerators can serve this purpose. Typically, large capacity (> 300 W at 77 K) single stage Gifford McMahon (GM) type cryocoolers are used because the operating temperatures of HTS cables are in the range of 50-75 K [107]. Two stage cryocoolers have been used for cables involving MgB2 superconductor at operating temperature of 20 K [108]. Single stage GM cryocoolers are available with large capacities of up to 600 W at 77 K, but are generally inefficient. Recent comprehensive reviews of many available types of cryocoolers and their operating principles are a good source of information for anyone considering a cryocooler based helium circulation system [113-114]. Figure 11 shows the helium circulation system used at the Center for Advanced Power Systems to demonstrate a HTS DC power cable system. The helium circulation system was supplied by DH Industries and uses a single stage Stirling unit (SPC-1, 650 W at 60 K) with a helium circulator manufactured by Cryozone (Bohmwind CryoFan). Large capacity helium liquefiers are also useful as sources of cooling power, particularly if the operating temperatures required are at 20 K or higher. Reverse Turbo-Brayton type cryogenic systems with large capacities and high efficiencies are available from Air Liquide for HTS cable applications [110]. Standard helium refrigerators up to 1 kW of cooling power at 20 K are available from Linde (models LR1420/LR1620) [109].

Figure 11 A picture of a cryogenic helium circulation system (Stirling Cryogenics GPC-1 with integrated CryoFan) similar to the one used at the Center for Advanced Power Systems in a recent demonstration of HTS DC power cable.

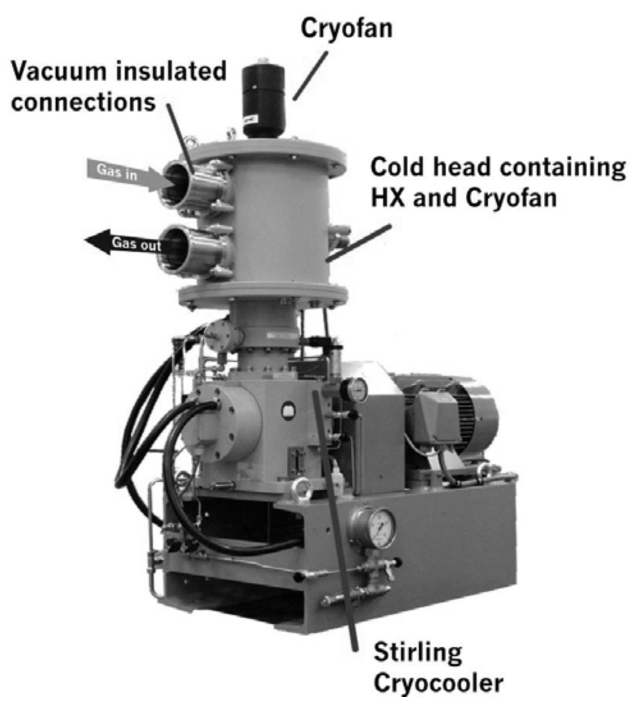

The second major component in cryogenic helium circulation systems is the gas circulator. Unlike some applications such as small superconducting magnet systems, HTS cables cannot use the primary helium loop of a refrigerator’s working helium gas and the cooling medium for the application. The primary reason for this difference is that there is a risk of contamination of the working fluid that would deteriorate the refrigerators efficiency or could damage it. Hence typical gaseous helium circulation systems use a secondary forced flow cooling loop that is thermally anchored to the cold source through a heat exchanger. The secondary helium loop requires a cryogenic circulator(s) to push the gas through the HTS cable system. The circulators come in a range of capacities [111] and are simply high speed centrifugal pumps. The cryogenic circulators are specially designed for required capacity and operating temperature range to minimize the static heat load. Unlike with liquid cryogens, obtaining large mass flow rates in a helium gas circulation system is difficult because of its low density. Operating pressures up to 20 bar are used to increase the density needed to obtain the required GHe mass flow rates. Typical GHe flow rates obtained are in the range of 10-50 g/s, depending on the operating pressure and temperature. Several firms offer cryogenic gas circulators with a range of capacities. The specifications of a cryo circulator that need to be considered for a given application are volume flow rate and the corresponding pressure drop that can be handled. The performance characteristics of a circulator are usually represented in a plot of volume flow rate (m^3/hr) versus pressure head (m). As with other cryogenic equipment, the larger the fan capacity the higher is the static heat load. Cryozone, Linde, Air Liquide, Barber Nicholes, and R&D Dynamics are some examples of commercial sources of helium circulators. Figure 12 shows pictures of cryogenic circulators commercially available from Cryozone. The selection of a circulator should consider several design factors such as required mass flow rates, operating temperature, static heat load limits, etc. A review of basic principles and design process of cryogenic gas circulators has been published recently [111].

Figure 12 Pictures of commercial helium circulators available from Cryozone.

Another critical component of a cryogenic helium circulation system is the heat exchanger that makes a thermal link between the source of cooling power such as the cold head of cryocooler and the secondary helium loop that collects the heat from the application and transfers to the cold head. The efficiency of the heat exchanger is important to be able to obtain the secondary loop temperature as close to the cold head temperature as possible. For large mass flow rates, it is not easy to design the heat exchanger that has the required heat transfer capability while keeping the pressure drop across the heat exchanges within the capability of the helium circulator being used. The heat exchangers are usually made of copper either as helically wrapped finned tubing or plate-fin heat exchangers [115-117]. There have been new developments in light weight metal and carbon foam heat exchangers with large surface area [115-119]. The objective the developments are to enhance heat transfer efficiency without increasing the pressure drop generated. Low pressure drop is particularly important for cryogenic helium circulation systems due to the limited pressure head available with helium circulators.

To achieve large cryogenic helium gas flow rates, multiple circulators were used in parallel configuration with the individual gas streams joining at the inlet and outlet. Test results of a large helium circulation system with four circulators, each serving a path with a cryocooler and associated heat exchanger, have been recently described [25]. Figure 13 shows a schematic of the GHe circulation system with four circulators in a parallel configuration.

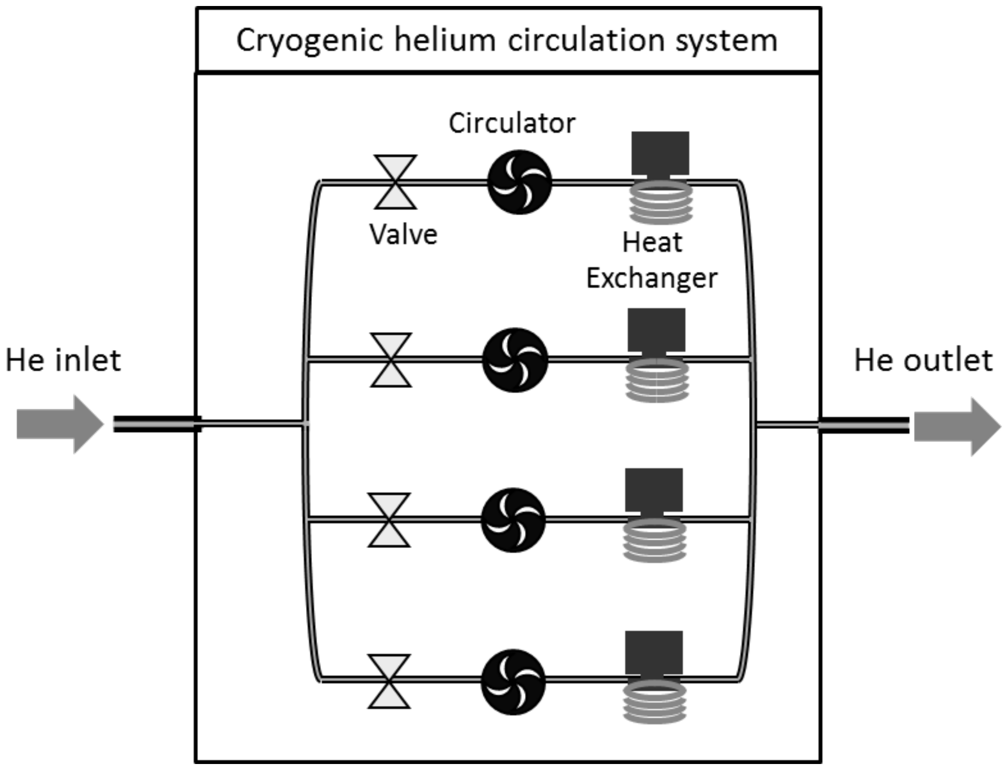

Figure 13 A schematic of the GHe circulation system with four circulators in parallel configuration that was used at FSU-CAPS.

Multiple circulators in series configuration have been used to counter the pressure drop across the application [120]. Figure 14 shows a schematic of a cryogenic helium circulation system with circulator fans both in series and in parallel configurations. These types of helium circulation systems were used to cool a 30 m long HTS DC cable system carrying up to 3 kA current. The temperature gradient across the cable system was as low as 3 K for a mass flow rate of about 10 g/s at 50 K inlet temperature [25, 98].

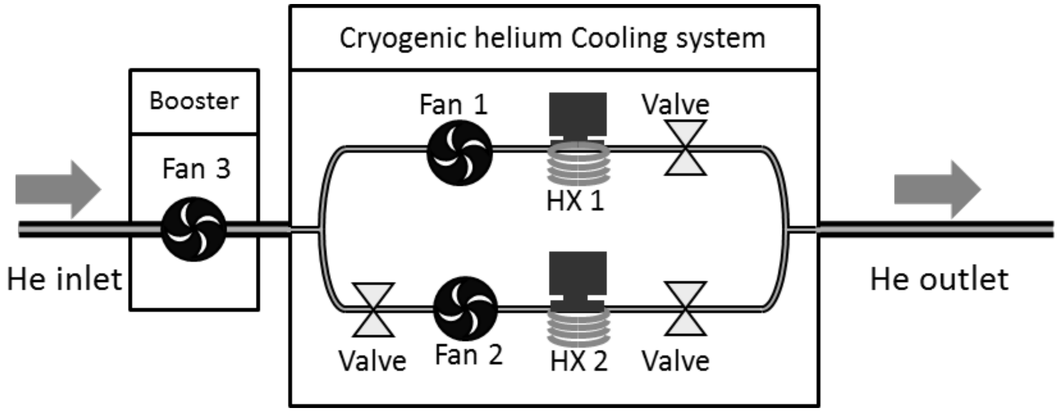

Figure 14 A schematic of a helium circulation system with multiple circulators in series and parallel configuration.

The total useful cooling power of a cryogenic helium the circulation system depends upon the mass flow rate ($\dot{m}$) and the temperature gradient (ΔT) between the inlet and outlet of the circulation system, and is given by:

$$Q = \dot{m} C_p \Delta T \quad (1)$$

where $\dot{m}$ is the mass flow rate and C_p is heat capacity (approximately 5 J/g-K between 20 and 80 K), and temperature gradient ΔT. As an example, a circulation system with a mass flow rate of 10 g/s and 5 K temperature gradient can provide useful cooling power of approximately 250 W. A typical 100 m long HTS cable requires about 250 W of cooling power if designed well. Heat load from commercial cable cryostats is approximately 1 W/m. heat leak from cable terminations usually add 25-30 W each [98]. The heat load from a HTS cable depends on its design and whether it is an AC or DC cable. HTS DC cables essentially no heat load except when there is significant AC ripple. AC cables will have AC losses in the cable and dielectric losses in the insulation if the cable uses cold-dielectric design.

8. Ongoing GHe cooled HTS Cable Projects

There are a few ongoing research and development activities on GHe cooled HTS power cables [120-124]. Florida State University Advanced Power Systems (FSU-CAPS) has been working on GHe cooled HTS DC cable project. FSU-CAPS has developed GHe circulation systems and conducted detailed cryogenic thermal studies on emulated cables using typical cryostats used for HTS cables [25]. In parallel to cryogenic thermal studies, FSU-CAPS studies many design variations of HTS DC cables cooled with GHe to understand the thermal and dielectric aspects of GHe cooled cables. Many experimental tools were established for characterizing short design cables and 30-m long prototype cables. At present United States Navy is the primary supporter of the work at FSU-CAPS on GHe cooled HTS cables and other power devices. US Navy is funding many small businesses to develop various components of GHe cooled HTS devices including cryogenic equipment and HTS cables and insulation materials. The funding from US Navy has contributed to a significant progress in understanding the challenges involved in GHe cooled HTS power cables and the development of innovative solutions that address the challenges. Recently, FSU-CAPS has successfully demonstrated a 30 m DC cable made with 2G HTS by operating at 3 kA at 60 K in GHe [121-122]. The dielectric design of the GHe cooled HTS cable has been validated up to 3.5 kV through high voltage DC soak tests that preceded and followed by partial discharge tests [87]. Ultera, a joint venture of Southwire Company and NKT Cables, fabricated the 30 m cable for FSU-CAPS project. Figure 15 shows a photograph of the GHe cable demonstration set us at FSU-CAPS. The picture shows the helium circulation system, the two cable terminations and part of the cable cryostat that houses the HTS cable.

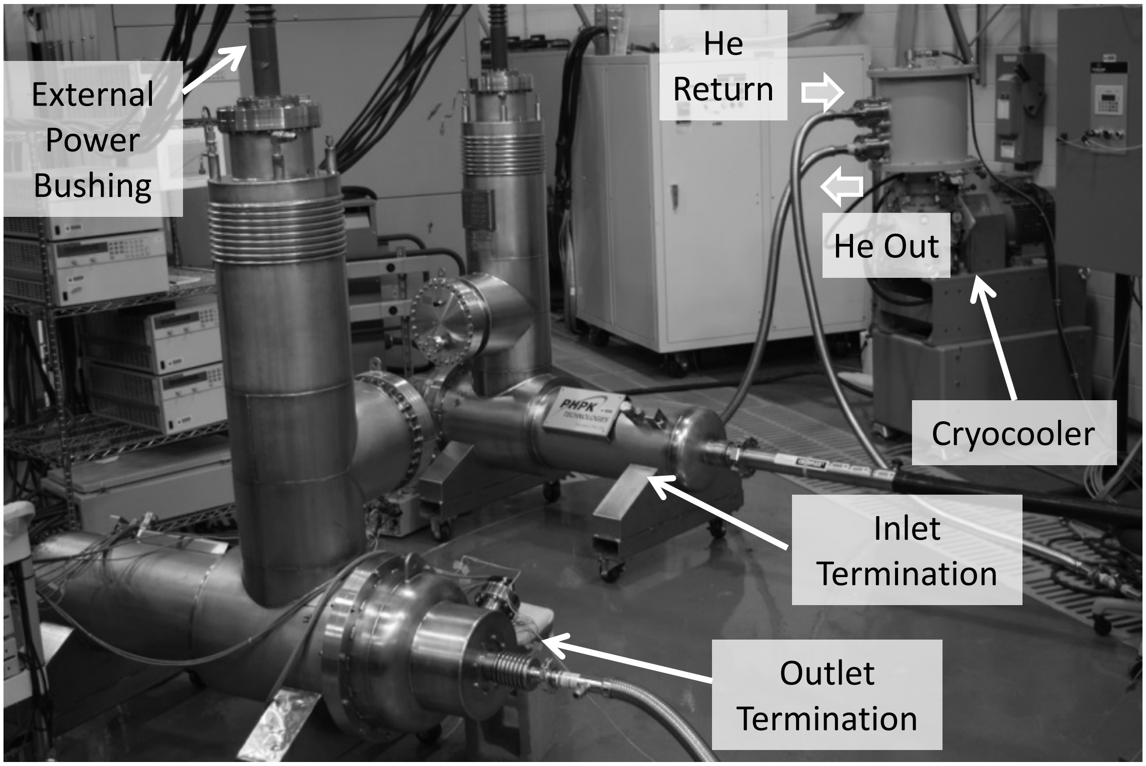

Figure 15 A picture of the GHe cooled HTS cable test facility at the FSU-CAPS.

Figure 16 shows the measured temperature rise across the prototype cable system demonstrated at FSU-CAPS at three different GHe mass flow rates. The cable system consists of the inlet and outlet terminations (described in section 6), and the 30 m long superconducting cable in a Nexans Cryoflex cryostat. As seen in the figure, the temperature rise was just 3 K for a current of 3 kA at GHe mass flow rate of 8.6 g/s. Figure 17 shows a plot of the voltage across the 30 m superconducting cable as a function of time while the cable is carrying 3 kA.. The data in plots 16 and 17 show that GHe is a viable cooling option for HTS cable systems and the behavior of the cables depends on the operating temperature, not the cryogenic media used for obtaining the operating conditions.

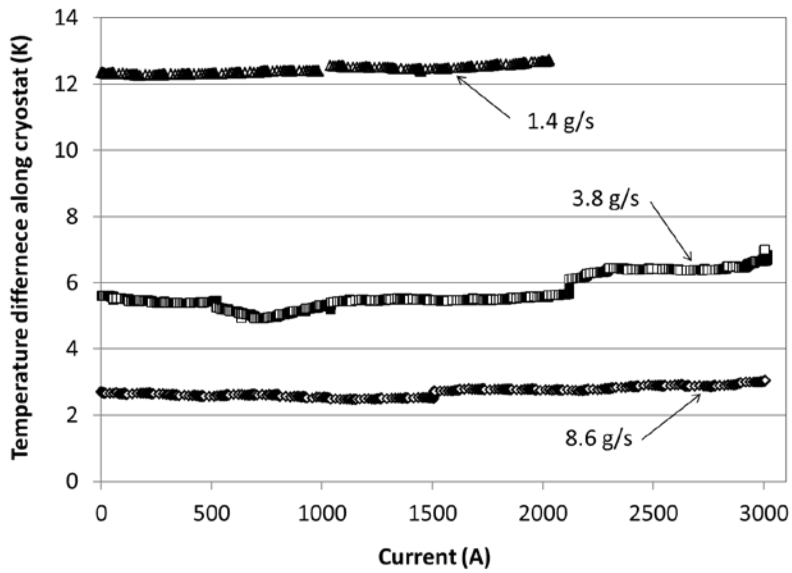

Figure 16 Temperature rise across the 30 m long HTS cable system at 3 kA current for three different GHe mass flow rates.

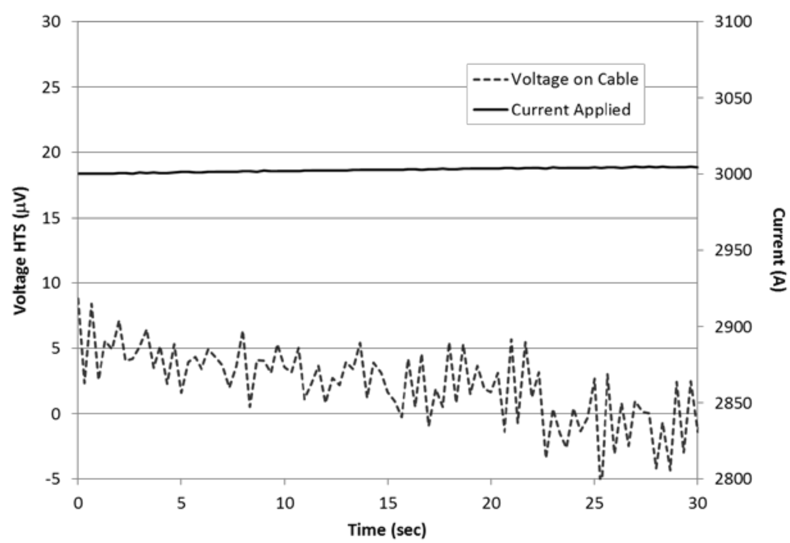

Figure 17 Current versus the electric field across the 30 m HTS cable during the GHe cooled demonstration at FSU-CAPS.

The Massachusetts Institute of Technology, in collaboration with Tsinghua University (China) and University of Cambridge (UK) has been working on the design of a GHe cooled HTS DC cable made of MgB2 superconducting wire for microgrid applications [27, 122]. The design incorporated a two stage current leads GN2 cooled copper leads and GHe cooled HTS.

Preliminary designs were rated for 1 kV and 1 kA cable with the ultimate goal of a 5 kA cable to be installed and tested at Tsinghua University in Beijing. The design and thermal models for the cable's cryogenic system has been published [27]. The HTS cable is designed to be cooled with forced flow GHe at 20-25 K. Both poles of the DC HTS cable are in separate tubular cryostats contained in one common vacuum envelope. Besides the GHE cooled MgB2 cable, MIT is also developing a high current 2G HTS cables for superconducting power transmission for directed energy and data center applications [123].

The European Organization for Nuclear Research (CERN) under the framework of High Luminosity LHC project, has been working on designs and prototype HTS cables for high current applications [28, 29, 74]. Recently, CERN demonstrated a 20 m long HTS cable made of MgB_2 superconductor for power transportation [124]. The MgB_2 cable was operated at 24 K under forced flow helium environment and carried at world record 20 kA. The project supported the development of round MgB2 wires at Columbus Superconductors. The ultimate goal of the project is to use similar MgB2 cables for connecting power converters that supply current to superconducting magnets in the tunnel of future LHC. It is necessary to move the power converters from the tunnel to the surface or other radiation free underground areas away from the magnets.

9. Summary

In recent years there has been a significant progress in GHe cooled HTS cable technology. High current GHe cooled HTS cables have been successfully demonstrated by multiple institutions. Many challenges of GHe HTS cables have been addressed through innovative solutions that resulted from systematic research and development studies in many research centers. The results of the studies suggest that GHe cooled cables are attractive for some high current cable applications. However, designers of GHe cooled HTS power cable systems have to keep in mind the limitations of GHe, when compared to the LN2 counter parts. Detailed studies on cryogenic thermal aspects of quench initiation, propagation and their implications on GHe systems need to be studied through detail modeling and experimentation. Such studies are in progress at many research institutes.

10. References

[1] P. A. Klaudy and J. Gerhold, *Advances in Cryogeninc Eng.,* vol. 11, p. 684, 1967.

[2] R. L. Garwin and J. Matisoo, "Superconducting Lines for the Transmission of Large Amounts of Electrical Power over Great Distances," *Proceedings of the IEEE,* vol. 55, no. 4, pp. 538-548, 1967.

[3] D. R. Edwards, *Electrical and Electronics Technician engineer,* vol. 1, 1968.

[4] R. W. Meyerhoff, "Superconducting power transmission," *Cryogenics,* vol. 11, no. 2, pp. 91-101, 1971.

[5] E. B. Forsyth, J. P. Blewett, R. B. Britton, M. Garber, D. H. Gurinsky, J. M. Hendrie, J. E. Jensen, G. H. Morgan and J. R. Powell, "Flexible Superconducting Power Cables," *IEEE Transactions on Power Apparatus and Systems,* Vols. PAS-92, no. 2, pp. 494-505, 1973.

[6] E. B. Forsyth, "Underground power transmission by superconducting cable," Brookhaven National Lab, Upton, NY, 1972.

[7] J. A. Baylis, "Superconducting Cables for a.c. and d.c. Power Transmission," *Philosophical Transactions of the Royal Society of London. Series A, Mathematical and Physical Sciences ,* vol. 275, no. 1248, pp. 205-224, 1973.

[8] H. L. Laquer, J. W. Dean and P. Chowdhuri, "Electrical, Cryogenic and System Design of a DC Superconducting Power Transmission line," *IEEE Transactions on Magnetics,* Vols. MAG-13, no. 1, pp. 182-187, 1977.

[9] P. Chowdhuri and H. L. Laquer, "Some Electrical Characteristics of a DR Superconducting Cable," *IEEE Transactions on Power Apparatus and Systems,* Vols. PAS-97, no. 2, pp. 399-408, 1978.

[10] P. I. Dolgosheyev, I. B. Peshkov, G. G. Svalov, I. M. Bortnik, V. L. Karapazyuk, L. P. Kubarev, A. A. Panov, Y. V. Petrovsky and V. A. Turket, "Design and first stage test of 50-meter flexible superconducting cable," *IEEE Transactions on Magnetics,* Vols. MAG-15, no. 1, pp. 150-154, 1979.

[11] M. Garber, "A 10 m Nb3Sn Cable for 60 Hz Power Transmission," *IEEE Transactions on Magnetics,* Vols. MAG-15, no. 1, pp. 155-158, 1979.

[12] P. A. Klaudy and J. Gerhold, "Practical Conclusions from Field Trials of a Superconducting Cable," *IEEE Transactions on Magnetics,* Vols. MAG-19, no. 3, pp. 656-661, 1983.

[13] E. B. Forsyth and R. A. Thomas, "Performance Summary of the Brookhaven Superconducting Power Transmission Systems," *Cryogenics,* vol. 26, no. 11, p. 599–614, 1986.

[14] C. S. Weber, R. Lee, S. Ringo, T. Masuda, H. Yumura and J. Moscovic, "Testing and Demonstration Results of the 350 m Long HTS Cable System Installed in Albany, NY," *IEEE Transactions on Applied Superconductivity,* vol. 17, no. 2, pp. 2038-2042, 2007.

[15] J. F. Maguire, J. Yuan, W. Romanosky, F. Schmidt, R. Soika, S. Bratt, F. Durand, C. King, J. McNamara and T. E. Welsh, "Progress and Status of a 2G HTS Power Cable to Be Installed in the Long Island Power Authority (LIPA) Grid," *IEEE Transactions on Applied Superconductivity,* vol. 21, no. 3, pp. 961-966, 2011.

[16] H. Yumura, Y. Ashibe, M. Ohya, H. Itoh, M. Watanabe, T. Masuda, H. Ichikawa, T. Mimura, S. Honjo, T. Hara, R. Ohno, M. Shimoda, N. Nakamura, T. Komagome and H. Yaguchi, "Update of YOKOHAMA HTS Cable Project (invited)," *IEEE Transactions on Applied Superconductivity,* vol. 23, no. 3, p. 5402306, 2013.

[17] L. Xiao, S. Dai, L. Lin, Z. Zhang and J. Zhan, "HTS Power Technology for Future DC Power Grid (Invited)," *IEEE Transactions on Applied Superconductivity,* vol. 23, no. 3, p. 5401506, 2013.

[18] C. Ryu, H. Jang, C. Choi, Y. Kim and H. Kim, "Current Status of Demonstration and Comercialization of HTS Cable System in Grid in Korea," *Proceedings of 2013 IEEE International Conference on Applied Superconductivity and Electromagnetic Devices,* pp. 539-542, October 2013.

[19] S. Dai, L. Xiao, H. Zhang, Y. Teng, X. Liang, N. Song, Z. Cao, Z. Zhu, Z. Gao, T. Ma, D. Zhang, F. Zhang, Z. Zhang, X. Xu and L. Lin, "Testing and Demonstration of a 10-kA HTS DC Power Cable," *IEEE Transactions on Applied Superconductivity,* vol. 24, no. 2, p. 5400104, 2014.

[20] M. Landgraf , "Operation of longest superconducting cable worldwide started," 2014. [Online]. Available: http://phys.org/news/2014-05-longest-superconducting-cable-worldwide.html. [Accessed 3 September 2014].

[21] S. Eckroad, "A Superconducting DC Cable," Electric Power Research Institute, Palo Alto, CA, 2009.

[22] W. V. Hassenzahl, S. E. Eckroad, P. M. Grant, B. Gregory and S. Nilsson, "A High-Power Superconducting DC Cable," *IEEE Transactions on Applied Superconductivity,* vol. 19, no. 3, pp. 1756-1761, 2009.

[23] S. Eckroad, "Novel Approaches and Alternative Cryogens for Cooling a Superconducting Cable: A Comparison of Liquid Air with Other Fluids," Electric Power Research Institute, Palo Alto, CA, 2012.

[24] V. V. Kostyuk, I. V. Antyukhov, E. V. Blagov, V. S. Vysotsky, B. I. Katorgin, A. A. Nosov, S. S. Fetisov and V. P. Firsov, "Experimental Hybrid Power Transmission Line with Liquid Hydrogen and MgB2-Based Superconducting Cable," *Technical Physics Letters,* vol. 38, no. 3, p. 279–282, 2012.

[25] S. V. Pamidi, C. H. Kim, J.-h. Kim, D. Crook and S. Dale, "Cryogenic Helium Gas Circulation System for Advanced Characterization of Superconducting Cables and Other Devices," *Cryogenics,* vol. 52, no. 4-6, p. 315, 2012.

[26] H. Rodrigo, F. Salmhofer, D. S. Kwag, S. V. Pamidi, L. Graber, D. Crook, S. L. Ranner, S. J. Dale and D. Knoll, "Electrical and thermal characterization of a novel high pressure gas cooled DC power cable," *Cryogenics,* vol. 52, p. 310, 2012.

[27] M. J. Cheadle, M. Woźniak, L. Bromberg, B. A. Glowacki, X. Jiang, R. Zeng, J. V. Minervini and J. G. Brisson, "DC Superconducting Cable Using MgB2 Wires," *IEEE Transactions on Applied Superconductivity,* vol. 23, no. 3, p. 6200805, 2013.

[28] A. Ballarino, "Design of an MgB2 feeder system to connect groups of superconducting magnets to remote power converters," *Journal of Physics: Conference Series,* vol. 234, p. 032003, 2010.

[29] A. Ballarino, "Development of Superconducting Links for the Large Hadron Collider Machine," *Superconductor Science and Technology,* vol. 27, no. 4, p. 044024, 2014.

[30] C. Starr, "National Energy Planning for the Century: The Continental SuperGrid," *Nuclear News,* pp. 31-35, February 2002.

[31] P. M. Grant, C. Starr and T. J. Overbye, "A Power Grid for the Hydrogen Economy," *Scientific American,* pp. 76-83, 295 2006.

[32] L. Trevisani, M. Fabbri and F. Negrini, "Long-term scenarios for energy and environment: Energy from the desert with very large solar plants using liquid hydrogen and superconducting technologies," *Fuel Processing Technology,* vol. 87, no. 2, pp. 157-161, 2006.

[33] P. M. Grant, "The SuperCable: Dual Delivery of Chemical and Electric Power," *IEEE Transactions on Applied Superconductivity,* vol. 15, no. 2, pp. 1810-1813, 2005.

[34] SuperPower, "SuperPower 2G HTS Wire Specifications," 2014. [Online]. Available: http://www.superpower-inc.com/system/files/SP_2G+Wire+Spec+Sheet_2014_web_v1.pdf. [Accessed September 2014].

[35] P. J. Ferrara, M. A. Uva and J. Nowlin, "Naval Ship-to-Shore High Temperature Superconducting Power," *IEEE Transactions on Applied Superconductivity,* vol. 21, no. 3, pp. 984-987, 2011.

[36] K. Allweins and E. Marzahn, "Feasibility of HTS DC Cables on Board a Ship," 2011. [Online]. Available: http://mydocs.epri.com/docs/publicmeetingmaterials/1110/7TNRSL46577/Meeting_Materials.pdf. [Accessed September 2014].

[37] B. K. Fitzpatrick, J. T. Kephart and E. M. Golda, "Characterization of Gaseous Helium Flow Cryogen in a Flexible Cryostat for Naval Applications of HighTemperature Superconductors," *IEEE TRANSACTIONS ON APPLIED SUPERCONDUCTIVITY,* vol. 17, no. 2, pp. 1752-1755, 2007.

[38] J. T. Kephart, B. K. Fitzpatrick, P. Ferrara, M. Pyryt, J. Penkos and E. M. Golda, "High Temperature Superconducting Degaussing From Feasibility Study to Fleet Adoption," *IEEE Transactions on Applied Superconductivity,* vol. 21, no. 32, pp. 2229-2232, 2011.

[39] H. Rodrigo, L. Graber, D. S. Kwag, D. G. Crook and B. Trociewitz, "Comparative study of high voltage bushing designs suitable for apparatus containing cryogenic helium gas," *Cryogenics ,* vol. 57, pp. 12-17, 2013.

[40] P. J. Masson, G. V. Brown, D. S. Soban and C. A. Luongo, "All Electric aircraft (update)," *Superconductor Science and Technology,* vol. 20, pp. 748-756, 2007.

[41] T. J. Haugan, J. D. Long, L. A. Hampton and P. N. Barnes, "Design of compact, lightweight power transmission devices for specialized high power applications," *SAE International Jounal of Aerospace,* vol. 1, p. 1088, 2008.

[42] M. Tomita, Y. Fukumoto, K. Suzuki and M. Miryala, "Development of prototype DC superconducting cable for railway system," *Physica C,* vol. 470, pp. s1007-s1008, 2010.

[43] H. Ohsaki, Z. Lv, M. Sekino and M. Tomita, "Application of superconducting power cables to DC electric railway systems," *Physics Procedia ,* vol. 36, p. 908 – 913, 2012.

[44] H. Ohsaki, N. Matsushita, T. Koseki and A. Tomita, "Characteristic Analysis of DC Electric Railway Systems with Superconducting Power Cables Connecting Power Substations," *Journal of Physics: Conference Series,* vol. 507, no. 11th European Conference on Applied Superconductivity, p. 032035, 2014.

[45] Pacific Gas and Electric Company, High performance data centers : a design guidelines sourcebook., Pacific gas and Electric Company, 2006.

[46] M. Ton, B. Fortenbery and W. Tschudi, "DC Power for Improved Data Center Efficiency," Lawrence Berkeley National Laboratory, Berkeley, CA, 2008.

[47] AMSC, "Superconductor LVDC Data Center Power Cables," 2012. [Online]. Available: http://www.amsc.com/documents/superconductor-lvdc-data-center-power-cables. [Accessed September 2014].

[48] J. G. Bednorz and K. A. Muller, "Possible highTc superconductivity in the Ba−La−Cu−O system," *Z. Physik B - Condensed Matter,* vol. 64, no. 2, pp. 189-193, 1986.

[49] H. Rogalla and P. H. Kes, 100 Years of Superconductivity, Boca Raton: CRC Press, 2012.

[50] S. S. Kalsi, Applications of High Temperature Superconductors to Electric Power equipment, 1st ed., Hoboken, New Jersey: Wiley-IEEE Press, 2011.

[51] D. C. Larbalestier, "The road to conductors of high temperature superconductors: 10 years do make a difference!," *IEEE Transactions on Applied Superconductivity,* vol. 7, no. 2, pp. 90-97, 1997.

[52] D. Larbalestier, A. Gurevich, D. M. Feldmann and A. Polyanskii, "High-Tc superconducting materials for electric power applications," *Nature,* vol. 414, pp. 368-377, 15 November 2001.

[53] R. M. Scanlan, A. P. Malozemoff and D. C. Larbalestier, "Superconducting materials for large scale applications (Invited)," *Proceedings of the IEEE,* vol. 92, no. 10, pp. 1639-1654, 2004.

[54] J. Jiang, W. L. Starch, M. Hannion, F. Kametani, U. P. Trociewitz, E. E. Hellstrom and D. C. larbalestier, "Doubled critical current density in Bi-2212 round wires by reduction of the residual bubble density," *Superconductor Science and Technology,* vol. 24, p. 082001, 2011.

[55] D. C. Larbalestier, J. Jiang, U. P. Trociewitz, F. Kametani, C. Scheuerlein, M. Dalban-Canassy, M. Matras, P. Chen, N. C. Craig, P. J. Lee and E. E. Hellstrom, "Isotropic Round-Wire Multifilament Cuprate Superconductor for Generation of Magnetic Fields above 30 T," *Nature Material,* vol. 13, no. 4, pp. 375-381, 2014.

[56] E. B. Callaway, G. Naderi, Q. van Le and J. Schwartz, "Statistical analysis of the relationship between electrical transport and filament microstructure in multifilamentary Bi2Sr2CaCu2Ox/Ag/Ag?Mg round wires," *Superconductor Science and Technology,* vol. 27, p. 044020, 2014.

[57] L. Masur, D. Parker, M. Tanner, E. Podtburg, D. Buczek, J. Scudiere, P. Caracino, S. Spreafico, P. Corsaro and M. Nassi, "Long length manufacturing of high performance BSCCO-2223 tape for the Detroit Edison Power Cable Project," *IEEE Transactions on Applied Superconductivity,* vol. 11, no. 1, pp. 3256-3260, 2001.

[58] L. J. Masur, J. Kellers, L. Feng, S. Fleshler and E. R. Podtburg, "Industrial high temperature superconductors: perspectives and milestones," *IEEE Transactions on Applied Superconductivity,* vol. 12, no. 1, pp. 1145-1150, 2002.

[59] H. P. Yi, Z. Han, J. S. Zhang, T. Liu, L. Liu, M. Y. Li, J. Fang, Q. Liu and Y. K. Zheng, "Research status of the manufacturing technology and application properties of Bi-2223/Ag tapes at Innost," *Physica C: Superconductivity,* Vols. 412-414, no. 2, pp. 1073-1078, 2004.

[60] Y. Yamada, M. Mogi and K. Sato, "Examples and Future Prospects of High-Temperature Superconductor Products," *SEI Technical Review,* vol. 65, pp. 51-59, 2007.

[61] Y. Yuan, J. Jiang, X. Y. Cai, D. C. Larbalestier, E. E. Hellstrom, Y. Huang and R. Parrella, "Significantly enhanced critical current density in Ag-sheathed (Bi,Pb)2Sr2Ca2Cu3Ox composite conductors prepared by overpressure processing in final heat treatment," *Applied Physics Letters ,* vol. 84, no. 12, pp. 2127-2129, 2004.

[62] T. Kato, S. Kobayashi, K. Yamazaki, K. Ohkura, M. Ueyama, N. Ayai, J. Fujikami, E. Ueno, M. Kikuchi, K. Hayashi and K. Sato, "Development of high performance Ag sheathed Bi2223 wire," *Physica C: Superconductivity,* Vols. 412-414, no. 2, p. 1066–1072, 2004.

[63] G. Osabe, N. Ayai, M. Kikuchi, K. Tatamidani, T. Nakashima, J. Fujikami, T. Kagiyama, K. Yamazaki, S. Yamade, E. Shizuya, S. Kobayashi, K. Hayashi, K. Sato, J. Shimoyama, H. Kitaguchi and H. Kumakura, "Recent progress of high performance Ag-sheathed Bi2223 wire," *Physica C: Superconductivity,* vol. 470, no. 20, pp. 1365-1368, 2010.

[64] N. Ayai, K. Hayashi and K. Yasuda, "Development of Bi-2223 superconducting wires for AC applications," *IEEE Transactions on Applied Superconductivity,* vol. 15, no. 2, pp. 2510-2513, 2005.

[65] V. Selvamanickam, Y. Chen, X. Xiong, Y. Xie, J. Reeves, X. Zhang, Y. Qiao, K. Lenseth, R. Schimidt, A. Rar, D. Hazelton and K. Tekletsadik, "Recent Progress in Second-Generation HTS Conductor Scale-Up at SuperPower," *IEEE Transactions on Applied Superconductivity,* vol. 17, no. 2, pp. 3231-3234, 2007.

[66] M. W. Rupich, X. Li, S. Sathyamurthy, C. L. H. Thieme, K. DeMoranville, J. Gannon and S. Fleshler, "Second Generation Wire Development at AMSC," *IEEE Transactions on Applied Superconductivity,* vol. 23, no. 3, p. 6601205, 2013.

[67] J. Maguire, D. Folts, J. Yuan, D. Lindsay, D. Knoll, S. Bratt, Z. Wolff and S. Kurtz, "Development and Demonstration of a Fault Current Limiting HTS Cable to be Installed in the Con Edison Grid," *IEEE Transactions on Applied Superconductivity,* vol. 19, no. 3, pp. 1740-1743, 2009.

[68] C. M. Rey, R. C. Duckworth, J. A. Demko, A. Ellis, D. R. James, M. J. Gouge and E. Tuncer, "Test Results For A 25 Meter Prototype Fault Current Limiting HTS Cable For Project Hydra," *Advances in Cryogenic Engineering: Transactions of the Cryogenic Engineering Conference,* vol. 55, pp. 453-460, 2010.

[69] Y. Shiohara, T. Taneda and M. Yoshizumi, "Overview of Materials and Power Applications of Coated Conductors Project," *Japanese Journal of Applied Physics,* vol. 51, p. 010007, 2012.

[70] K. R. Marken, "Status of Coated Conductor Activities in the United States. No. LA-UR-11-06650," Los Alamos National Laboratory, Los Alamos, 2011.

[71] D. C. van der Laan, X. F. Lu and L. F. Goodrich, "Compact GdBa2Cu3O7-δ coated conductor cables for electric power transmission and magnet applications," *Superconductor Science and Technology,* vol. 24, p. 042001, 2011.

[72] M. Takayasu, L. Chiesa, L. Bromberg and J. V. Minervini, "HTS twisted stacked-tape cable conductor," *Superconductor Science and Technology,* vol. 25, p. 014011, 2012.

[73] W. Goldacker, F. Grilli, E. Pardo, A. Kario, S. K. Schlachter and M. Michal Vojenčiak, "Roebel cables from REBCO coated conductors: a one-century-old concept for the superconductivity of the future," *Superconductor Science and Technology,* vol. 27, p. 093001, 2014.

[74] A. Ballarino, "Alternative Design Concepts for Multi-Circuit HTS Link Systems," *IEEE Transactions on Applied Superconductivity,* vol. 21, no. 3, pp. 980-983, 2011.

[75] S. Jin, H. Mavoori, C. Bower and R. B. van Dover, "High critical currents in iron-clad superconducting MgB2 wires," *Nature,* vol. 411, pp. 563-565, 31 May 2001.

[76] H. Kumakura, A. Matsumoto, H. Fujii and K. Togano, "High transport critical current density obtained for powder-in-tube-processed MgB2 tapes and wires using stainless steel and Cu-Ni tubes," *Applied Physics Letters,* vol. 79, pp. 2435-2437, 2001.

[77] S. Soltanian, X. L. Wang, J. Horvat, S. X. Dou, M. D. Sumption, M. Bhatia, E. W. Collings, P. Munroe and M. Tomsic, "High transport critical current density and large Hc2 and Hirr in nanoscale SiC doped MgB2 wires sintered at low temperature," *Superconductor Science and Technology,* vol. 18, pp. 658-666, 2005.

[78] M. Tomsic, M. Rindfleisch, J. Yue, K. McFadden, J. Phillips , M. D. Sumption, M. Bhatia, S. Bohnenstiehl and E. W. Collings, "Overview of MgB2 Superconductor Applications," *International Journal of Applied Ceramic Technology,* vol. 4, no. 3, pp. 250-259, 2007.

[79] A. Malagoli, C. Bernini, V. Braccini, C. Fanciulli, G. Romano and M. Vignolo, "Fabrication and superconducting properties of multifilamentary MgB2 conductors for AC purposes: twisted tapes and wires with very thin filaments," *Superconductor Science and Technology,* vol. 22, p. 105017, 2009.

[80] R. Musenich, M. Greco, M. Razeti and G. Tavilla, "Electrical characterization of a multi-strand MgB2 cable," *Superconductor Science and Technology,* vol. 20, no. 3, pp. 235-238, 2007.

[81] M. Stemmle, F. Merschel, M. Noe and A. Hobl, "Ampacity Project - Worldwide First Superconducting Cable And Fault Current Limiter Installation In A German City Center," Stockholm, 2013.

[82] W. -J. Shin, J. -S. Hwang, J. -K. Seong, J. -G. Lee and B. -W. Lee, "Breakdown Characteristics of Liquid Nitrogen for Transmission-Class Superconducting Electric Equipment," Bali, Indonesia, 2012.

[83] I. Sauers, R. James , A. Ellis, E. Tuncer, G. Polizos and M. Pace, "Effect of Bubbles on Liquid Nitrogen Breakdown in Plane-Plane Electrode Geometry From 100-250 kPa," *IEEE Transactions on Applied Superconductivity,* vol. 21, no. 3, pp. 1892 - 1895, 2011.

[84] A. Küchler, Hochspannungstechnik, Heidelberg: Springer, 2005.

[85] H. Rodrigo, D. Kwag, L. Graber, B. Trociewitz and S. Pamidi, "AC Flashover Voltages Along Epoxy Surfaces in Gaseous Helium Compared to Liquid Nitrogen and Transformer Oil," *IEEE Transactions on Applied Superconductivity,* vol. 24, no. 3, p. 7700506, 2014.

[86] L. Graber, H. Rodrigo, F. Salmhofer, D. Knoll and D. G. Crook, "Experimental Determination of Dielectric Properties of Cryoflex in High Pressure Cold Helium Gas," Hannover, Germany, 2011.

[87] L. Graber, C. H. Kim, S. V. Pamidi, H. Rodrigo and D. Knoll, "Dielectric Design Validation of a Helium Gas Cooled Superconducting DC Power Cable," Philadelphia, PA, USA, 2014.

[88] J. A. Demko, J. W. Lue, M. J. Gouge, D. Linsay, M. Roden, D. Willen, M. Daumling, J. E. Fesmire and S. D. Augustynowicz, "Cryostat Vacuum Thermal Considerations for HTS Power Transmission Cable Systems," *IEEE Transactions on Applied Superconductivity,* vol. 13, no. 2, pp. 1930 - 1933, 2003.

[89] N. Kelley, M. Nassi and L. Masur, "Application of HTS Wire and Cables to Power Transmission: State of the Art and Opportunities," Columbus, OH, USA., 2001.

[90] P. M. Grant, W. V. Gregory and S. W. Eckroad, "Design Criteria for Warm Temperature Dielectric Superconducting DC Cable: Impact of Co-Pole magnetic Fields," in *8th european Conference on Applied Superconductivity*, 2007.

[91] M. Kosaki, M. Nagao, Y. Mizuno, N. Shimizu and K. Horii, "Development of extruded polymer insulated superconducting cable," *Crogenics,* vol. 32, no. 10, p. 885–894, 1992.

[92] J. W. Ekin, "Experimental Techniques for Low-Temperature Measurements," Oxford University Press, pp. 234-235, 2006.

[93] S. J. Rigby and B. M. Weedy, "Liquid Nitrogen-Impregnated Tape Insulation for Cryoresistive Cable," *IEEE Transactions on Electrical Insulation,* vol. 10, no. 1, pp. 1 - 9, 1975.

[94] E. Tuncer, Y. L. Zuev, I. Sauers, D. R. James and A. R. Ellis, "Electrical Properties of Semiconducting Tapes Used in HTS Power Cables," *IEEE Transactions on Applied Superconductivity,* vol. 17, no. 2, pp. 1497 - 1500, 2007.

[95] J.-K. Seong, W. Choi, W.-J. Shin, J.-S. Hwang and B.-W. Lee, "Experimental and Analytical Study on DC Breakdown Characteristics of Butt Gap Condition in LN2/PPLP Composite System," *IEEE Transactions on Applied Superconductivity,* vol. 23, no. 3, p. 5401604, 2013.

[96] D. S. Kwag, V. D. Nguyen, S. M. Baek, H. J. Kim, J. W. Cho and S. H. Kim, "A Study on the Composite Dielectric Properties for an HTS Cable," *IEEE Transactions on Applied Superconductivity,* vol. 15, no. 2, pp. 1731 - 1734, 2005.

[97] M. Fenger, "Partial Discharge in Cables: Lowering the Risk of Unforeseen Cable Insulation Failures," San Diego, CA, USA, 2010.

[98] C. H. Kim, S.-K. Kim, L. Graber and S. V. Pamidi, "Cryogenic thermal studies on terminations for helium gas cooled superconducting cables," Enschede, The Netherlands, 2014a.

[99] R. McFee, "Optimum Input Leads for Cryogenic Apparatus," *The Review of Scientific Instruments,* vol. 30, no. 2, pp. 98-102, 1959.

[100] N. Suttel, C. H. Kim, J. Ordonez, D. Shah, L. Graber and S. Pamidi, "Thermal Modeling of Gaseous Helium as a Cryogen for High Temperature Superconducting Cable Components," *IEEE Transactions on Applied Superconductivity,* Submitted.

[101] D. G. Crook, L. Graber and S. V. Pamidi, "Cryogenic heat sink for gas cooled superconducting power devices". US Patent 8809679 B1, 2014.

[102] M. Stemmle, F. Merschel, M. Noe and A. Hobl, "AmpaCity - Advanced superconducting medium voltage system for urban area power supply," Chicago, 2014.

[103] R. C. Lee, A. Dada and S. M. Ringo, "Cryogenic refrigeration system for HTS cables," *IEEE Transactions on Applied Superconductivity,* vol. 15, no. 2, pp. 1798-1801, 2005.

[104] C. S. Weber, C. T. Reis, A. Dada, T. Masuda and J. Moscovic, "Overview of the underground 34.5 kV HTS power cable program in albany, NY," *IEEE Transactions on Applied Superconductivity,* vol. 15, no. 2, pp. 1793-1797, 2005.

[105] J. A. Demko, I. Sauers, D. R. James, M. J. Gouge, D. Lindsay, M. Roden, J. Tolbert, D. Willen, C. Traholt and C. T. Nielsen, "Triaxial HTS Cable for the AEP Bixby Project," *IEEE Transactions on Applied Superconductivity,* vol. 17, no. 2, pp. 2047-2050, 2007.

[106] Cryomech, Inc., "Cryorefrigerators," [Online]. Available: http://www.cryomech.com/products/cryorefrigerators/. [Accessed September 2014].

[107] Stirling Cryogenics, "Stirling Cryogenics," [Online]. Available: http://www.stirlingcryogenics.com/. [Accessed September 2014].

[108] Linde Cryogenics, "Linde Cryogenics," [Online]. Available: http://www.linde-kryotechnik.ch/public/datenblaetter/helium_eng_einzeln.pdf. [Accessed September 2014].

[109] Air Liquide, "Air Liquide," [Online]. Available: http://airliquideadvancedtechnologies.com/file/otherelementcontent/pj/f8/a4/5a/58/turbo-brayton_sd1997969771067587692.pdf. [Accessed September 2014].

[110] H. Vermeuleun, "Cryogenic Circulators: The Solution for Cooling Problems?," *Cold Facts,* vol. 29, pp. 46-48, 2013.

[111] Cryomech, Inc., "Cold Helium Circulation Systems at Cryomech," [Online]. Available: http://www.cryomech.com/products/cold-helium-circulation/. [Accessed September 2014].

[112] R. Radebaugh, "Cryocoolers: the state of the art and recent developments," *Journal of Physics: Condensed Matter,* vol. 21, p. 164219, 2009.

[113] R. Radebaugh, "Refrigeration for Superconductors (Invited)," *Proceedings of the IEEE,* vol. 92, no. 10, p. 1719, 2004.

[114] A. Boman and D. Doty, "Design and manufacture of ultra-low-mass, cryogenic heat exchangers," *Cryogenics,* vol. 41, pp. 797-803, 2002.

[115] R. Barron, Cryogenic Heat Transfer, Taylor & Francis, 1999.

[116] N. C. Gallego and J. W. Klett, "Carbon Foams for Thermal Management," *Carbon,* vol. 41, no. 7, pp. 1461-1466, 2003.

[117] A. G. Straatman, N. C. Gallegob, B. E. Thompsonc and H. Hangan, "Thermal characterization of porous carbon foam-convection in parallel flow," *International Journal of Heat and Mass Transfer,* vol. 49, no. 11-12, pp. 1991-1998, 2006.

[118] G. Venkatarathnam and S. Sarangi, "Matrix Heat Exchangers and Their Application in Cryogenic Systems," *Cryogenics,* vol. 30, no. 11, pp. 907-908, 1990.

[119] J. J. Kuang, T. Kim, M. L. Xu and T. J. Lu, "Ultra-lightweight Compact Heat Sinks with Metal Foams Under Axial Fan Flow Impingement," *Heat Transfer Engineering,* vol. 33, no. 7, pp. 642-650, 2012.

[120] C. H. Kim, J.-G. Kim and S. V. Pamidi, "Cryogenic Thermal Studies on Cryocooler Based Helium Circulation System for Gas Cooled Superconducting Power Devices," Syracuse, NY, 2014b.

[121] Florida State University, 2013. [Online]. Available: http://news.fsu.edu/More-FSU-News/24-7-News-Archive/2013/December/Florida-State-Center-for-Advanced-Power-Systems-researchers-achieve-major-breakthrough. [Accessed September 2014].

[122] EPRI-Pamidi, "Installation and Testing of Helium Gas Cooled Superconducting DC Cable at FSU-CAPS," 2013. [Online]. Available: http://mydocs.epri.com/docs/PublicMeetingMaterials/MRNYPKPLTGV/19-PAMIDI-Helium_Cooled_DC_Cable.pdf. [Accessed September 2014].

[123] EPRI-Minervini, "Development of HTS High Current Cables and Joints for DC Power and High Field Magnet Applications," 2013. [Online]. Available: http://mydocs.epri.com/docs/PublicMeetingMaterials/MRNYPKPLTGV/15-MINERVINI-HTS_Cables_for_DC_Apps.pdf.

[124] A. Del Rosso, "World-record current in a superconductor," 2014. [Online]. Available: http://home.web.cern.ch/about/updates/2014/04/world-record-current-superconductor.

Appendix D

Presented at the Applied Superconductivity Conference 2014, August 10-15, 2014, Charlotte, NC.

Presentation ID: 4LPo1J-06

Effects of Longitudinal Variations in Critical Current and n Value of Individual Tapes on the Performance of Superconducting Cables

Venkata Pothavajhala, Lukas Graber, Chul Han Kim, and Sastry Pamidi

Center for Advanced Power Systems, Florida State University, 2000 Levy Avenue, Tallahassee, FL- 23210

1. Introduction

- Advantages of superconducting cables compared to Cu cables:
  - Higher current density
  - Lower losses
  - Lower size and weight
- Effects of non-uniform current distribution among tapes
  - Reduction in rated capacity
  - Higher AC losses due to uneven temperature and self-field
  - Potential damage when operated close to the design capacity

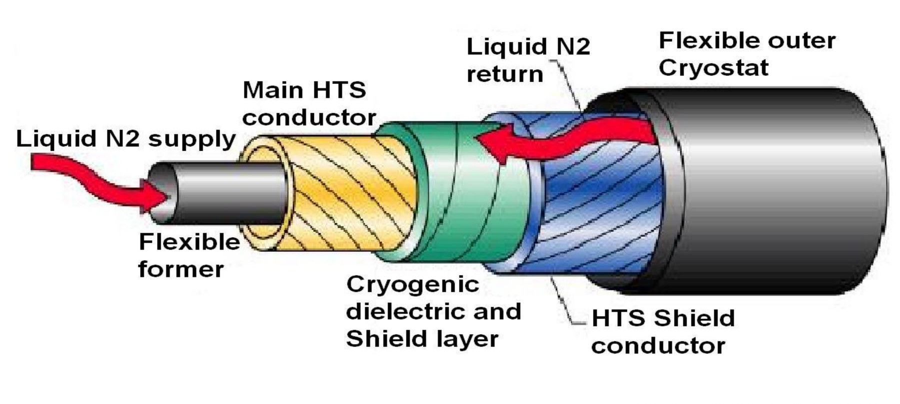

Fig. 1. Superconducting cable showing multiple tapes per layer and and multiple layers

- Longitudinal variations in critical current (I_c) and n-value
  - Commercially available tapes have variations in I_c and n-value along their length
  - Variations in local temperature, magnetic field also cause variations in I_c and n-value
  - Compressive, torsional strain and transverse loading on tapes of cable also cause these variations
  - The overall I_c (end to end)of tape masks the sections with low I_c
  - Lead to reduction in apparent I_c

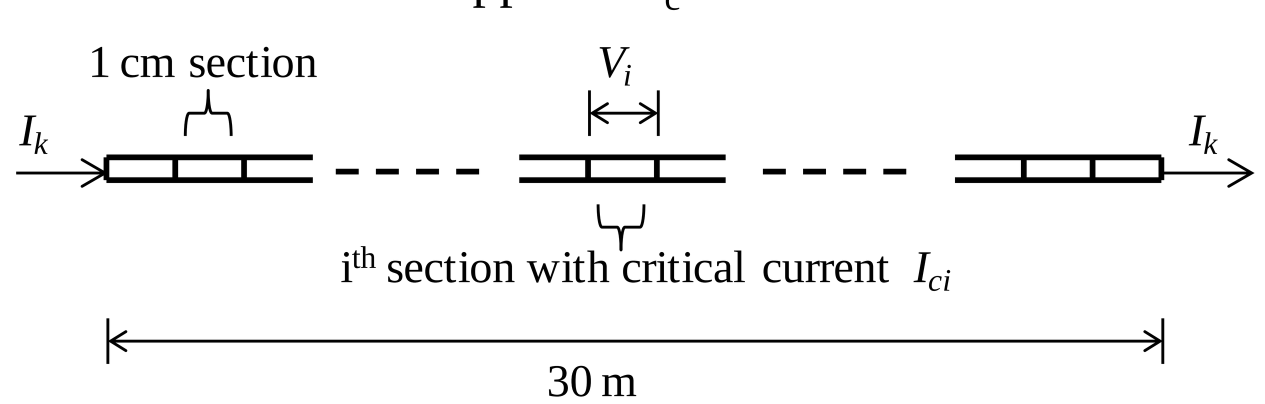

Fig. 2. Model tape in HTS cable divided into several 1 cm sections with varying I_c values, used for simulating the effect of these variations

2. Longitudinal variations in critical current - analysis using Monte Carlo method

- 30 m HTS tape used for the cable fabrication was considered to have different I_cs for each centimeter section of its length.
- To test the effect of sections with low I_cs on the overall performance, the following distribution was considered

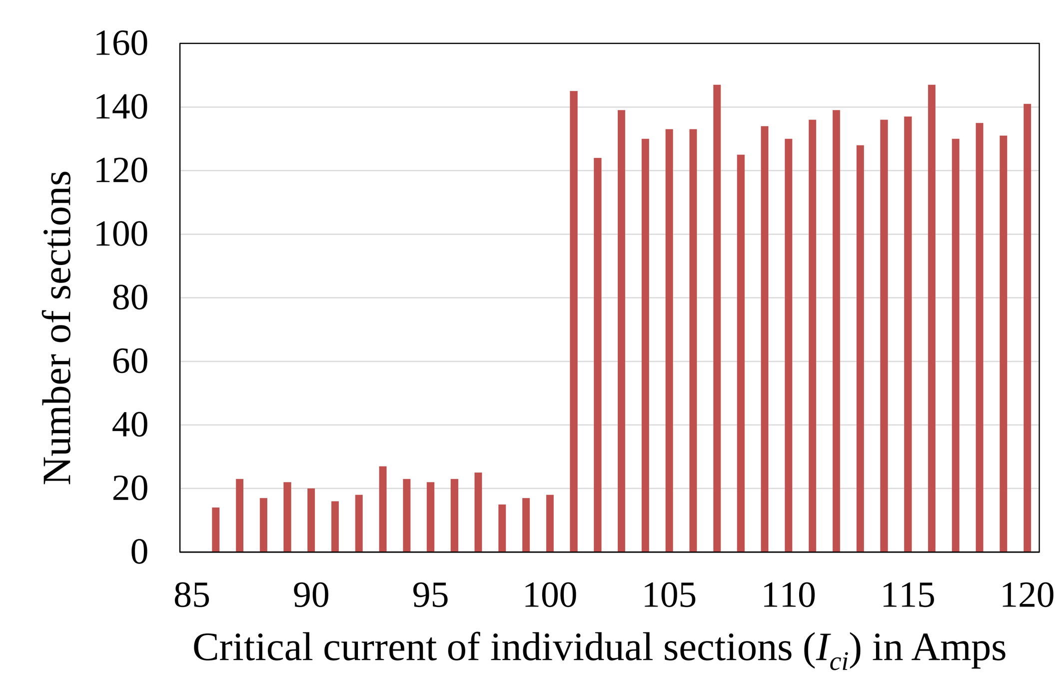

Fig. 3. Mathematically equivalent model of the experimental setup

- 300 sections: Uniform distribution of I_c :[85,100] A
- 2700 sections: Uniform distribution of I_c:[100,120] A
- Voltage generated by each section was calculated for currents from 1 A to 120 A

$$V_i = E_c \left(\frac{I_k}{I_{ci}}\right)^{n_i} \qquad V_t = \sum_{i=1}^{3000} V_i$$

Apparent I_c of the tape = 96 A

- Reduction in apparent I_c for normally distributed random values of I_{ci}s along the length:

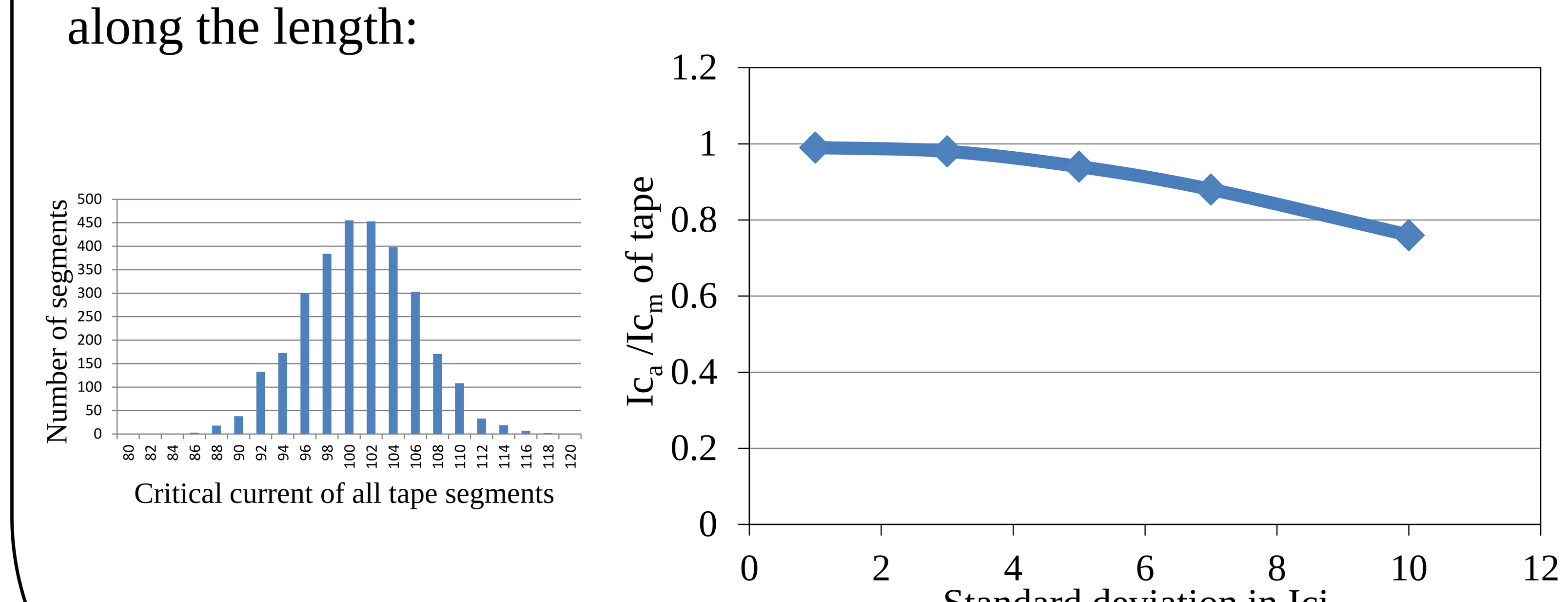

Fig. 4. Reduction in I_{ca} for certain longitudinal variation in I_{ci}

3. Longitudinal variations in n value

- n: μ=30, σ=1,3,5,7

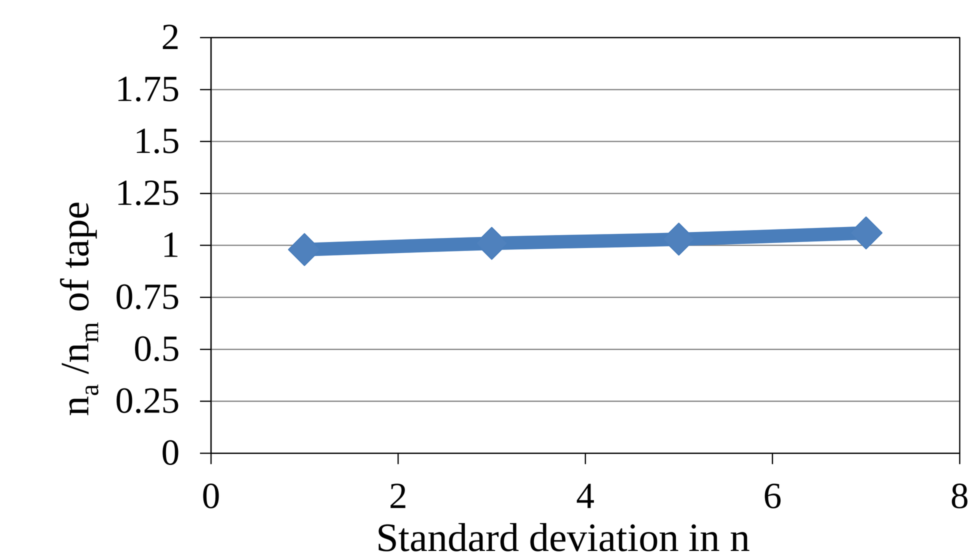

Fig. 5. Apparent n of the cable as function of cable mean n for a certain standard deviation in n_i along the length of individual tapes of the cable.

4. Conclusions

- Effect of longitudinal variations on cable characteristics
- Model cable: 30 m, 3 kA, 30 tapes
- Generated 50 cables from 1500 tapes simulated with μ I_c =100 A, σ =1 A ,3 A, 5 A,7 A and 10 A

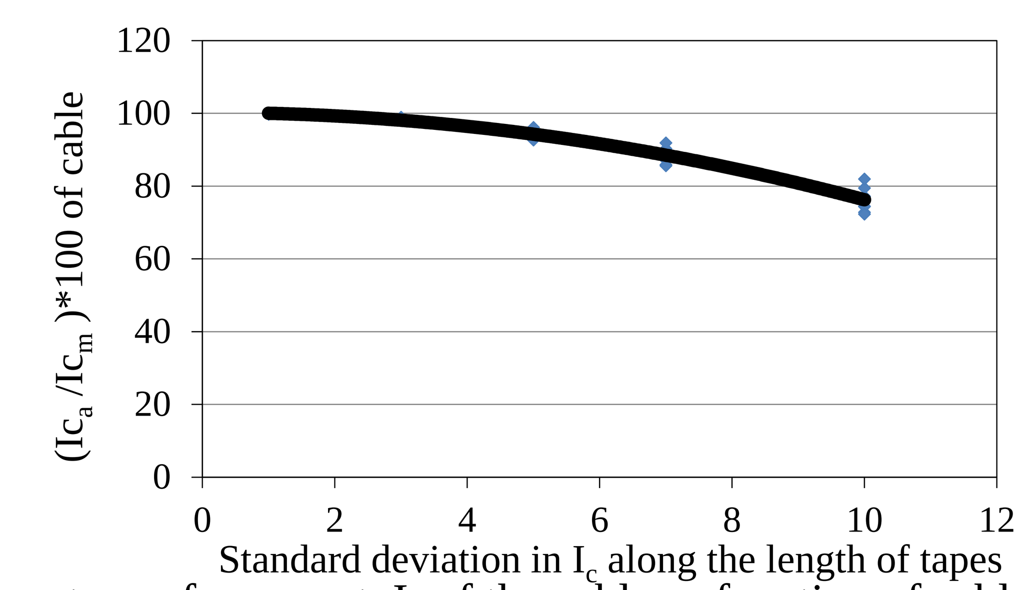

Fig. 6. Percentage of apparent I_c of the cable as function of cable mean I_c for a certain standard deviation in I_{ci} along the length of individual tapes of the cable.

Reduction in cable I_c could be as high as 20% for σ of 10

- Longitudinal variations in I_c of the tapes reduce the design/rated capacity of the cable and have significant effect on its performance.
- This is because the voltage produced by the lower I_c sections would be high enough to push the tape to reach its critical current well before the average I_c of the tape. Hence the longitudinal property distribution in I_c should be considered for best performance of superconducting cable design.

APPENDIX E

Presented at the Applied Superconductivity Conference 2014, August 10-15, 2014, Charlotte, NC.

4LPo1I-03

Thermal Network Model for HTS Cable Systems and Components Cooled by Helium Gas

Darshit Shah, Chul Han Kim, Lukas Graber, Sastry Pamidi, and Juan Ordonez

Center for Advanced Power Systems, Florida State University, Tallahassee, Florida

N00014-14-1-0198

Thermal Network Models

- Thermal network models (TNM) are frequently used to model stationary and transient heat flux and temperature conditions in power apparatus.
- The thermal network approach is based on the similarity between electrical and thermal field.
- Conductive, convective and radiative heat transfer can be modeled by thermal resistances (resistors), heat capacities by capacitors, temperature differences by voltage sources, and heat fluxes by current sources.
- Kirchhoff's Laws and the superposition principle remain valid.
- The method results in computationally efficient simulations that allow for design optimizations over wide parameter spaces
- TNMs can also be coupled with Joule heating and allows to model material parameters as a function of temperature.
- The PLECS toolbox ("Piecewise Linear Electrical Circuit Simulation") in the MATLAB-Simulink environment is suitable for TNMs since it natively supports the thermal-electrical coupling through heat sinks
- PLECS is predominatly designed for power electronics, we extended its utility for modeling of combined cryogenic thermal and electrical problems.

The Need for Coupled Thermal and Electrical Models

- FSU-CAPS has been working on gaseous helium cooled HTS cables
- There is a need for understanding the dynamic response of gaseous helium cooled cables under various scenarios to devise risk mitigation techniques.
- We use FEM methods with COMSOL to assess finer details of thermal maps of HTS devices. These methods are, however, slow.
- Thermal Network Models are easier to modify and allow easier modification and seep wide parameter range.
- Because they are fast, Thermal Network Models are useful in understanding dynamic response of HTS cable systems
- FSU-CAPS has many sets of experimental data on prototype HTS cable systems.
- Comparison of the results from the models with experimental data allows for refinement of the models.

Conclusions

- Thermal field in the cable termination was studied using thermal network models
- The results were compared with those of COMSOL models and experimental observations
- The results match with the measurements within ±5%
- The computational effort needed for thermal network models is significantly less than that for finite element analysis.
- The simulation time is on the range of a few seconds with a regular personal computer.
- The MATLAB/Simulink toolbox PLECS allowed to easily couple thermal and electrical networks.
- The models are useful for design optimizations to reduce the sizes and heat loads in various components of HTS cables.

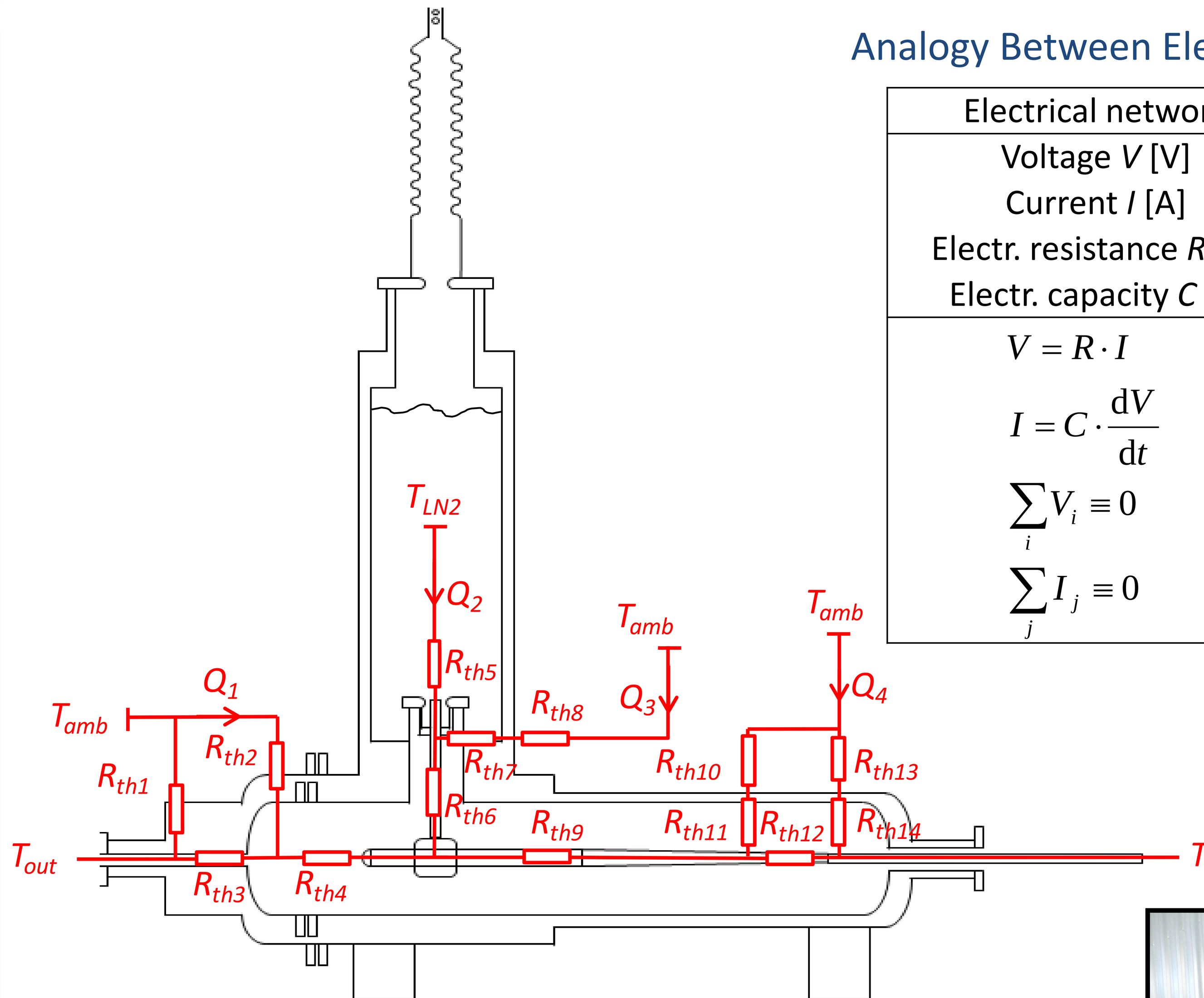

Discretization of geometry, introducing heat sources, temperature potentials, thermal resistances.

Analogy Between Electrical and Thermal Networks

Electrical network	Thermal network
Voltage V [V]	Temp. difference ΔT [K]
Current I [A]	Heat flux Q [W]
Electr. resistance R [Ω]	Therm. resist. R_{th} [K/W]
Electr. capacity C [F]	Therm. capacity C_{th} [J/K]
$V = R \cdot I$	$\Delta T = R_{th} \cdot Q$
$I = C \cdot \frac{dV}{dt}$	$Q = C_{th} \cdot \frac{dT}{dt}$
$\sum_i V_i \equiv 0$	$\sum_i T_i \equiv 0$
$\sum_j I_j \equiv 0$	$\sum_j Q_j \equiv 0$

PLECS (Piecewise Linear Electrical Circuit Simulation) is a Simulink toolbox for system-level simulations of electrical circuits

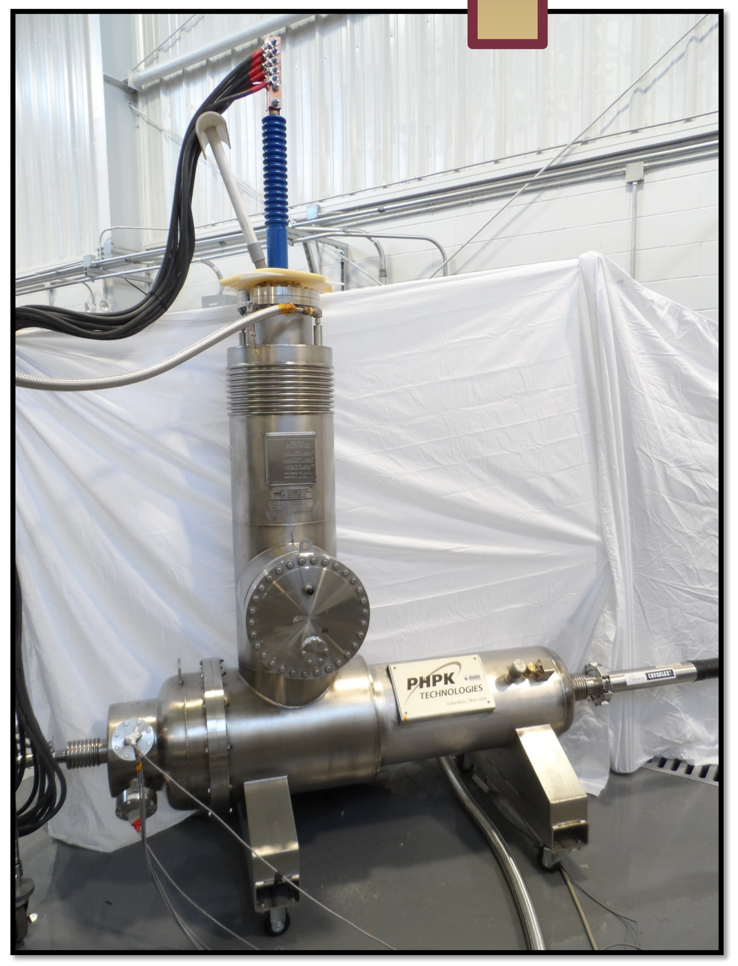

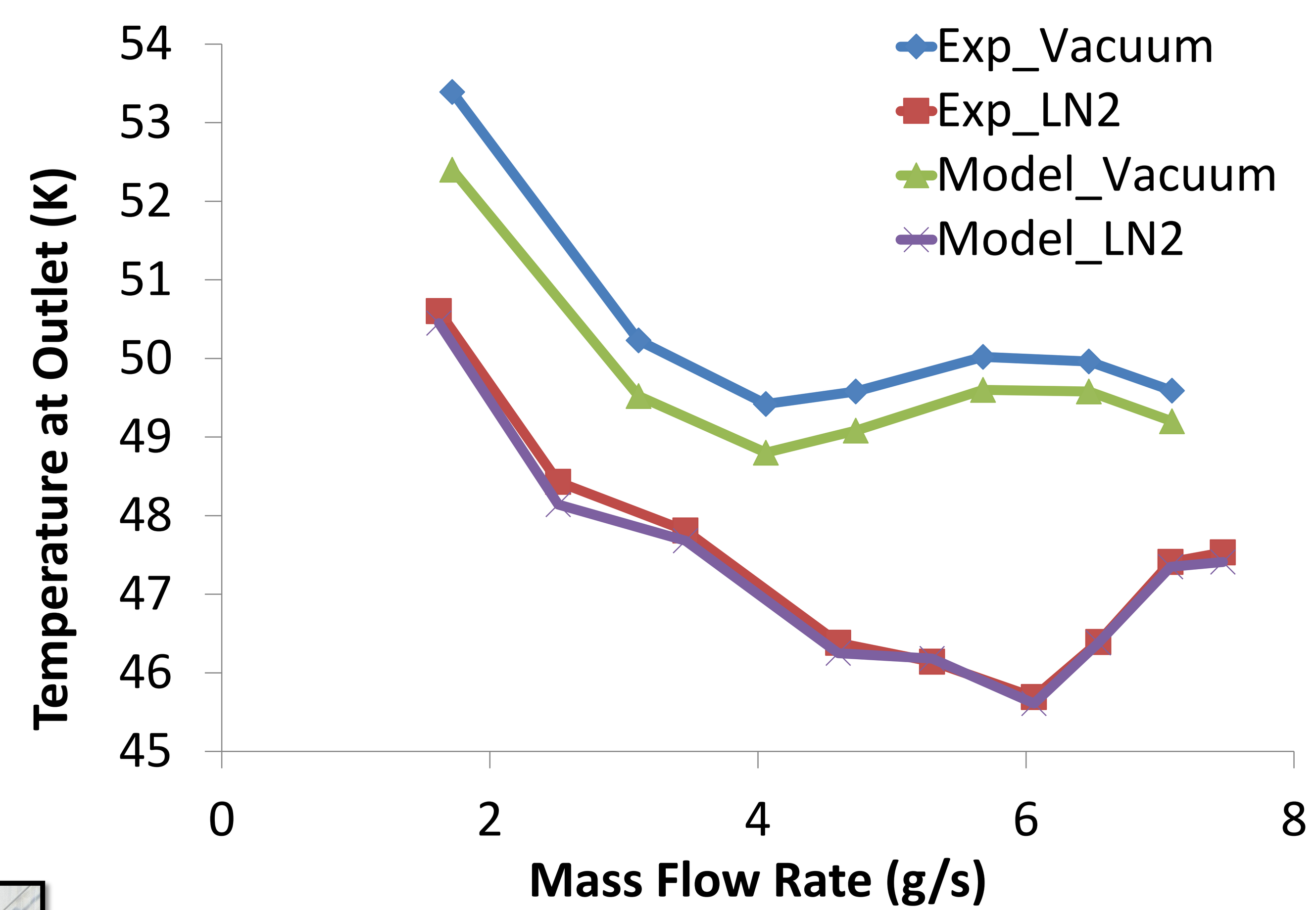

Comparison of model results with experimental data for the HTS cable termination for various gHe flow rates with no current

Equivalent circuit diagram of cable termination using PLECS

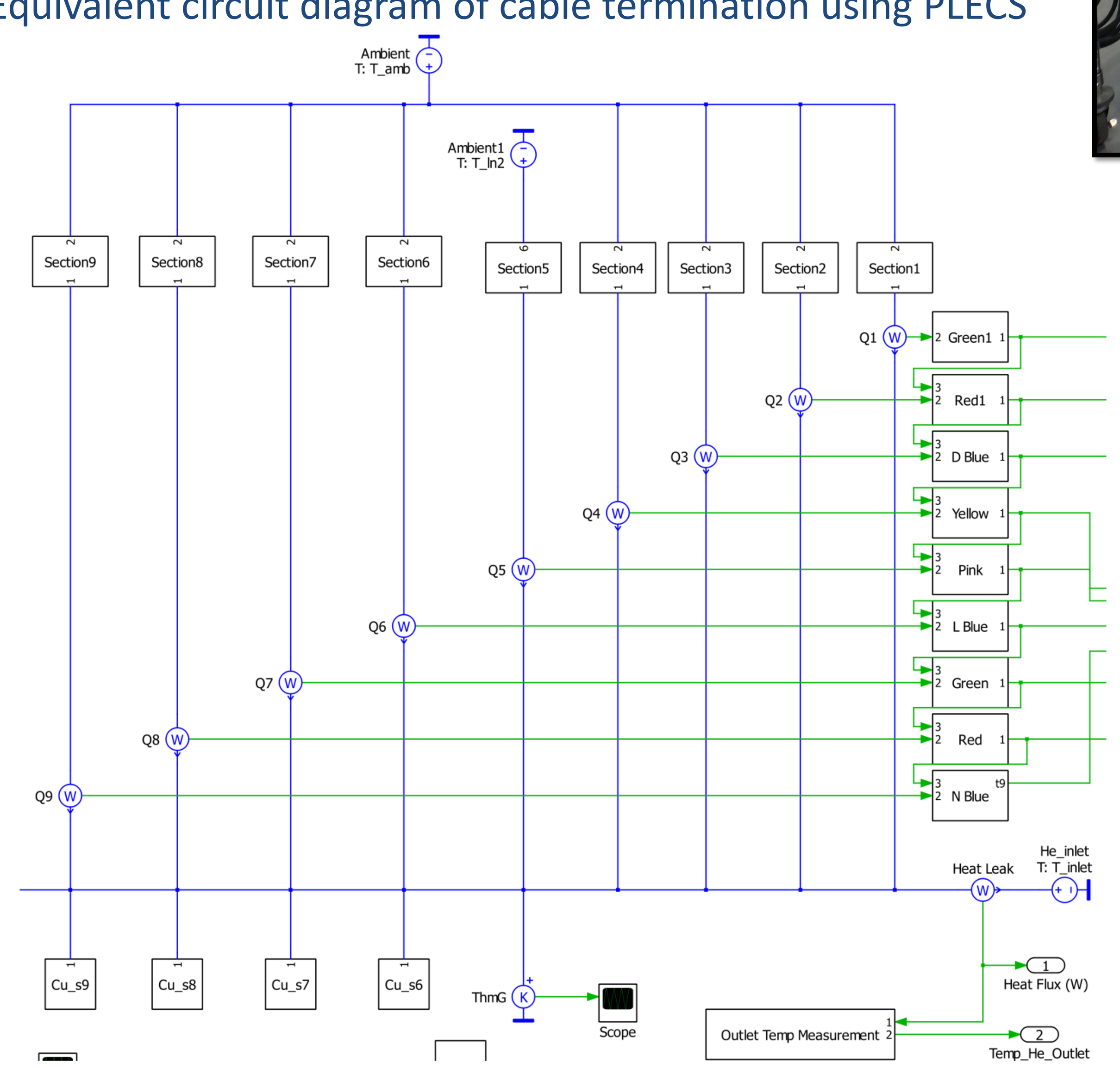

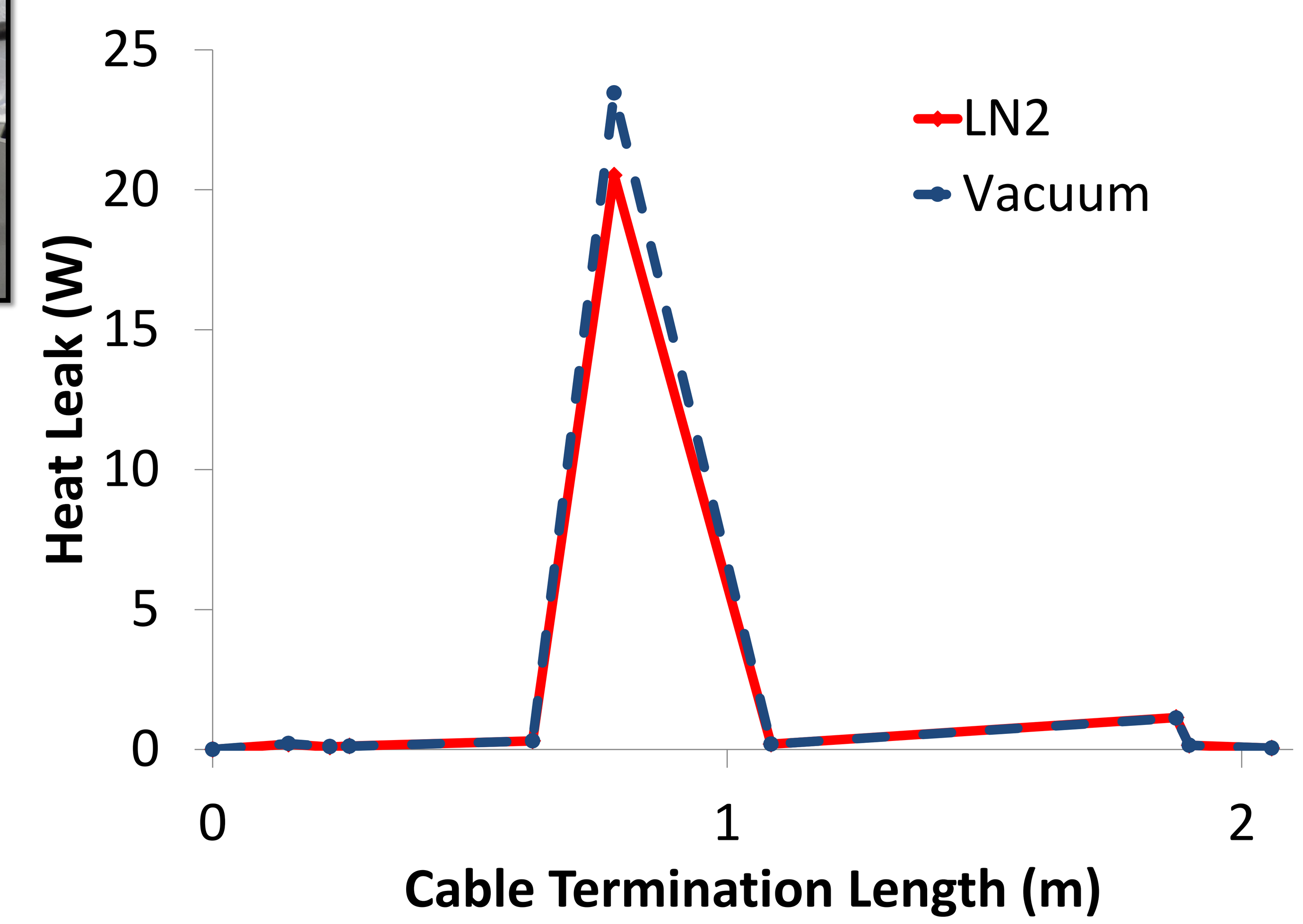

Heat leak predicted by the model along the length of the HTS cable for both the vacuum and LN2 bath cases with no current.

APPENDIX F

Thermal Modeling of Cryogenic Helium Gas-Cooled Superconducting Cable Terminations

N. Suttell, C.H. Kim, D. Shah, L. Graber, J.C. Ordonez, S. Pamidi
Center for Advanced Power Systems, Department of Mechanical Engineering, Florida State University, Tallahassee, FL 32310

Poster ID: 4LPo1I-04: 172

NEEC Naval Engineering · Center for Advanced Power Systems · Florida A&M University - Florida State University College of Engineering · Electric Ship Research and Development Consortium ESRDC · Department of the Navy ONR Science & Technology

Presented at the Applied Superconductivity Conference 2014, August 10-15, 2014, Charlotte, NC.

Abstract

- High temperature superconducting (HTS) power cables are being considered for a variety of electric power grid, naval, and aviation applications.
- The superconducting cable system is comprised of two terminations and a superconducting cable in a long cryostat.
- This study focuses on the modeling of the components for a gaseous helium cooled second generation HTS cable system for the purpose of optimization.
- The termination cryostats are where the room temperature copper lead interfaces with the superconducting cable at cryogenic temperatures.
- Excessive temperature gradients in the termination cryostat reduce operating margins of the cables and increase the risks of damage.

Termination Cryostat Located at The Center for Advanced Power Systems (CAPS) at Florida State University

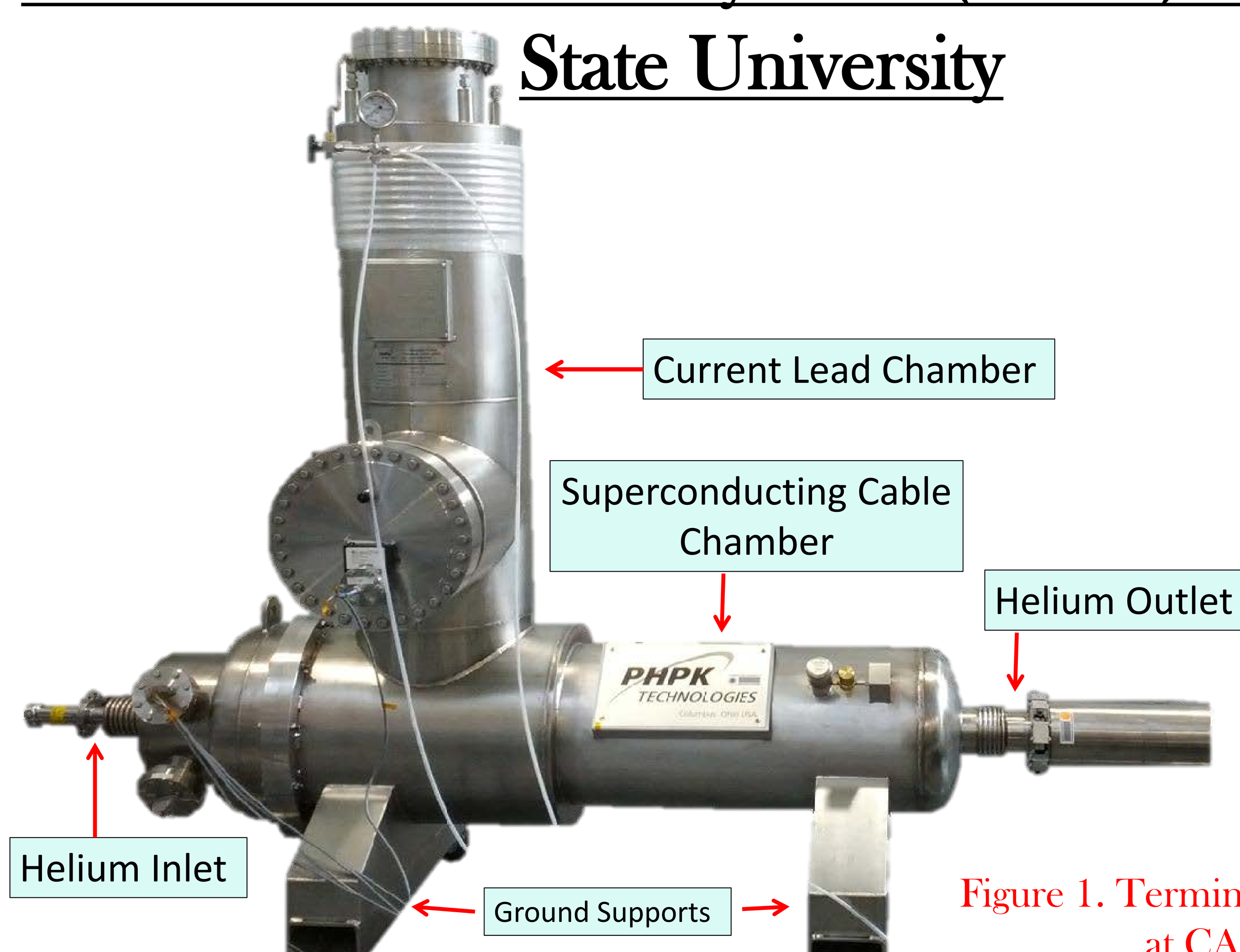

Figure 1. Termination Cryostat at CAPS

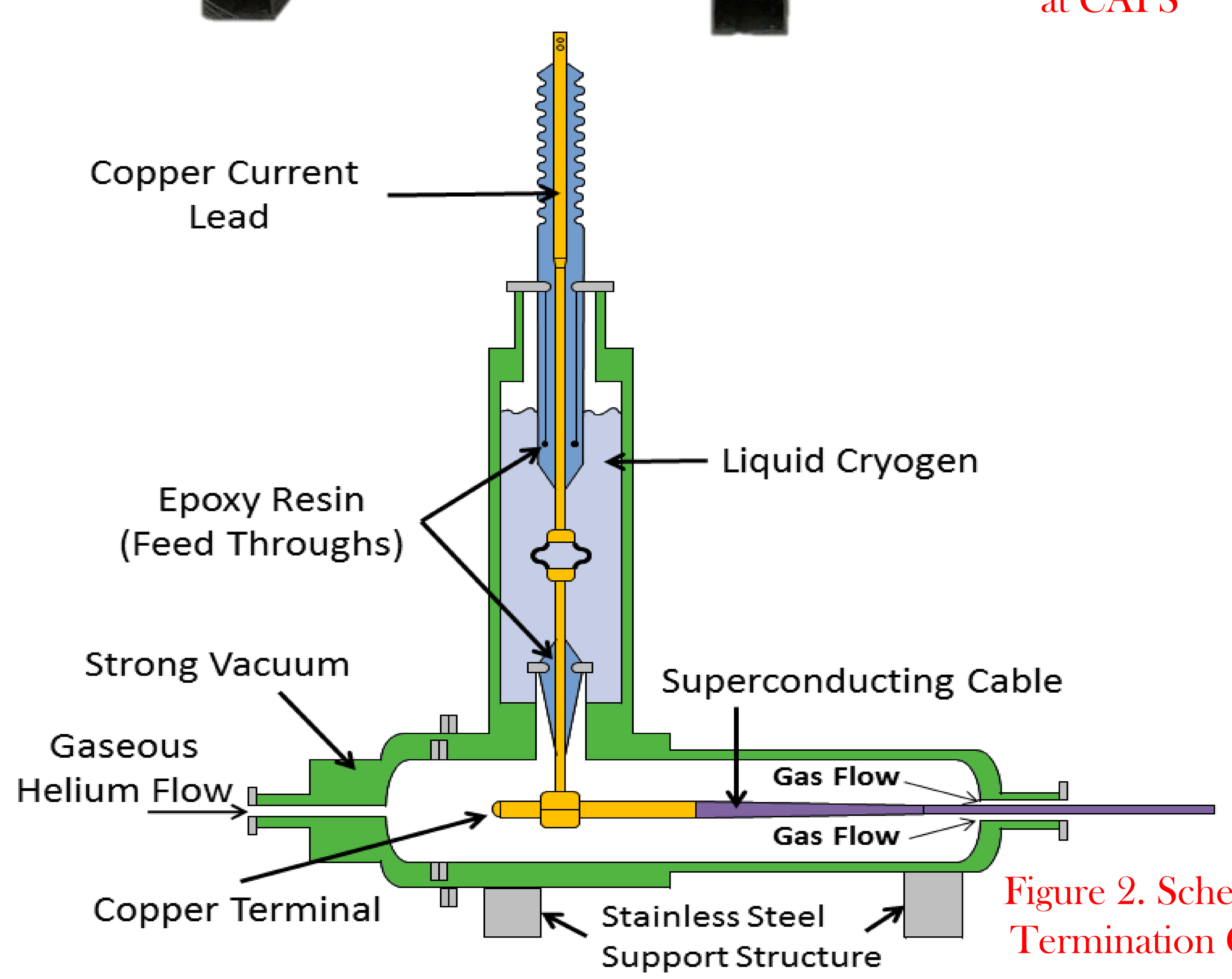

Figure 2. Schematic of Termination Cryostat

Modeling Technique

- COMSOL *Multiphysics* was used to develop a thermal model of the termination.
- A 2D Axis-symmetric geometry was designed that couples the $\kappa - \omega$ Turbulent Flow Module with the Heat Transfer in Solids and Fluids Module.
- Two cases are modeled: when the current lead chamber is under vacuum (Case 1), and when the current lead chamber is filled with LN2 (Case 2).
- The purpose of the model is to match with experimental results, locate maximum heat leak, optimize geometry for shipboard applications, and abandon the need for LN2.

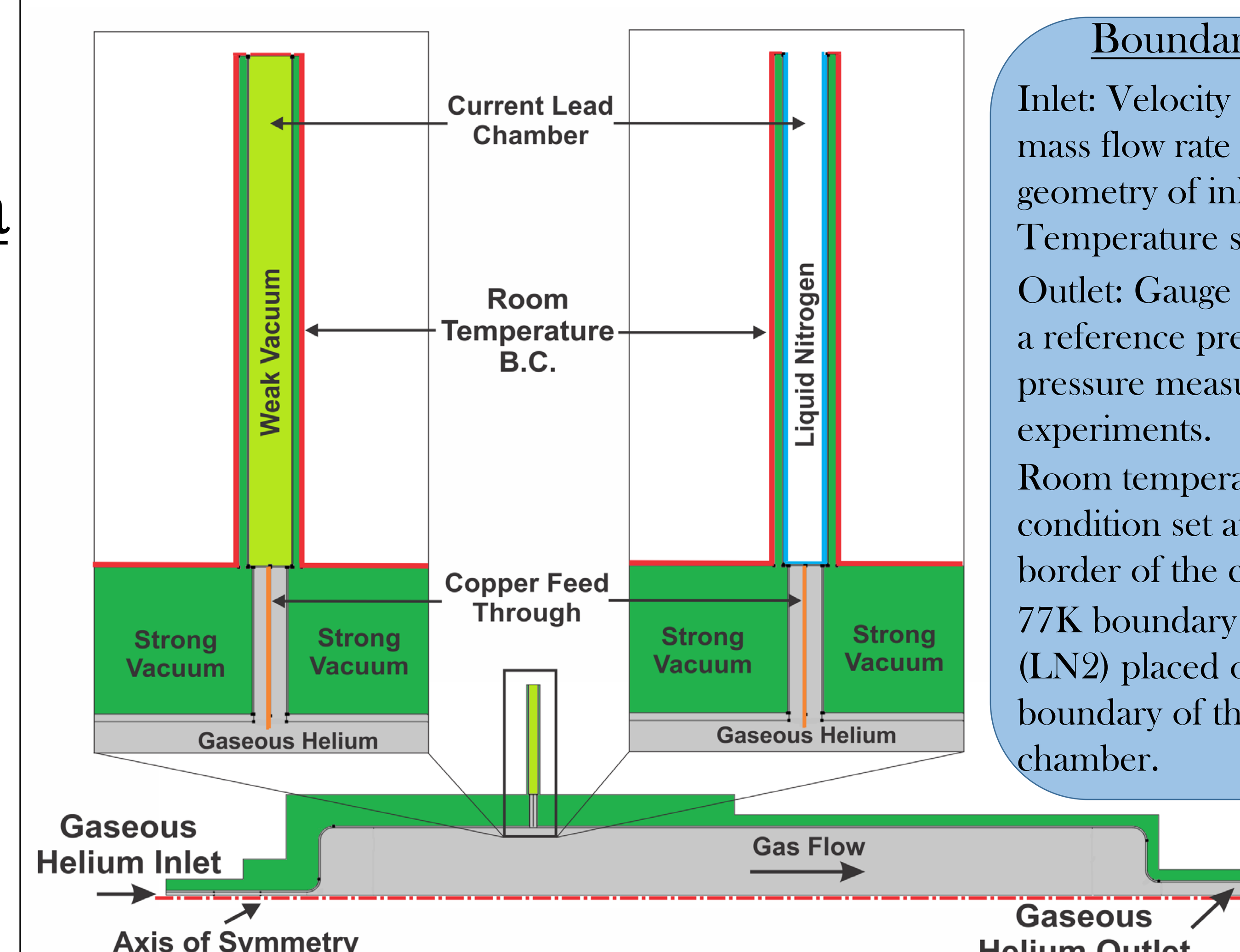

Figure 3. Schematic of 2D axis-symmetric COMSOL model

Boundary Conditions

Inlet: Velocity specification based on mass flow rate (1-7 g/s) and geometry of inlet channel. Temperature specification (43-48K).

Outlet: Gauge pressure set at 0 with a reference pressure of the absolute pressure measured during experiments.

Room temperature boundary condition set at 293.15K around the border of the cryostat.

77K boundary condition for Case 2 (LN2) placed on the inside boundary of the current lead chamber.

Navier-Stokes Equations

Turbulent Conservation of Momentum

$$\rho(\mathbf{u}\cdot\nabla)\mathbf{u} = \nabla\cdot\left[-p\mathbf{I} + (\mu+\mu_T)(\nabla\mathbf{u}+(\nabla\mathbf{u})^T) - \frac{2}{3}(\mu+\mu_T)(\nabla\cdot\mathbf{u})\mathbf{I} - \frac{2}{3}\rho\kappa\mathbf{I}\right] + \mathbf{F}$$

Continuity Equation

$$\nabla\cdot(\rho\mathbf{u}) = 0$$

Energy Equation

$$\rho C_p \mathbf{u}\cdot\nabla T = \nabla\cdot(k\nabla T) + Q + Q_{vh} + W_p$$

The turbulent kinetic energy and dissipation ($\kappa - \omega$) model for turbulent flow calculation in COMSOL was used to close the Reynolds-averaged Navier-Stokes equations.

$$\rho(\mathbf{u}\cdot\nabla)\kappa = P_\kappa - \rho\beta^*\kappa\omega + \nabla\cdot((\mu+\sigma^*\mu_T)\nabla\kappa)$$

$$\rho(\mathbf{u}\cdot\nabla)\omega = \alpha\frac{\omega}{\kappa}P_\kappa - \rho\beta\omega^2 + \nabla\cdot((\mu+\sigma\mu_T)\nabla\omega)$$

Turbulent viscosity

$$\mu_T = \rho\frac{\kappa}{\omega}$$

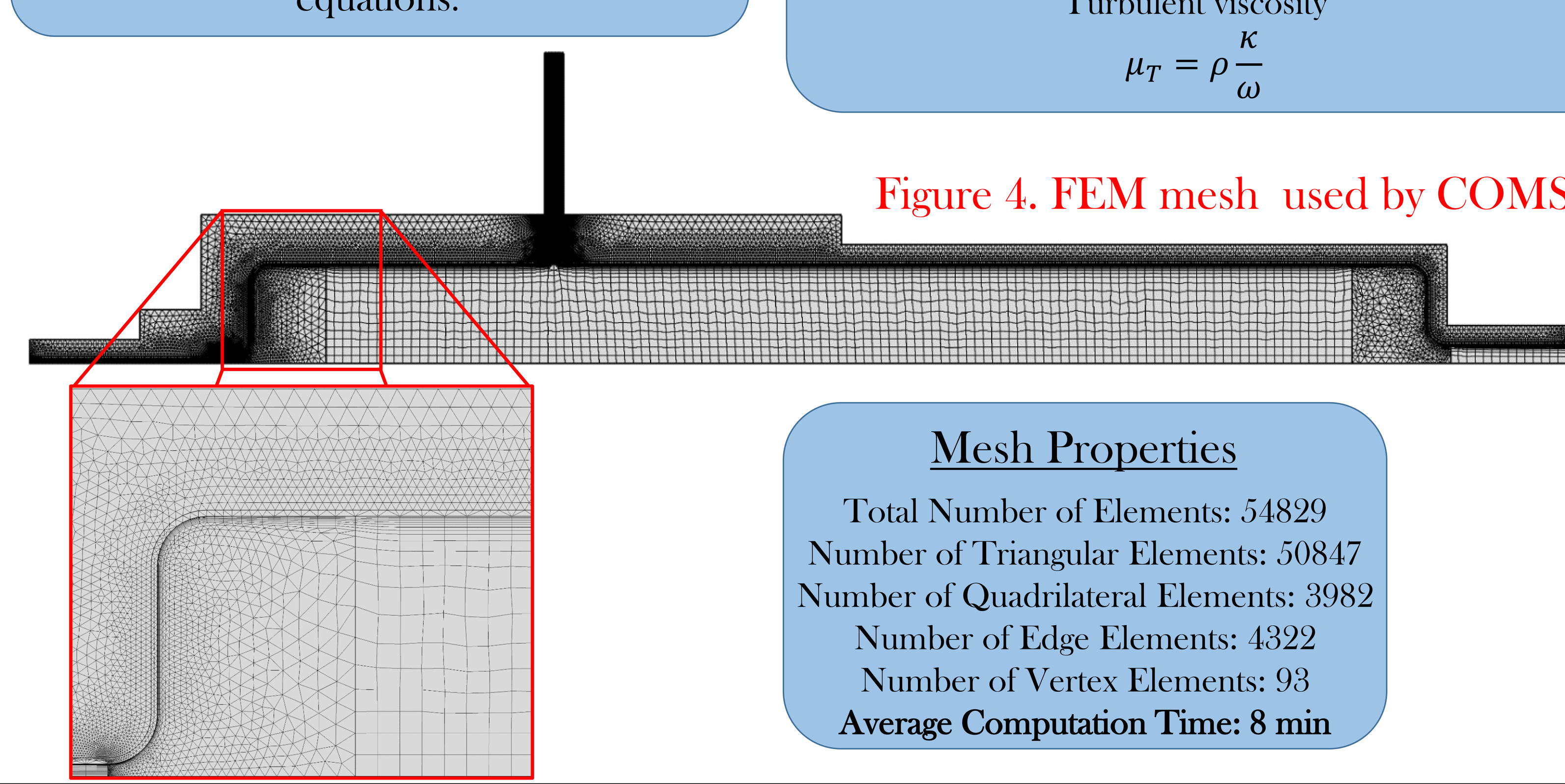

Figure 4. FEM mesh used by COMSOL

Mesh Properties

Total Number of Elements: 54829
Number of Triangular Elements: 50847
Number of Quadrilateral Elements: 3982
Number of Edge Elements: 4322
Number of Vertex Elements: 93
Average Computation Time: 8 min

Model Results

- The model produces a 3D rendition of the termination cryostat with an adjusted geometry for the current lead chamber.
- A full and detailed thermal map and velocity profile can now be produced.
- All kinds of parameters can be analyzed including pressure drop, heat leak, locations of vortices and eddy currents, and large density variations.
- The model solves within a very reasonable timeframe which is good for making adjustments and optimization.

Results for termination cryostat: inlet mass flow rate = 4.06 g/s, inlet temperature = 47.52K

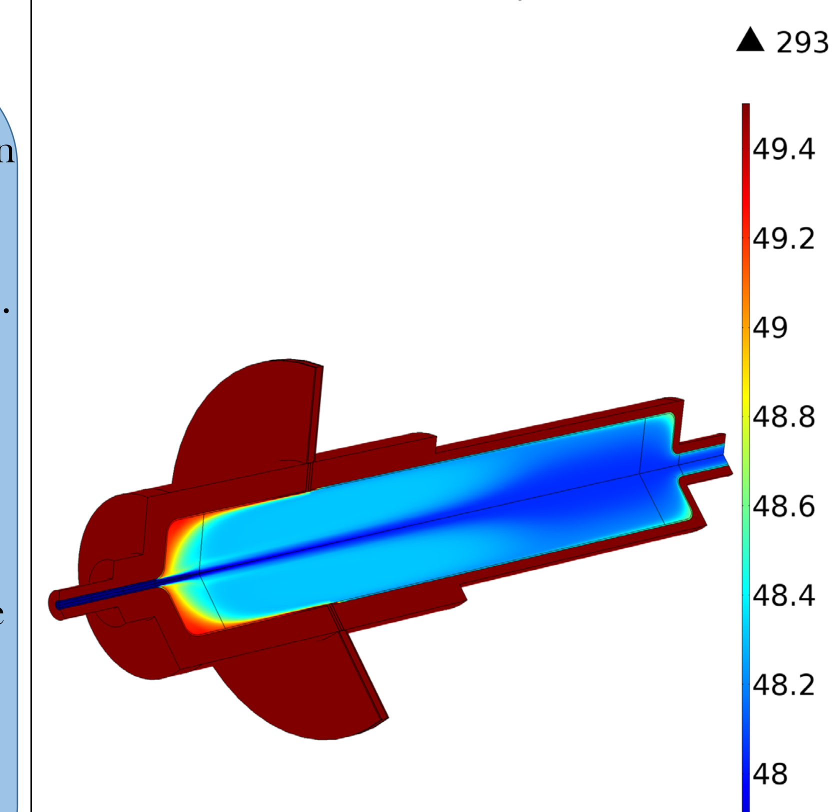

Figure 5. Temperature Field (K)

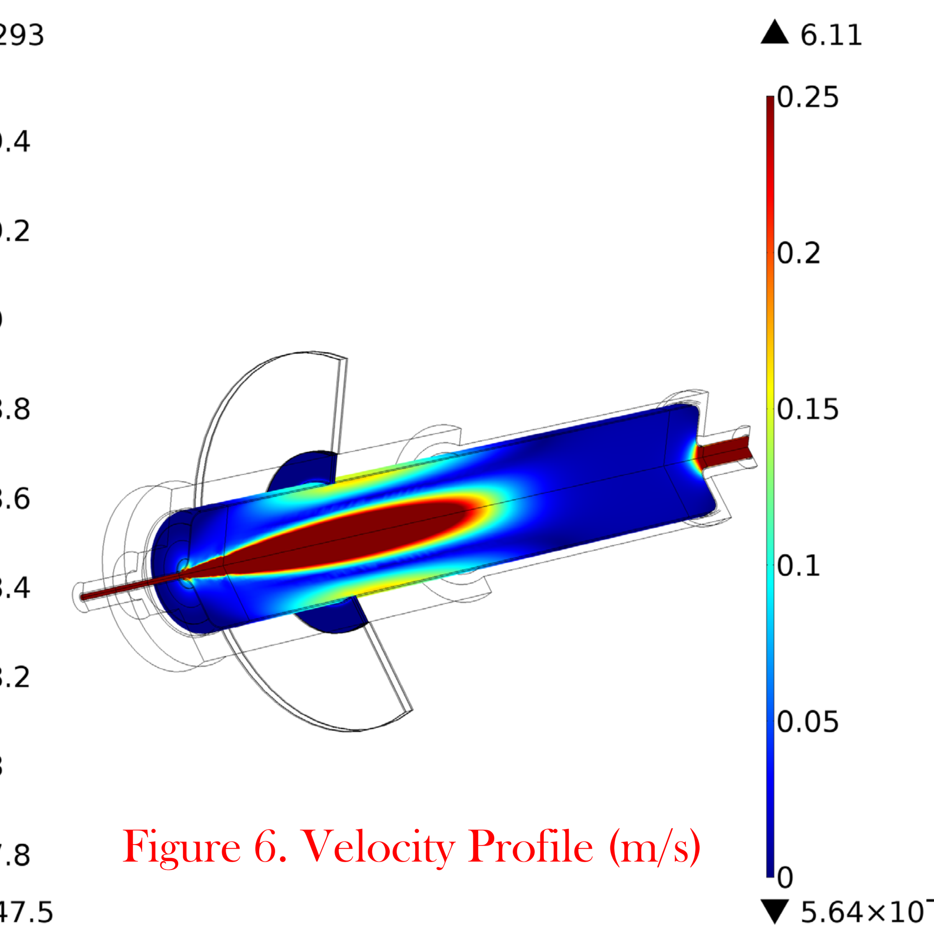

Figure 6. Velocity Profile (m/s)

Conclusion

- Results of the COMSOL model are congruent with the experimental results as well as the results by PLECS (Piecewise Linear Electrical Circuit Simulation) model.
- Results are better for Case 2 (current lead chamber filled with LN2), because the 77K boundary condition is more accurate. Also it has smaller delta T
- 3D model will be developed in the near future to test validity of 2D axis-symmetric model.

Figure 7. Comparison of Model Results to Experimental Results for Case 1 (Vacuum)

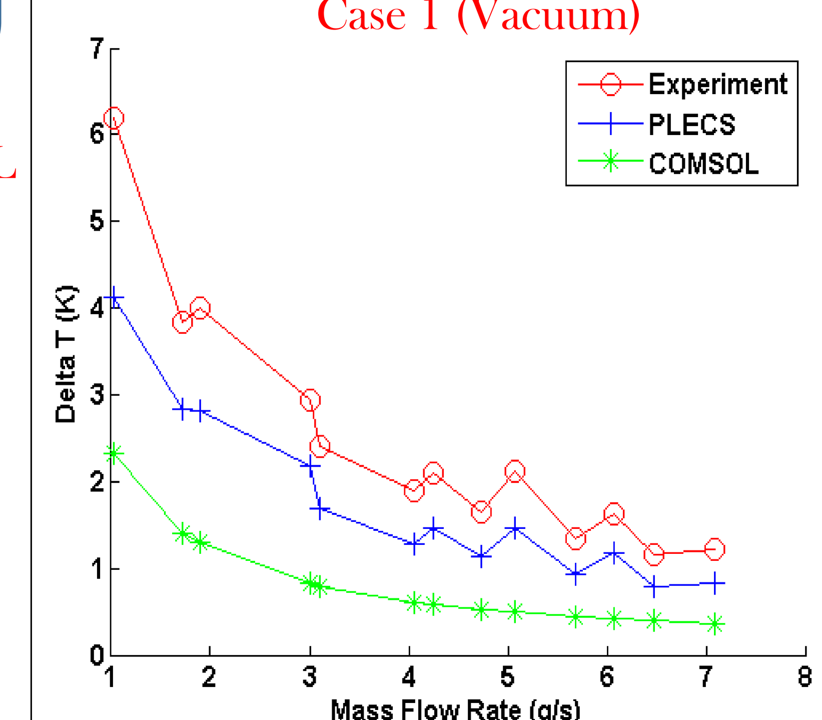

Figure 8. Comparison of Model Results to Experimental Results for Case 2 (LN2)

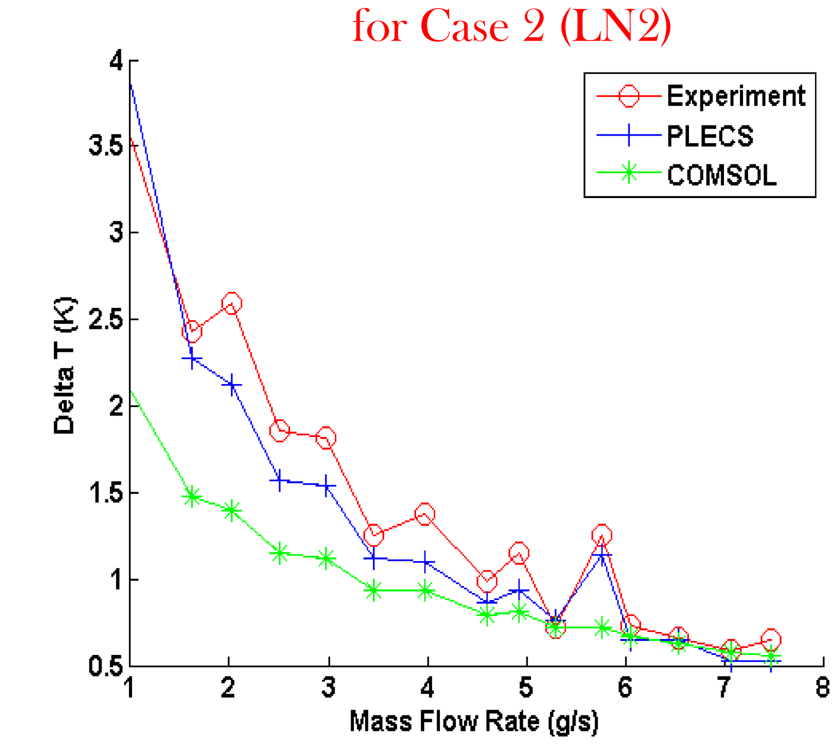

APPENDIX G

Effects of Longitudinal Variations in Critical Current and n-Value of Individual Tapes on the Performance of Superconducting Cables

Venkata Pothavajhala, *Student Member, IEEE,* Chul H. Kim, *Member, IEEE*, Lukas Graber, *Senior Member , IEEE,* and Sastry Pamidi, *Senior Member, IEEE*

***Abstract*— This paper presents results and analysis of simulations on critical current of superconducting cable affected by longitudinal variations of superconducting properties typically observed in commercial second generation high temperature superconducting (2GHTS) tapes. It was observed that the apparent critical current derived from measurements of long tape sections and cables mask the sections with lower critical current. Monte Carlo simulations coupled with mathematical models of superconducting cables made from multiple tapes were sued to assess potential risks in cable operations that are caused by longitudinal variations in I_c and *n*-value of the conductor used to fabricate long cables. It is shown that the variations in I_c reduce the designed capacity of the cables and increase the chances of catastrophic damage when a cable is operated close to its critical current.**

***Index Terms*—current distribution, critical current, mathematical model, superconducting DC cables.**

I. Introduction

High temperature superconducting (HTS) power cables are highly efficient for power distribution and transmission compared to conventional cables [1]. HTS DC transmission systems have the advantages of high transport current capability and zero resistive loss [2]. Studies show that HTS DC power cables can be used in future power grids [3]. Recent developments also include design, fabrication and istallation of 2GHTS power cables in power grid [4]-[7].

Current distribution among the tapes of HTS cables was found to be an important aspect to ensure optimal and reliable operation of the cable [8]. The effect of critical current (I_c), index (*n*) value and contact resistances were investigated and the results indicate that the uneven current distirbution due to differences in these parameters among the tapes could lead to catastrophic damage to the cables [9] [10]. The non uniform current distribution also reduces the cpacity of cable and lead to higher losses [11]. Current distribution is also important issue for resistive superconducting fault current limiters [12] [13]. During the processing and operation of 2GHTS tapes, they might be subjected to mechanical, thermal and electromagnetic stresses which can result in degradation of I_c. The effect of bending on I_c and minimmum bending radius of the tape to avoid degradation with and without stabilizers were studied in [14]. Compression, torsional strains and transverse loading on the tapes of the cable also cause variations in I_c along the length [15]-[17]. The importance of the uniformity in the I_c for practical applications of HTS coated conductors was emphasized by measuring the local I_cs for various tensile strains in [18]. The I_c of commercially available 2GHTS tapes varies along the length [19] [20]. Sometimes, the variation in I_c along the length could be as high as 10% compared to the average or minimum I_c. The variation of I_c and n value along the length of YBCO coated conductor commercially manufactured by MOD/RABiTS process was studied by the Los Alamos National Laboratory in self field and in applied field and were found to be significant [21]. Another important aspect is that these variations would have significant impact on performance of helium gas cooled cables that support higher power densities when operated at 50-60 K [22]. This is due to lower heat capacity of the helium gas. Commerical tapes from multiple vendors were procured and characterized to assess the extent of variations to be used in the models.

2GHTS is relatively new technology and involves complex multilayers including epitaxial layers to accomplish the biaxial texture needed to achive high critical current densitiy [23]. The manufacturers are devising quality control tools to accomplish narrow distribution of superconducting properties along the length which is also related to enhancing the yield of the production. It will take some time for the manufacturing processes to reach a level of quality control in all the subprocesses in the manufacturing. Meanwhile, it is important to understand the implications of longitudinal variations in 2GHTS tape propoerties on the characteristics of power devices made from them. Many HTS cables have successfully been demonstrated, but studies on the effects of longitudinal variations in superconducting poperties have not been reported.

This paper presents the effects of the longitudinal variations in I_c and *n* value of individual tapes on the overall performance of the superconducting cables. Commerical tapes from multiple vendors were procured and characterized to assess the extent of variations in I_c, and *n* value and the data were used in the mathematical models presented. Monte Carlo [24] [25] - a statistical computational method of solving problems involving computer generated random values, was used for analyzing the effect of variations in tape parameters on performance of superconducting cables calculated using

Automatically generated dates of receipt and acceptance will be placed here; authors do not produce these dates. This work was supported in part by the Office of Naval Research under Grant N00014-14-1-0198.
Venkata Pothavajhala (Phone: 850 284 2660; e-mail: pothavajhala@mail.caps.fsu.edu), Sastry Pamidi (e-mail: pamidi@caps.fsu.edu), Lukas Graber (e-mail: grabber@caps.fsu.edu) and Chul Han Kim (e-mail: ckim@caps.fsu.edu) are with Center for Advanced Power Systems, Florida State University, Tallahassee, FL 32310

mathematical cable model. These simulations were used to understand the nature and extent of the variations on the performance HTS cable systems. 10 cables were modeled using 300 tapes in which each tape is divided into 3000 sections and simulated with certain standard deviation of I_c and similarly for n values along their lengths.

II. Longitudinal Variation in Critical Current

As HTS tapes used for manufacturing superconducting cables have some variations in I_c along their length, a mathematical model was developed for a 30 m cable made of 30 superconducting tapes in parallel configuration. HTS tapes were considered to have different $I_c s$ for each centimeter section along the length as shown in Fig. 1.

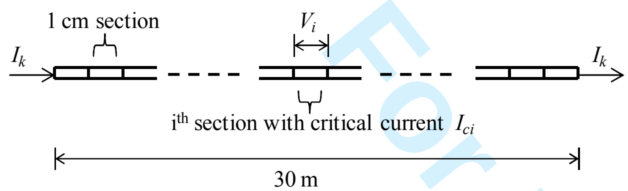

Fig. 1. A model tape in a HTS cable divided into several 1cm sections with varying I_c values.

I_k is the total current passing through the tape (varying from 1 A to 120 A), V_i is the voltage produced by ith section of the tape having critical current of I_{ci} and index-value of n_i.

$$V_i = E_c\left(\frac{I_k}{I_{ci}}\right)^{n_i} \tag{1}$$

E_c is the electric field criterion, 1µV/cm. The total voltage (V_t) produced by the 30 meter long tape is the sum of voltages produced by N (3000) sections

$$V_t = \sum_{i=1}^{N} V_i \tag{2}$$

The apparent critical current (I_{ca}) of the whole 30 m tape can be calculated using the Electric field of the tape (E)

$$E = \frac{V_t}{\sum_{i=1}^{N} l_i} \tag{3}$$

Here, l_i is the length of ith section of the tape, which is equal to 1 cm in this case. In designing a HTS superconducting cable with a required I_c, typically the average Ic of superconducting tape is used. The actual supplied tape has a range of Ic values and manufacturers have the ability to measure and supply the data for every 5 cm or even every cm.

To test the effect of the sections that have I_{ci} lower than the average I_{ci} of the tape, the following I_{ci} distribution (Fig. 2) was considered with 10 % of tape sections having I_{ci} less than 100 A and with a constant n of 30 for all sections.

The I_{ca} of the tape obtained in this case was 96 A. From this result it was clear that though 90% of the tape sections have I_{ci}s more than 100 A, the resulting I_{ca} of whole tape was reduced by 4 A. This was because the sections of tape (10%) with I_{ci}s lower than 100 A produce more voltage at higher currents causing the electric field to reach its criterion (1µV/cm) before the current reaches 100 A.

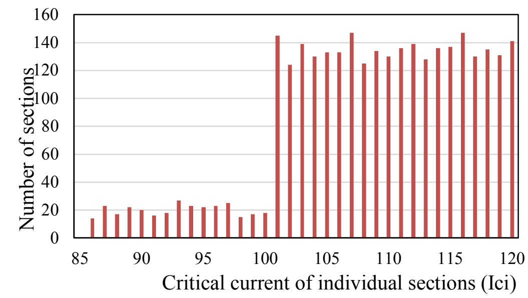

Fig. 2. Distribution of critical current of tape sections

To study a more realistic case, all the 3000 sections of tape were assigned normally distributed random values for their I_{ci}s with a mean of 100 A (I_{cm}) and varying standard deviation (σ_{Ici}) of 1 A, 3 A, 5 A, 7 A and 10 A.

$$\sigma_{I_{ci}} = \sqrt{\frac{1}{3000}\sum_{i=1}^{3000}\left(I_{ci} - I_{cm}\right)^2} \tag{4}$$

The I_{ca} of the tape was calculated for each case of σ_{Ici}. Monte Carlo method was used to simulate large number (about 50) of such tapes and the average value of I_{ca} was calculated. The standard deviation (σ_{Ici}) in I_{ci}s was calculated as in Eq. 4 and plotted against I_{ca}/I_{cm} in Fig. 3.

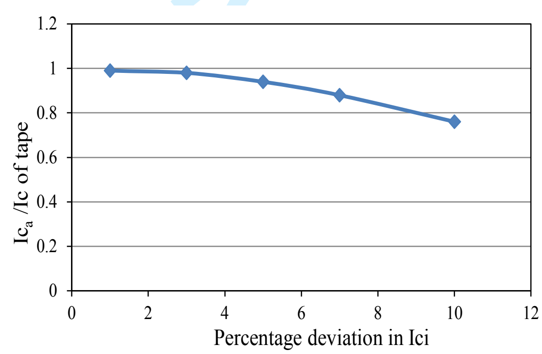

Fig. 3. Reduction in I_{ca} for certain longitudinal variation in I_{ci}

Fig. 3 indicates that as the standard deviation of critical current density along the length increases, the extent of reduction of the apparent critical current density from the average value also increases. The critical current as measured from end to end of a tape using the 1μV/cm electric field criterion masks the variation and gives a value mostly represented by the sections with lower values of critical current.

To investigate the effect of tapes having longitudinal variations in their characteristics on the performance of the whole cables fabricated using such tapes, models were generated for 300 tapes, each 30 meter long, with certain standard deviation in the I_{ci} along their length, and with a mean I_c of 100 A. 30 of these tapes were randomly selected to form each model cable of a set of 10 with a design I_c of 3 kA. The apparent I_c of the whole cable is nothing but the sum of I_{ca}s of individual tapes in this case because the contact resistances and n values of all tapes are assumed to be equal. Ten such model cables were formed with each cable having 30 tapes of certain standard deviation in I_c along their length. The n value of all tapes was assumed to be equal to 30 in this case. The summary results for the set of 10 cables is shown in Fig. 4. As seen from the figure, the higher the standard deviation of critical current of individual tapes, the larger is the reduction of measured critical current of the cable relative to the design value. The reduction is a result of the use of average I_c value for design purposes, as is typically done.

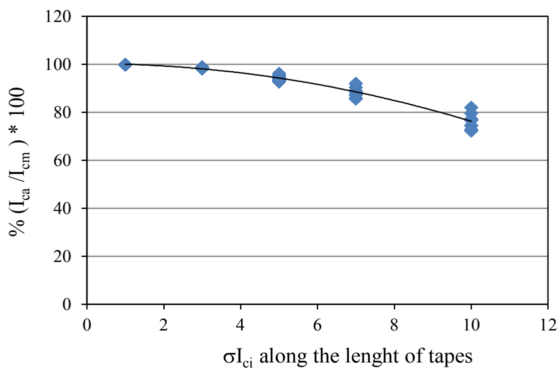

Fig. 4. Percentage of apparent I_c of the cable as function of cable mean I_c for a certain standard deviation in I_{ci} along the length of individual tapes of the cable.

III. Longitudinal Variation in Index Value

The effect of longitudinal variation of n value was also studied taking normally generated random values for different sections of the tape with mean n- value (n_m) of 30. The I_c of the tape was assumed to be constant along the length at 100 A. The individual section voltages were calculated using Eq. 1. After calculating the total voltage generated using Eq. 2, the E of the tape was calculated using Eq. 3 and resulting E-I curve was fitted using power law from which the apparent index value (n_a) was extracted. Monte Carlo method was used to simulate about 50 such tapes and the average n_a was calculated. The ratio of n_a and n_m is plotted against the standard deviation in n value of the tape (as in Eq. 5) and plotted in Fig. 5.

$$\sigma_{n_i} = \sqrt{\frac{1}{3000}\sum_{i=1}^{3000}\left(n_i - n_m\right)^2} \qquad (5)$$

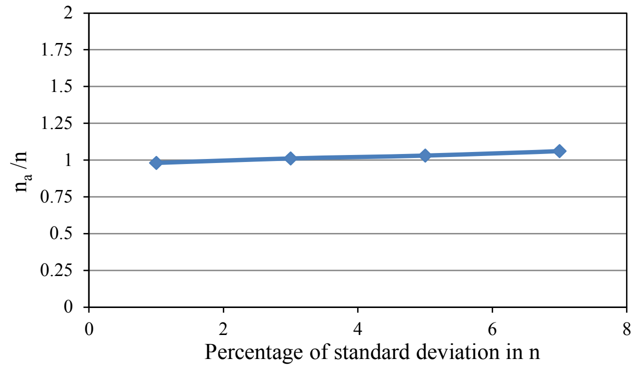

Fig. 5. Apparent n of the cable as function of cable mean n for a certain standard deviation in n_i along the length of individual tapes of the cable.

As seen from Fig. 5, there is no significant change in n_a of the tape due to longitudinal variations in n value. This is because the voltages generated by the sections with lower n-value are compensated by the voltages generated by sections with higher n-value. This indicates that the apparent n-value of the whole cable would be close to the mean n of tapes even if there are significant longitudinal variations in n-values of tapes.

IV. Conclusion

Monte Carlo simulations on superconducting tapes in long cable applications indicate that the longitudinal variations in I_c of the tapes reduce the design/rated capacity of the cable and have significant effect on its performance. Generally, manufacturers of superconducting tape provide the minimum I_c for the batch of superconductor, but short sectional variations of tape also affect the cable performance in a long length application. This is because the voltage produced by the lower I_c sections would be high enough to push the tape to reach its critical current well before the average I_c of the tape. The longitudinal variations in n value do not seem to effect the cable performance as long as these variations are distributed normally around the mean n value. Hence the sectional property distribution in I_c should also be considered for best performance of superconducting power cable design. In general, to minimize operational risk that some sections of the cable produce additional heat and cause potential damage, particularly when the cable is operated close to its rated capacity, tapes with a narrow distribution of superconducting parameters are preferred.

References

[1] J. X. Jin, "High efficiency dc power transmission using high-temperature superconductors," *Physica C,* Vols. 460-462, pp. 1443-1444, 2007.

[2] H. Zhao, J. Jin and X. Lu, "Advantages of HTS DC power transmission," in *IEEE International Conference on Applied Superconductivity and Electromagnetic Devices*, Chengdu, 2009.

[3] L. Xiao, S. Dai, L. Lin, Z. Zhang and J. Zhang, "HTS Power Technology for Future DC Power Grid," *IEEE Transactions on Applied*

Superconductivity, vol. 23, p. #5401506, 2013.

[4] D. Lindsay and B. Mehraban, "World's First Demonstration of a New 13.2 kV Triax Superconducting Cable," in *IEEE Power Engineering Society General Meeting*, Tampa, 2007.

[5] C. Weber, C. Reis, A. Dada, T. Masuda and J. Moscovic, "Overview of the underground 34.5 kV HTS power cable program in albany, NY," *IEEE Transactions on Applied Superconductivity,* vol. 15, no. 2, pp. 1793-1797, 2005.

[6] J. Maguire, J. Yuan, W. Romanosky, F. Schmidt, R. Soika, S. Bratt, F. Durand, C. King, J. McNamara and T. Welsh, "Progress and Status of a 2G HTS Power Cable to be Installed in the Long Island Power Authority (LIPA) Grid," *IEEE Transactions on Applied Superconductivity,* vol. 21, no. 3, pp. 961-966, 2011.

[7] M. Stemmle, F. Merschel, M. Noe and A. Hobl, "AmpaCity — Installation of advanced superconducting 10 kV system in city center replaces conventional 110 kV cables," in *IEEE International Conference on Applied Superconductivity and Electromagnetic Devices (ASEMD)*, Beijing, 2013.

[8] J.-H. Kim, C. H. Kim, V. Pothavajhala and S. V. Pamidi, "Current sharing and redistribution in superconducting DC cable," *IEEE Transactions on Applied Superconductivity,* vol. 23, no. 3, p. #4801304, 2013.

[9] V. Pothavajhala, L. Graber, C. H. Kim and S. Pamidi, "Experimental and Model Based Studies on Current Distribution in Superconducting DC Cables," *IEEE Transactions on Applied Superconductivity,* vol. 24, no. 3, p. #48000505, 2014.

[10] M. Takayasu, L. Chiesa, L. Bromberg and J. Minervini, "Cabling Method for High Current Conductors Made of HTS Tapes," *IEEE Transactions on Applied Superconductivity,* vol. 21, no. 3, pp. 2340-2344, 2011.

[11] S. Choi, S.-J. Suh, W. Nah, Y. H. Ma, K.-W. Ryu, J. H. Kim, J. Joo, M.-H. Sohn and Y.-k. Kwon, "Influence of Non-Uniform Current Distribution on AC Transport Current Loss in Bi-2223/Ag Tapes," *IEEE Transactions on Applied Superconductivity,* vol. 16, no. 2, pp. 154-157, 2006.

[12] T. Nitta, T. Matsumura, J. Baba, M. Ainslie, S. Torii, H. Kado, T. Kumagai and M. Shibuya, "Tests for Conceptual Design of 6.6 kV Class Superconducting Fault Current Limiter With YBCO Thin Film Elements," *IEEE Transactions on Applied Superconductivity,* vol. 19, no. 3, pp. 1964-1967, 2009.

[13] M. Ainslie, J. Baba, V. Salvucci, T. Nitta, T. Fukunaga, M. Shibuya, S. Torii, T. Matsumura and T. Kumagai, "Superconducting Fault Current Limiter Design Using Parallel-Connected YBCO Thin Films," *IEEE Transactions on Applied Superconductivity,* vol. 19, no. 3, pp. 1918-1921, 2009.

[14] M. Polikarpova, P. Lukyanov, I. Abdyukhanov and V. Pantsyrny, "Bending Strain Effects on the Critical Current in Cu and Cu–Nb–Stabilized YBCO-Coated Conductor Tape," *IEEE Transactions on Applied Superconductivity,* vol. 24, no. 3, p. #6600604, 2014.

[15] L. Chiesa, M. U. Medford, N. Allen and M. Takayasu, "Electromechanical Investigation of 2G HTS Twisted Stacked-Tape Cable Conductors," *IEEE Transactions on Applied Superconductivity,* vol. 24, no. 3, p. #6600405, 2013.

[16] G. Majkic, R. J. Mensah, V. Selvamanickam, Y. Xie and K. Salama, "Electromechanical behavior of IBD/MOCVD YBCO coated conductors subjected to torsion and tension loading," *IEEE Transactions on Applied Superconductivity,* vol. 19, no. 3, pp. 3003-3008, 2009.

[17] H. S. Shin, J. R. C. Dizon, T.-H. Kim, D.-W. Ha and S.-S. Oh, "Critical current degradation behavior in YBCO coated conductors under torsional strain," *IEEE Transactions on Applied Superconductivity,* vol. 17, no. 2, pp. 3274-3277, 2007.

[18] S.-S. Oh, H.-S. Kim, D.-W. Ha and H.-S. Ha, "Variation of Local Critical Current Due to Mechanical Strain in RCE-REBCO Coated Conductors," *IEEE Transactions on Applied Superconductivity,* vol. 24, no. 3, p. #6900204, 2014.

[19] V. Selvamanickam, Y. Chen, X. Xiong, Y. Xie, J. Reeves, X. Zhang, Y. Qiao, K. Lenseth, R. Schmidt, A. Rar, D. Hazelton and K. Tekletsadik, "Recent Progress in Second-Generation HTS Conductor Scale-Up at SuperPower," *IEEE Transactions on Applied Superconductivity,* vol. 17, no. 2, pp. 3231-3234, 2007.

[20] M. Rupich, X. Li, S. Sathyamurthy, C. Thieme, K. DeMoranville, J. Gannon and S. Fleshler, "Second Generation Wire Development at AMSC," *IEEE Transactions on Applied Superconductivity,* vol. 23, no. 3, p. #6601205, 2013.

[21] J. Willis, J. Coulter and M. Rupich, "n-Value Analysis of Position-Dependent Property Variability in Long-Length Coated Conductors," *IEEE Transactions on Applied Superconductivity,* vol. 21, no. 3, pp. 2988-2991, 2011.

[22] P. Ferrara, M. Uva and J. Nowlin, "Naval Ship-to-Shore High Temperature Superconducting Power Transmission Cable Feasibility," *IEEE Transactions on Applied Superconductivity,* vol. 21, no. 3, pp. 984-987, 2011.

[23] R. H. Ono, "Thin Film Processing of Complex Multilayer Structures of High-Temperature Superconductors," *Material Resrarch Society Bulletin,* pp. 34-38, August 1992.

[24] N. Metropolis and S. Ulam, "The Monte Carlo Method," *Journal of the American Statistical Association,* vol. 44, no. 247, pp. 335-341, 1949.

[25] C. C. Herd, "A Note On Early Monte Carlo Computations and Scientific Meetings," *Annals of the History of Computing,* vol. 7, no. 2, pp. 141-155, 1985.

APPENDIX H

Thermal Modeling of Gaseous Helium as a Cryogen for High Temperature Superconducting Cable Components

Nick Suttell, Chul H. Kim, *Member, IEEE*, Juan Ordonez, Darshit Shah, Lukas Graber, *Senior Member, IEEE*, Sastry Pamidi, *Senior Member, IEEE*

***Abstract*—A fluid mechanics and cryogenic thermal study of the termination system of a gaseous helium cooled second generation high temperature superconducting (HTS) cable is presented. This includes a discussion on the development of a 2D turbulent model that uses finite element method within COMSOL to assess the temperature profiles in the terminations and the comparison of the model results with those obtained experimentally. Temperature gradients across the cable system were measured before an actual HTS cable was installed to ensure that they are within an acceptable range and to validate the cryogenic design of the cable terminations. The experiments were conducted at the gaseous helium cooled superconducting cable test facility at the Florida State University, Center for Advanced Power Systems (CAPS). The thermal model presented here confirms that temperature gradients across a 30 meter long HTS cable system operating at around 50 K can be maintained below 6 K with helium gas mass flow rates of < 10 g/s. The results of the thermal models agree with the experimental results. The modeling methods used and the resulting thermal model reported will be useful for future design studies in optimizing the cryogenic thermal and fluid flow designs of superconducting cables.**

Index Terms*—Helium Gas, COMSOL, Turbulent Flow, RANS, Superconducting Cable

I. Introduction

GASEOUS helium as a cryogen for cooling high temperature superconducting power devices is a relatively recent development. The concept requires more studies and testing to understand the implications of low thermal capacity and other differences in properties of helium gas compared to liquid nitrogen. Naval applications including degaussing cables [1], propulsion motors, and power transmission systems [2]-[5] have been at the heart of cryogenic gaseous helium research. Several universities [6], [7] and power research institutions including the Electric Power Research Institute (EPRI) [8] have also conducted similar studies for utility applications. Benefits of using gaseous helium over other gaseous and liquid cryogens for naval applications include reduced risk of asphyxiation, single-phase flow, lower operational temperature leading to higher HTS current densities, and light weight. However, gaseous helium has a low thermal capacity compared to liquid cryogens at the same temperature and pressure [9], and it has a low dielectric strength [10]. The low heat capacity requires a careful design, and thus intensive modeling and experimentation must be performed in order to understand the properties of gaseous helium exposed to large temperature gradients.

Mechanical issues also arise during thermal cycles of HTS cable systems due to the fact that different materials have different coefficients of thermal contraction while cooling. Therefore, it is important to investigate methods of reducing mechanical deformation of HTS cable system components. Locations susceptible to mechanical failures are typically around the soldered joints at the terminations [11].

This paper is on modeling studies for cryogenic thermal analysis of a high temperature superconducting cable termination cryostat cooled with gaseous helium. Two different cases were studied: In Case 1, the chamber containing the current lead is under vacuum, and in Case 2, the same current lead chamber is filled with liquid nitrogen. It should be noted that this study does not consider Joule heating. Most of the copper and HTS material was replaced with temperature sensor bars in these tests. The focus was on understanding the cryogenic thermal aspects of the physical structure of the terminations. The results from the model were compared to experimental results for which many different cases have been investigated. These cases include a range of mass flow rates from 1-7.5 g/s, gaseous helium pressures from 200-1100 kPa, and inlet temperatures from 43-50 K. The model that is described in this paper uses the flow of helium gas in the turbulent regime and heat transfer through the termination. Reynolds numbers have been calculated up to 120,000 for the inlet channel, and 5,600 for the main channel, so the turbulent flow assumption is valid. The model takes into account the heat transfer throughout the entire termination. The goal of this study is to model the termination cryostat, compare results to those obtained by the experiments, investigate optimization opportunities, and assess the need of using any liquid cryogens in the process.

Manuscript submitted August 12, 2014, 2014.
This work was supported in part by the Naval Engineering Education Center.
This work was supported in part by the Office of Naval Research under Grant N00014-14-1-0198.
The authors are with the Center for Advanced Power Systems, Florida State University, Tallahassee, FL, 32310 USA; ngs07@my.fsu.edu.
Nick Suttell and Juan Ordonez are also with the Department of Mechanical Engineering at FAMU-FSU College of Engineering, Tallahassee, FL, 32310 USA.

II. Experimental Setup

The Center for Advanced Power Systems (CAPS) at Florida State University houses a 30 m HTS cable test facility that uses helium gas as the cryogen. Fig. 1 shows a schematic of the termination system used for the models and for the experiments. The experimental system involves two termination cryostats on either end of a 30 m long HTS cable cryostat and a cryogenic system that circulates the helium. The termination facilitates current injection into the cable and houses the superconducting cable ends that are attached to copper leads using low resistive solder joints. The termination tanks have vacuum jacketing to minimize heat leak into the cryogenic helium environment. There are two chambers that make up the termination cryostat. A horizontal chamber (that houses the superconducting cable ends and contains the cryogenic helium gas environment) is 2.05 m long and a vertical chamber (the current lead chamber) 1.17 m tall is connected vertically on top of the horizontal chamber. Most of the heat load on the superconducting cable system comes from the two terminations. Fig. 2 shows a schematic of the fully assembled termination that includes the superconducting cable ends and current leads. The system that was modeled does not have the cable ends because the purpose of the model and the experimental data were to assess the heat load on the terminations coming from the ambient environment. Hence there is no Joule heating included in the model. In the system that was analyzed, the copper feed through is the only conductive material present, and it is there solely for structural purposes (a pressure seal between the current lead chamber and the horizontal chamber). The feedthrough does, however, increase heat transfer from the helium gas due to its higher thermal conductivity and must be accurately modeled. The copper feedthrough has a diameter of 19.1 mm and a length of 82.0 mm.

Minimal heat penetrates the termination through the vacuum jacket, and the ground supports have been carefully designed to minimize heat conduction into the system. The helium gas enters the termination from the left side and exits at the right side of the horizontal chamber as shown in Fig. 2. There is no helium present in the current lead chamber. Eight temperature sensors were strategically placed throughout the first termination to accurately record the temperature field within. Of the 28 cases of non-Joule heating experiments that have been conducted, 15 of them were carried out while the current lead chamber was under vacuum (Case 1). This vacuum is separate and operates independently from the vacuum jacket that surrounds the entire termination. The other 13 cases were done while the current lead chamber was filled with liquid nitrogen (LN2) (Case 2). The purpose of testing these two conditions is to determine the role of liquid nitrogen and to estimate the heat load savings achieved by intercepting the heat leak from the current lead whose top section resides in LN2 or in vacuum depending on the case.

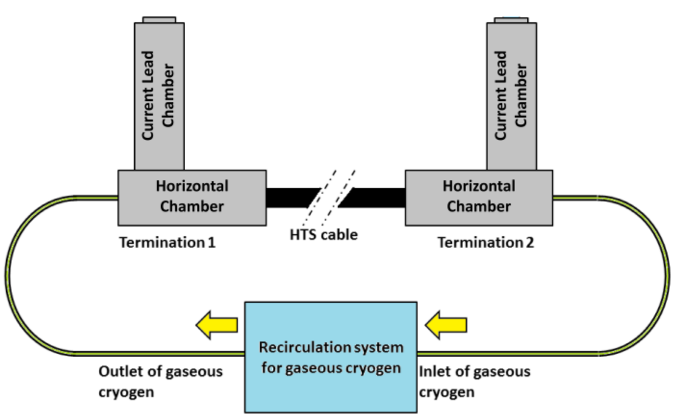

Fig. 1. Gaseous Helium Circulation System

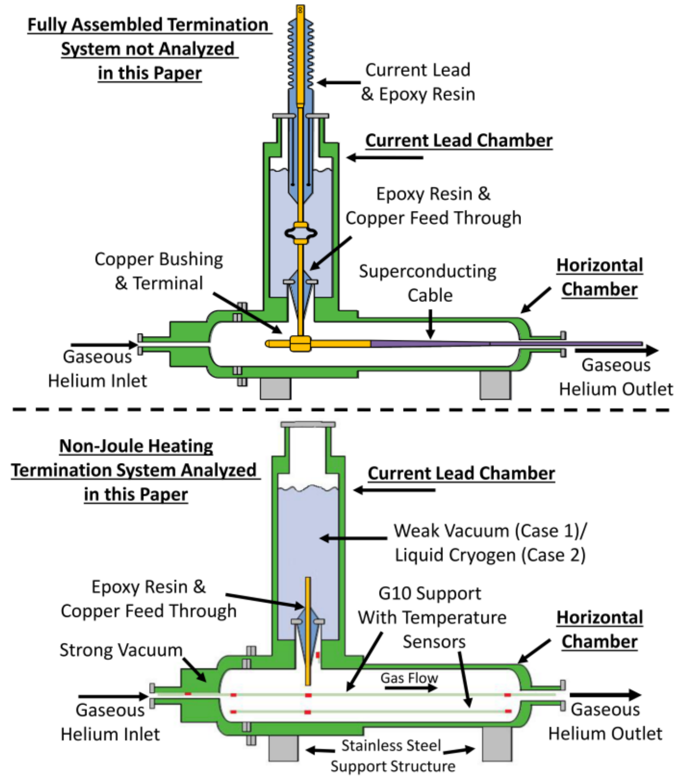

Fig. 2. Termination Cryostat. Top shows the fully functioning termination. Bottom shows the termination set-up analyzed in this paper.

III. Modeling Technique

A 2-dimensional axisymmetric model was developed to analyze the thermal map of the gaseous helium throughout the horizontal chamber at steady state. The axis of symmetry was chosen to be through the center of the horizontal chamber. To simplify the model, some assumptions and geometrical approximations were made.

1. The heat leak due to Joule heating is neglected because the experimental results used for comparison were collected without current flowing through the cable.
2. The axis through the center of the horizontal chamber was selected as the axis of symmetry. Because of this, the geometry of the current lead chamber and the feed through had to be properly adjusted so that it would maintain an equivalent surface and cross sectional area as it revolves around the horizontal axis of symmetry. This creates a disk-shape structure around the superconducting chamber when extrapolated in 3 dimensions, and it is why the current lead chamber is much smaller than the

horizontal chamber in the model. However the cross-sectional area is equivalent.

3. The supports have been carefully designed to minimize heat conduction into the system from the ground and are neglected in the model. Geometry for the steel shell on the outside of the vacuum jacket was also neglected because it was assumed to have a constant temperature (293.15 K) throughout.
4. Heat leak due to radiation is negligible since extensive amounts of Mylar was installed around the horizontal chamber in vacuum jacket.

Fig. 3 shows a 2D quadrant of the termination model, and it also helps describe the two different cases.

For Case 1, air was added in the model as a solid domain for the vacuum chamber inside the current lead chamber with a low conductivity equivalent to the overall heat transfer coefficient of the vacuum chamber. A correlation to calculate an equivalent conductivity of both vacuum chambers was found in [12]. Instead of modeling the complex physics of convection, conduction, and radiation in the insulation space, an equivalent conduction term is obtained from this correlation. The thermal conductivity in this low pressure theory is as follows:

$$K_e = K_0/(1 + C/PP), \tag{1}$$

where K_e is the thermal conductivity of air at the reduced pressure, K_0 is the thermal conductivity at 1 bar, C is a constant equal to 7.6e-05, and PP is the pressure parameter equal to:

$$PP = Pd/T, \tag{2}$$

where P is the pressure of the air in Pascals, d is the plate distance in meters, and T is the temperature in Kelvin.

The effective conductivity calculated for the vacuum jacket was 1.14×10^{-4} W/(m·K), and the effective conductivity calculated for the current lead chamber vacuum was 1.77×10^{-2} W/(m·K).

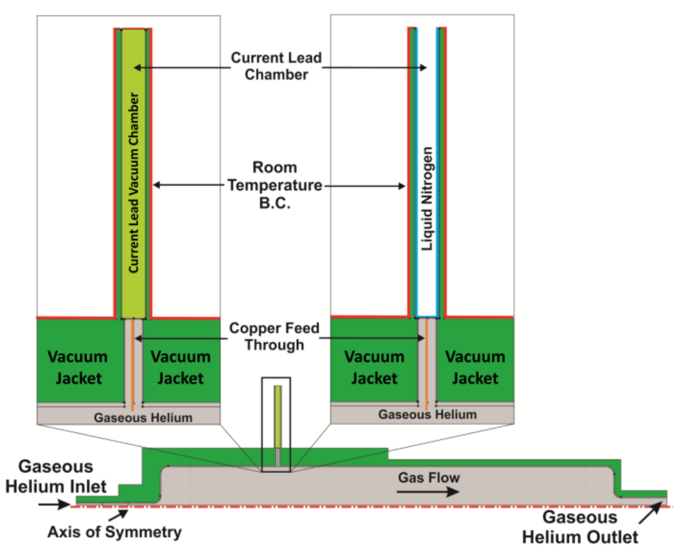

Fig. 3. Model Diagram (Case 1: current lead chamber under vacuum; Case 2: current lead chamber filled with LN2

In Case 1, there are two separate vacuum chambers (the vacuum jacket and the vacuum within the current lead chamber) that operate independently from each other. For Case 2, a boundary condition on the inside wall of the current lead chamber was set to 77 K with no material within the domain. The difference between Case 1 and Case 2 in terms of heat transfer is that, for Case 1, heat transfer from the 300 K environment to the horizontal chamber is considered including leaks through the top plate and the stainless steel wall structure of the current lead chamber. For Case 2, heat leaks only by conduction through the copper feed through at the bottom of current lead chamber where the temperature is 77 K.

The turbulent flow physics for compressible flow used by COMSOL divides the flow into 2 regimes: large, resolved scales; and small, unresolved scales. The large scales use the Navier-Stokes equations, and the small scales use a turbulence model that includes Reynolds-averaged Navier-Stokes (RANS) equations associated with the Wilcox $k - \omega$ Turbulent Model [13]. The way the RANS model solves for scalar quantities is it divides them into an averaged value and a fluctuating part

$$\phi = \overline{\phi} + \phi', \tag{3}$$

where ϕ can represent any scalar quantity of the flow, $\bar{\phi}$ is the averaged value, and ϕ' is the fluctuating value. RANS models are numerically less expensive than resolving all present scales. The model couples the $\kappa - \omega$ turbulent flow physics with heat transfer in fluids and solids. The Navier-Stokes equations used in the stationary turbulence model for compressible flow and the energy balance for heat transfer are as follows:

$$\rho(\boldsymbol{u}\cdot\nabla)\boldsymbol{u} = \nabla\cdot\Big[-p\boldsymbol{I} + (\mu+\mu_T)(\nabla\boldsymbol{u} + (\nabla\boldsymbol{u})^T) - \frac{2}{3}(\mu+\mu_T)(\nabla\cdot\boldsymbol{u})\boldsymbol{I} - \frac{2}{3}\rho k\boldsymbol{I}\Big] + \boldsymbol{F}; \tag{4}$$

$$\nabla\cdot(\rho\mathbf{u}) = 0; \tag{5}$$

$$\rho C_p\mathbf{u}\cdot\nabla T = \nabla\cdot(k_c\nabla T) + Q + Q_{vh} + W_p, \tag{6}$$

where ρ is the density of the gaseous helium, $\mathbf{u}$ is the velocity field, p is the absolute pressure, μ is the viscosity, μ_T is the turbulent viscosity, T is the absolute temperature, k is the turbulent kinetic energy, $\mathbf{F}$ is the volume force, C_p is the specific heat at constant pressure, k_c is the temperature dependent thermal conductivity, Q_{vh} is the viscous heating term, Q contains heat sources other than viscous heating, and W_p is the pressure work term. The turbulent model introduces two additional transport equations along with two additional dependent variables to close the RANS equations: the turbulent kinetic energy, κ, and the dissipation per unit turbulent kinetic energy, ω.

$$\rho(\mathbf{u}\cdot\nabla)k = P_k - \rho\beta^* k\omega + \nabla\cdot\big((\mu + \sigma^*\mu_T)\nabla k\big) \tag{7}$$

$$\rho(\mathbf{u}\cdot\nabla)\omega = \omega\alpha P_k/k - \rho\beta\omega^2 + \nabla\cdot\left((\mu+\sigma\mu_T)\nabla\omega\right) \quad (8)$$

These two additional terms are related to each other through the turbulent dynamic viscosity, μ_{T},

$$\mu_T = \rho k/\omega. \quad (9)$$

The rest of the symbols in (7) and (8) are reported in Table 1. These constants are closure coefficients, and they provide algebraic expressions of known mean-flow and turbulence properties in place of unknown double and triple correlations. Because the Wilcox $k-\omega$ theory is not exact, the values of the closure coefficients are set to assure agreement with observed properties of turbulence. More information on this can be found in Wilcox's book [13].

TABLE I
CONSTANTS WITHIN THE ADDITIONAL TURBULENT EQUATIONS AND THEIR CORRESPONDING RELATION

Constant	Relation
α	$13/25$
β	$\beta_0 f_\beta$
β^*	$\beta_0^* f_\beta$
σ	$1/2$
σ^*	$1/2$
β_0	$13/125$
f_β	$(1+70\chi_\omega)/(1+80\chi_\omega)$
χ_ω	$\lvert\Omega_{ij}\Omega_{jk}S_{ki}/(\beta_0^*\omega)^2\rvert$
β_0^*	$9/100$
f_{β^*}	$\begin{cases} 1, & \chi_\kappa < 0 \\ \dfrac{(1+680\chi_k^2)}{(1+400\chi_k^2)}, & \chi_\kappa \geq 0 \end{cases}$
χ_k	$(\nabla k\cdot\nabla\omega)\omega^{-2}$

The finite element method implementation used 206,108 total mesh elements. Fig. 4 shows the mesh convergence test done on the model for a Case 1. In this case, the inlet mass flow rate is 4.2 g/s, and the inlet temperature is 47.5 K. After approximately 205,000 mesh elements, there is no significant gain in the solution's accuracy, and therefore that number of mesh elements was selected for the model.

A boundary layer mesh is imposed at the fluid-wall boundary to resolve the velocity profile and heat transfer near the wall, and a swept mesh is generated through the constant cross-section of the superconducting chamber. Analytical expressions known as wall functions are imposed at the wall to efficiently describe the flow [14]. The wall functions are an accurate approximation that starts where the logarithmic layer meets the viscous sublayer (neglecting the buffer layer in between). The heat transfer is also accurately adjusted for using these wall functions.

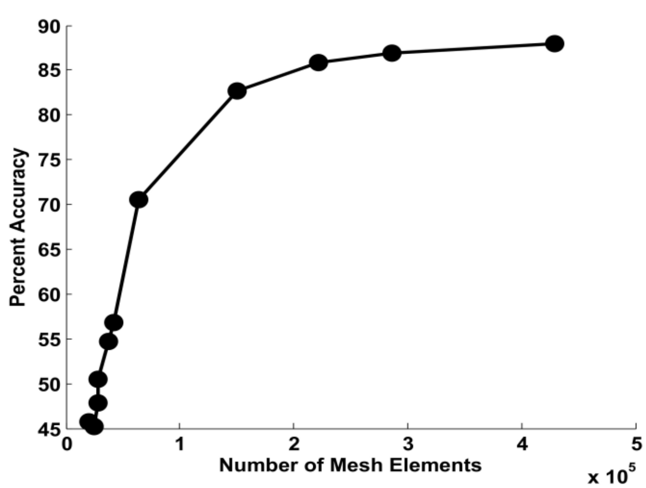

Fig. 4. Mesh Convergence Test for Case 1. Mass Flow Rate = 4.1 g/s, Inlet Temperature = 47.5 K

IV. RESULTS AND DISCUSSION

The computational model was run for all 28 cases of thermal experiments of the cable system at CAPS. Figs. 5 and 6 show the temperature field and velocity magnitude profile, respectively, for Case 1 where the mass flow rate is 4 g/s and the inlet temperature is 47.5 K. The gradients within the superconducting channel for both temperature and velocity can be seen in these plots. The peak velocity of the helium gas was 5.89 m/s located in the center of the channel, and the average peak temperature of the helium gas was 73.2 K at a location near the current lead chamber. Velocity streamlines in Fig. 6 show a vortex which causes higher velocity magnitudes near the wall. The heat flux was integrated along the outer boundary of the system. It was found to be a maximum at 16.3 W for Case 1 when $\dot{m} = 6.1$ g/s and a minimum at 9.6 W for Case 2 when $\dot{m} = 1.0$ g/s.

The temperature rise from the inlet of the cryostat to the outlet was the parameter chosen to compare the theoretical results to the experiment. Figs. 7 and 8 show these comparisons for Case 1 and Case 2, respectively. The results for Case 2 agree better with the experiment than for Case 1 possibly because the boundary condition of 77 K imposed in Case 2 is stronger and can exclude uncertainties that can come from additional heat transfer simulation in the domain of the current lead chamber.

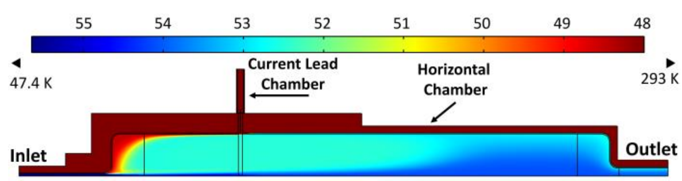

Fig. 5. Temperature Field for Case 1. (Unit for color bar is in Kelvin)

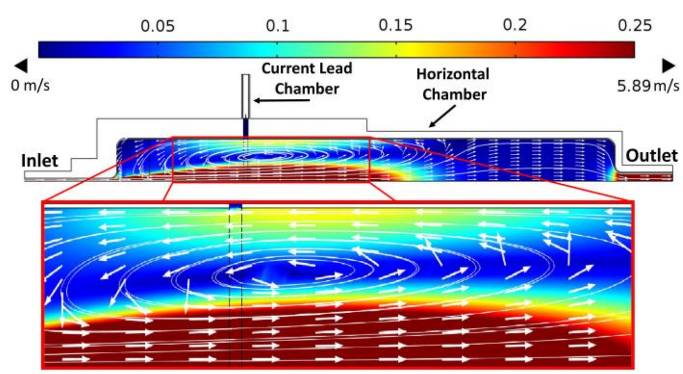

Fig. 6. Velocity Profile with Streamlines for Case 1. (Unit for color bar is in m/s)

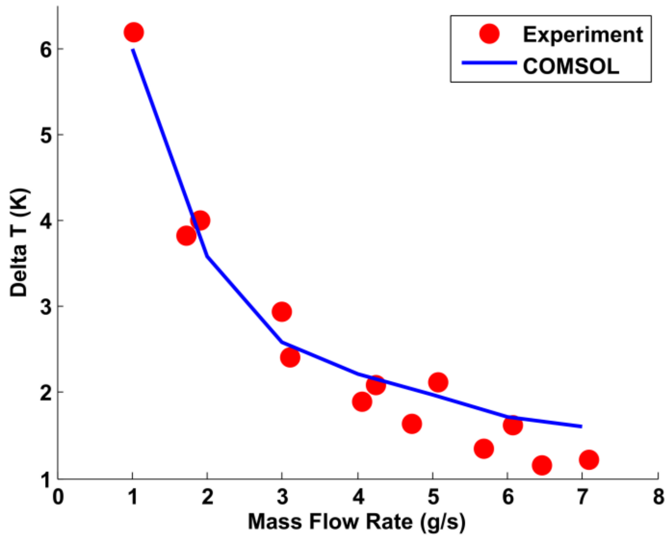

Fig. 7. Comparison of the temperature rise between the inlet and outlet for the experimental and computational results for Case 1 (Vacuum)

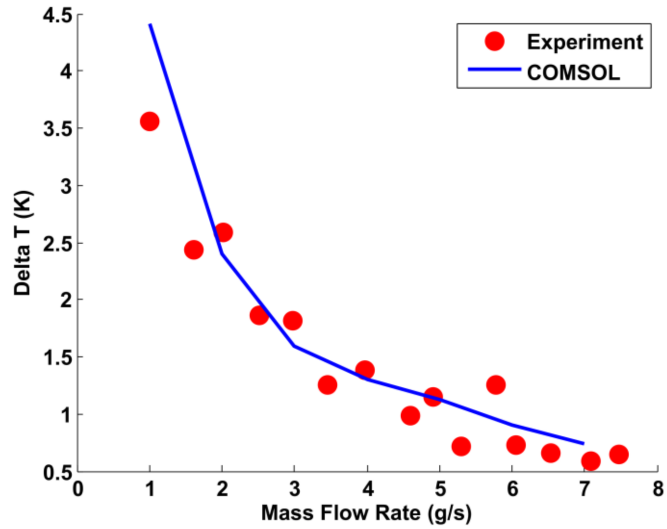

Fig. 8. Comparison of the temperature rise between the inlet and outlet for the experimental and computational results for Case 2 (LN2)

V. Conclusion

A 2D axis-symmetric, $k-\omega$ turbulent model was implemented to analyze fluid flow and heat transfer in the termination cryostat of an HTS cable cooled with gaseous helium as the cryogen. This study is one of the first attempts to computationally model a termination as a necessary first step for further optimization. The results agree well with the experimental data for both cases. The model shows better agreement with the experiment when temperature boundary conditions are set as close to the horizontal chamber as possible. This is the case for Case 2 where the 77 K boundary condition is set at the bottom of the current lead chamber. Some perspective conclusions could be made throughout the development of this model:

1. The flow is within the turbulent regime, and a 2D axis-symmetric turbulent model can solve in a short time.
2. Most of the heat leak experienced by the termination is through the current lead chamber.
3. The presence of the copper feed through is necessary to properly simulate heat transfer due to conduction since it is also an important heat transfer path in termination design.

A 3D model will be developed to further test the validity of the 2D axis-symmetric model. This is desirable because the geometry can be accurately reproduced (especially the current lead chamber), electrical characteristics can be introduced more conveniently, and improved optimization studies can be made. The 3D model will be tested against the 2D axis-symmetric model to determine if its improved accuracy outweighs the higher computing power requirements.

VI. References

[1] J. T. Kephart, B. K. Fitzpatrick, P. Ferrara, M. Pyryt, J. Pienkos and E. M. Golda, "High Temperature Superconducting Degaussing from Feasibility Study to Fleet Adoption," *IEEE Transactions on Applied Superconductivity*, vol. 21, no. 3, pp. 2229-2232, 2011.

[2] B. K. Fitzpatrick, J. T. Kephart and E. M. Golda, "Characterization of Gaseous Helium Flow Cryogen in a Flexible Cryostat for Naval Applications of High Temperature Superconductors," *IEEE Transactions on Applied Superconductivity*, vol. 17, no. 2, pp. 1752-1755, 2007.

[3] J. T. Kephart, B. K. Fitzpatrick, P. Ferrara, M. Pyryt, J. Miller and C. Nadig, "Flow Resistance Experiments in HTS Cable Form," *IEEE Transactions on Applied Superconductivity*, vol. 23, no. 3, p. 4, 2013.

[4] J. C. Ordonez, J. A. Souze, D. R. Shah, J. V. C. Vargas and R. Hovsapian, "Temperature and Pressure Drop Model for Gaseous Helium Cooled Superconducting DC Cables," *IEEE Transactions on Applied Superconductivity*, vol. 23, no. 3, p. 5402005, 2013.

[5] H. Rodrigo, F. Salmhofer, D. S. Kwag, S. V. Pamidi, L. Graber, D. G. Crook, S. L. Ranner, S. J. Dale and D. Knoll, "Electrical and thermal characterization of a novel high pressure gas cooled DC power cable," *Cryogenics*, vol. 52, no. 4, pp. 310-314, 2012.

[6] J. A. Demko and W. V. Hassenzahi, "Thermal management of long-length HTS Cable Systems," *IEEE Transactions on Applied Superconductivity*, vol. 21, no. 3, p. 957, 2011.

[7] M. Wozniak, L. Bromberg, B. A. Glowacki, J. Xiaohua, Z. Rong, J. V. Minervini and J. G. Brisson, "DC Superconducting Cable Using MgB2 Wires," *IEEE Transcations on Applied Superconductivity*, vol. 23, no. 3, p. 6200805, 2013.

[8] EPRI, "Program on Technology Innovation: A Superconducting DC cable," Electric Power Research Institute, Inc., Palo Alto, 2009.

[9] S. V. Pamidi, C. H. Kim, D. Crook and S. Dale, "Cryogenic helium gas circulation system for advanced characterization of superconducting cables and other devices," *Cryogenics*, vol. 52, no. 4, pp. 315-320, 2012.

[10] L. Graber, C. H. Kim, S. V. Pamidi, H. Rogrigo and D. Knoll, "Dielectric design validation of a helium gas cooled superconducting DC power cable," in *Electrical Insulation Conference (EIC)*, Philadelphia, PA, 2014.

[11] A. Ballarino, "Development of Superconducting Links for the LHC," *Journal of Physics: Conference Series*, vol. 27, no. 4, p. 044024, 2014.

[12] C. J. M. Lasance, "Electronics-Cooling," 1st November 2002. [Online]. Available: http://www.electronics-cooling.com/2002/11/the-thermal-conductivity-of-air-at-reduced-pressures-and-length-scales/. [Accessed December 2013].

[13] D. C. Wilcox, Turbulence Modeling for CFD, La Canada, California: DCW Industries, Inc., 1993.

[14] H. Grotjans and F. R. Menter, "Wall Functions for General Application CFD Codes," *ECCOMAS 98, Proceedings of the Fourth European Computational Fluid Dynamics Conference*, pp. 1112-1117, 1998.